VOLUME 30 MARCH 1952 NUMBER 2

Canadian Journal of Physics

Editor: G. M. VOLKOFF

Published by THE NATIONAL RESEARCH COUNCIL
OTTAWA CANADA

CANADIAN JOURNAL OF PHYSICS

(*Formerly Section A, Canadian Journal of Research*)

The CANADIAN JOURNAL OF PHYSICS is published bimonthly by the National Research Council of Canada under the authority of the Chairman of the Committee of the Privy Council on Scientific and Industrial Research. Matters of general policy are the responsibility of a joint Editorial Board consisting of members of the National Research Council of Canada and the Royal Society of Canada.

The National Research Council of Canada publishes also: *Canadian Journal of Botany, Canadian Journal of Chemistry, Canadian Journal of Medical Sciences, Canadian Journal of Technology, Canadian Journal of Zoology.*

Manuscripts should be addressed to:

DR. LÉO MARION,
Editor-in-Chief,
Canadian Journal of Physics,
National Research Council,
Ottawa, Canada.

Each manuscript should be typewritten, double-spaced, and the original and one extra copy submitted (see **Notice to Contributors,** inside of back cover).

Subscription, renewals, and orders for back numbers should be addressed to:

Administrative Services,
National Research Council,
Ottawa, Canada.

Subscription rate: $3.00 a year; single numbers: 50 cents. Special rates can be obtained for subscriptions to more than one of the Journals published by the National Research Council.

**Deceased.*

Canadian Journal of Physics

Issued by THE NATIONAL RESEARCH COUNCIL OF CANADA

VOLUME 30 MARCH, 1952 NUMBER 2

ROTATIONAL WINGS OF RAMAN BANDS AND FREE ROTATION IN LIQUID OXYGEN, NITROGEN, AND METHANE[1]

BY M. F. CRAWFORD, H. L. WELSH, AND J. H. HARROLD[2]

ABSTRACT

Rotation-vibrational Raman bands have been observed in liquid oxygen, nitrogen, and methane, and in solid methane. In every case the Q branches associated with isotropic Raman scattering are sharp lines; but the Q branches and rotational wings associated with anisotropic scattering form broad continuous bands, with extent and intensity distribution consistent with free molecular rotation. The lack of discrete structure in the broad bands is attributed to a removal of the m degeneracy of the rotational energy levels in the intermolecular force fields. Removal of the m degeneracy broadens those transitions for which the transition probability depends on the anisotropic part of the rate of change of the polarizability, but not those for which J and m are unchanged and for which the transition probability depends only on the isotropic part. The Raman spectrum of liquid oxygen yields no evidence for O_4 aggregates. The Raman spectrum of liquid methane displays all fundamental vibrations of the molecule and two overtones, with Raman shifts (in cm.$^{-1}$): 1300, band (ν_4); 1535, band (ν_2); 2570, line, and 2600, band ($2\nu_4$); 2906, line (ν_1); 3020, band (ν_3); 3053, line ($2\nu_2$).

INTRODUCTION

The rotational structure of Raman bands predicted by the theory of Placzek and Teller (14) and verified quantitatively for a few simple gases is in general absent in the Raman spectra of liquids. The vibrational Raman bands of most liquids are in fact quite sharp. The faint wings that have been observed around Rayleigh lines and vibrational Raman lines (2) show a rapid continuous decrease of intensity outward from the center, without the subsidiary maxima in the wings characteristic of free rotation. This lack of rotational structure has been attributed to hindering of the molecular rotation by intermolecular forces in the liquid state.

Discrete rotational Raman lines for a pure substance in the liquid state have been observed only in hydrogen (8). For hydrogen the spacing of the rotational energy levels is very large ($B = 60$ cm.$^{-1}$), and the intermolecular forces are so small that the rotation of the molecules is not appreciably hindered. Other simple molecules with hydrogen as a constituent have relatively large rotational energy constants, but do not show free rotation in the liquid state because dipole moments and hydrogen bonding produce relatively large molecular interactions. For such molecules, the Raman spectra show marked and irregular differences between the gaseous and the liquid state which can

[1] *Manuscript received August 1, 1951.*
Contribution from the McLennan Laboratory, University of Toronto, Toronto 5, Ont.
[2] *Holder of National Research Council Studentship, 1946-7; N.R.C. Fellowship, 1947-8; Research Council of Ontario Scholarship, 1948-9.*

be attributed to molecular association. Examples are water (11) and ammonia (19).

Detailed investigations of the Raman effect are lacking for the liquid state of most of the other simple molecules with reasonably large rotational constants and with comparatively small molecular interactions, i.e. for substances with low boiling points and small latent heats. Oxygen, nitrogen, and methane have these properties; and discrete rotational structure has been observed (18, 12, 4) in the Raman spectra of these as gases. However, the literature contains no mention of rotational wings around the vibrational Raman lines of liquid oxygen and nitrogen, and the published work on rotation-vibrational Raman bands of liquid methane (9, 15) is inconclusive concerning the question of free rotation. Wings around Rayleigh lines have been reported for some liquids, in particular, for liquid oxygen by Saha (16). None of the investigators attempted to correct their results for the scattering in the photographic emulsion of the very intense Rayleigh light; consequently, no great reliance can be placed on any of the conclusions hitherto reported.

This paper presents the results of a detailed study of the Raman spectra of liquid oxygen, nitrogen, and methane. The results show that the molecular rotation is relatively unhindered for these substances in the liquid state. Freedom of molecular rotation in solid methane has been repeatedly suggested and cessation of this rotation has been proposed in explanation of the λ-point at 20° K. in the specific heat curve (13). However, the recent results of Thomas, Alpert, and Torrey (17) on the nuclear magnetic resonance absorption show no change in the line width at 20° K. and eliminate the possibility of a rotational transformation at this temperature. Their data on both line width and spin-lattice relaxation time indicate that appreciable activity persists in the solid just below its melting point. The investigation of the Raman spectrum presented here shows that molecular rotation is in fact essentially free in solid methane at a temperature 12° below its melting point.

EXPERIMENTAL PROCEDURES

The procedures for photographing the Raman spectra and for obtaining intensity and frequency calibrations were essentially the same as those of Welsh, Crawford, and Scott (20). The water-cooled mercury lamps subsequently developed in this laboratory were used. With these lamps the exposures required were not unduly long, and it was possible to measure relative intensities in the Raman spectra directly with a photoelectric recording spectrometer (10).

In studying pure rotational Raman effect, the distribution of intensity in the wings of the Rayleigh line obtained directly from the spectrogram was corrected for the scattering of Rayleigh light in the emulsion. To determine this correction the spectrum of the mercury lamp was photographed with an exposure such that the intensities of the weaker mercury lines were equal to the intensities of these same lines in the Raman spectrogram. The intensity distribution measured for the exciting lines in the mercury lamp spectrum was

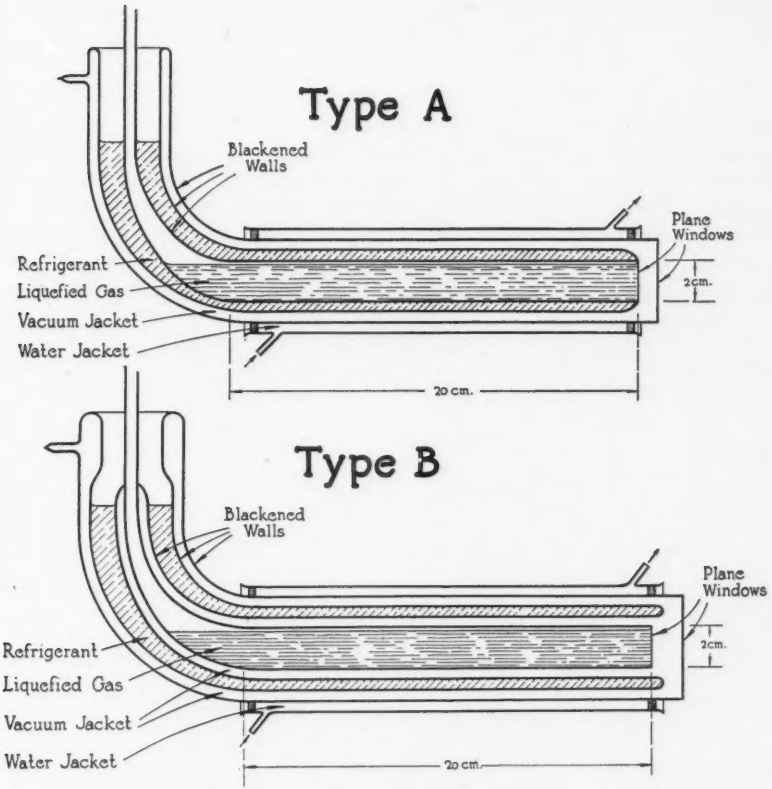

FIG. 1. Raman tubes for liquefied gases: Type *A*, direct cooling; Type *B*, indirect cooling.

then subtracted from the intensity distribution in the Raman spectrogram, and the residual intensity was taken as due solely to the Raman effect.

The Raman tubes for liquid oxygen, nitrogen, and methane are of conventional design, with the addition of vacuum jackets to permit operation at liquid air temperatures. Fig. 1 shows two typical designs. Plane-parallel Pyrex windows are fused to the Raman tubes to allow the scattered light to emerge without focusing effects. Raman tubes of Type A, in which the refrigerant was in direct contact with the innermost tube containing the sample, were used for liquid oxygen and nitrogen. The Type B tube was used for liquid methane. In this tube the vacuum jacket, extending around the sample tube as far as the horn, insulated the liquid methane (m.p. $-184°$ C.) from the refrigerant, liquid nitrogen (b.p. $-196°$ C.), which was more satisfactory than liquid air because of the constancy of its boiling point.

The illuminated portion of the tube was surrounded by a water jacket to

absorb heat from the lamps. A filter solution of sodium nitrite in water was circulated through this jacket when it was desired to remove the Raman lines excited by the 4047A group of mercury lines. A thickness of 9 mm. of this solution, saturated at 30° C., transmitted only 0.1% at 4047A, but nearly 90% at 4358A.

Gases from storage cylinders were passed through soda lime and phosphorus pentoxide traps into the evacuated sample tubes, and there liquefied directly by the refrigerant. The methane used was a C.P. grade (99%), the oxygen was a hospital grade, and the nitrogen was the ordinary grade fractionated from liquid air. The sample tubes were not filled completely. The vapor in the space above the liquid under study equalized the temperature throughout the liquid, and prevented it from boiling at the window.

The temperatures of the liquids were estimated from their vapor pressures, as measured with a mercury barometer attached to the sample tube. The

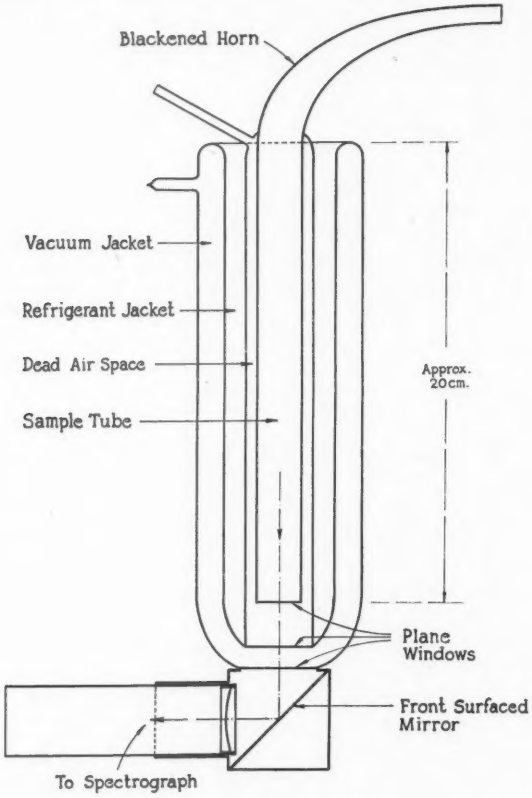

FIG. 2. Raman tube for solid methane.

barometer also served as a safety valve for the disposal of the methane. The liquid oxygen and methane were at pressures below atmospheric during the exposures, and the liquid nitrogen was under an excess pressure of 3 p.s.i.

The degree of polarization of some of the Raman bands of liquid methane was determined to check the assignment of the bands to the vibrational modes of the methane molecule. The experimental arrangement followed closely that described by Welsh, Crawford, and Scott (20). However, the approximation to unidirectional irradiation was poor, because of the several cylindrical layers of fluids surrounding the sample tube. The arrangement of the apparatus was such that the intensities of a depolarized line in the two spectra polarized at right angles were equal. Thus an apparent value of 1.0 was obtained for the depolarization factor ($\rho = 0.86$) of depolarized lines. For the symmetrical vibration ν_1, which Bhagavantam (1) has shown to be highly polarized in the gas ($\rho = 0.08$), the apparent value of ρ was 0.25. From these limiting values it was possible to determine approximately the degree of polarization of the other Raman bands.

Fig. 2 shows the Raman tube used for solid methane. In this tube the space between the sample tube and the refrigerant served a dual purpose. It

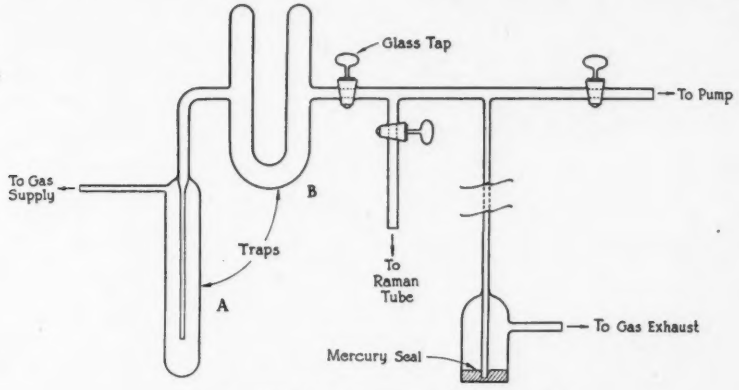

FIG. 3. Distillation apparatus for methane.

was evacuated during the filling of the sample tube to prevent the methane from solidifying rapidly into an apparently amorphous solid. Then, after large crystals of methane had formed, dry air was admitted to this space to maintain the methane appreciably below its melting point. The methane was distilled into the sample tube to remove traces of insoluble impurities (see Fig. 3). The gas was first liquefied in the Trap A by immersing the trap in liquid oxygen. The flask containing the liquid oxygen was then lowered, and the methane allowed to boil off slowly into Trap *B*, in which it was again liquefied by filling the cup of the trap with liquid oxygen. The liquid methane dripping from the bottom of the cup evaporated and was condensed for a third

time in the sample tube. During this final condensation the refrigerant jacket was completely filled with liquid nitrogen. As the level of the liquid in the sample tube rose, the methane slowly solidified upwards from the window and inwards from the walls. The bulk of the solid was fairly transparent, except near the window where there was a concentration of small crystals forming a translucent pyramidal structure extending upwards about 3 cm. from the window. The sample tube was filled with solid methane in about three hours, and the final vapor pressure was below that given in the standard physical tables for solid methane at the melting point (−184° C.).

The translucent structure near the window greatly increased the flux of Rayleigh light and seriously reduced the flux of Raman light entering the photoelectric recording spectrometer. The Rayleigh light was reduced by using a monochromator (10) set to exclude 4358A and all radiations of shorter wave lengths. However, the intensities of the Rayleigh lines of longer wave lengths were so great that only the clear region between 4358A and 4916A was suitable for the study of the Raman spectrum. The intensity of the Raman light was increased by using a new high-current mercury lamp. For the regular lamps, in which only the electrode pools are water-cooled, the rate of increase of intensity with current decreases sharply above 15 amp., and the Pyrex coils carrying the discharge tend to become overheated. For the high-current lamp, the cooling water was carried from end to end of the lamp by a small Pyrex tube within the discharge tube, and a constant rate of increase of intensity with current was obtained up to 35 amp. As for the regular lamps, the mercury lines were sharp and very little continuum was present.

RESULTS AND DISCUSSION

Liquid Oxygen and Nitrogen

An intense Raman spectrum of liquid oxygen, excited in a tube of Type A with dimensions as in Fig. 1 (*a*) by one water-cooled helical lamp, was recorded with an $f/4$ spectrograph in five hours. Rotational wings were plainly evident, extending 100 cm.$^{-1}$ on either side of the vibrational Raman line and showing no discrete structure. Since the slit had a spectral width of 3 cm.$^{-1}$ compared to the line spacing of 11.5 cm.$^{-1}$ in the pure rotational Raman effect of the gas (18), clearly these wings are continuous. Fig. 4 gives the intensity distribution in the rotational wings of the Raman band, as determined from the spectrograms. The density of the Q branch was too great for reliable determination of its intensity relative to that of the wings.

The pure rotational Raman spectrum of liquid oxygen, excited in a 45 cm. Raman tube of Type A by two helical lamps, was recorded with a Hilger E-1 spectrograph in seven hours. Again no discrete structure was observed, using a slit of spectral width 2.5 cm.$^{-1}$ The intensity distribution in the rotational Raman spectrum also is plotted in Fig. 4. This intensity distribution, which has been corrected for the scattering of the Rayleigh light in the emulsion as previously described, agrees closely with that found in the rotation-vibrational Raman band. The distribution is not in agreement with that

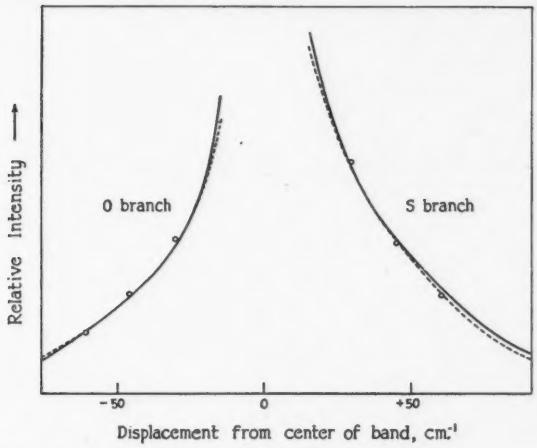

FIG. 4. Intensity distribution in rotational wings for liquid oxygen:
——— Rotational Raman band (4358A).
- - - - - Rotation-vibrational Raman band (photographic).
° ° ° ° ° Rotation-vibrational Raman band (photoelectric).

estimated by Saha (16) for the rotational wings of the Rayleigh lines of the liquid. A bulge in the microphotometer trace of the Stokes wing, which he interpreted as a maximum of intensity, is actually due to the scattering in the emulsion, for which he made no correction.

Further exposures with the *E*-1 spectrograph with slits of spectral width down to 1.0 cm.$^{-1}$ showed that the half-width of the *Q* branch of the vibrational Raman band is less than 1 cm.$^{-1}$ The frequency shift of the *Q* branch is 1552.0 cm.$^{-1}$, as compared to 1556.4 cm.$^{-1}$ calculated for the vibrational frequency of oxygen molecules from the electronic spectrum of the gas.

A similar study of the pure rotational Raman effect of liquid nitrogen showed that it also has a continuous intensity distribution. However, the intensity was much less than that for liquid oxygen, and therefore the study of liquid nitrogen was not pursued further by the photographic method.

The vibrational Raman bands of liquid oxygen and nitrogen, excited in the 45 cm. tube, were also recorded photoelectrically, using matched entrance and exit slits of spectral width 10 cm.$^{-1}$ The intensity distribution in the wings of the vibrational band of liquid oxygen confirms that obtained photographically for displacements from the band center greater than 30 cm.$^{-1}$ (see Fig. 4). For displacements less than 30 cm.$^{-1}$ the intensity changes so rapidly that a comparison is not significant because of the difference in slit widths.

Figs. 5 and 6 show the intensity distributions in the vibrational bands of liquid oxygen and nitrogen obtained by photoelectric recording. Clearly the contour in each case is quite similar to that predicted for freely rotating diatomic molecules, an intense *Q* branch and extensive rotational wings, except

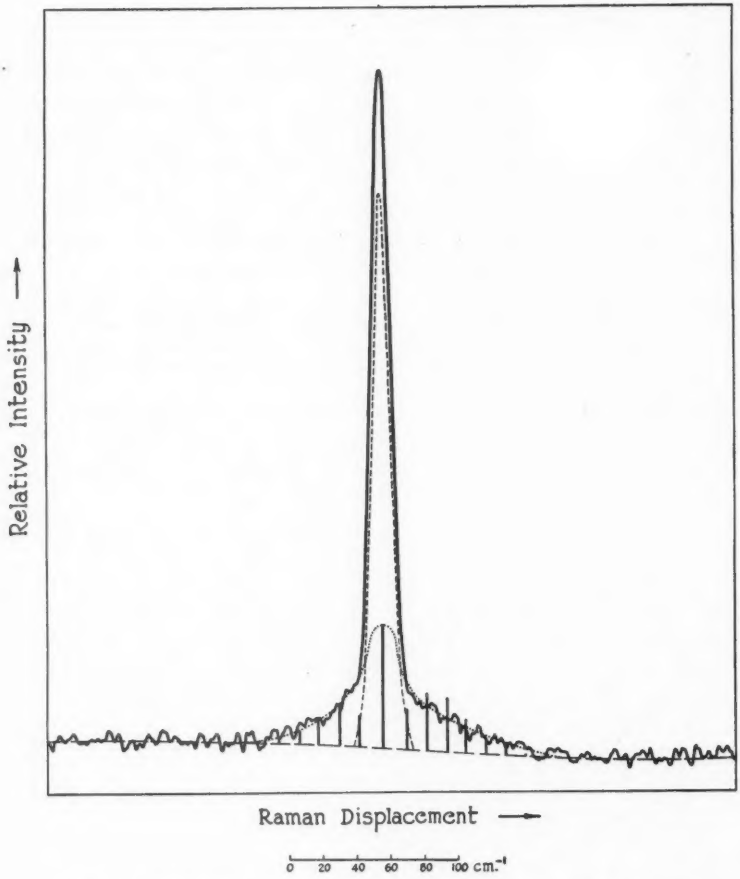

FIG. 5. Intensity distribution in vibrational Raman band of liquid oxygen.

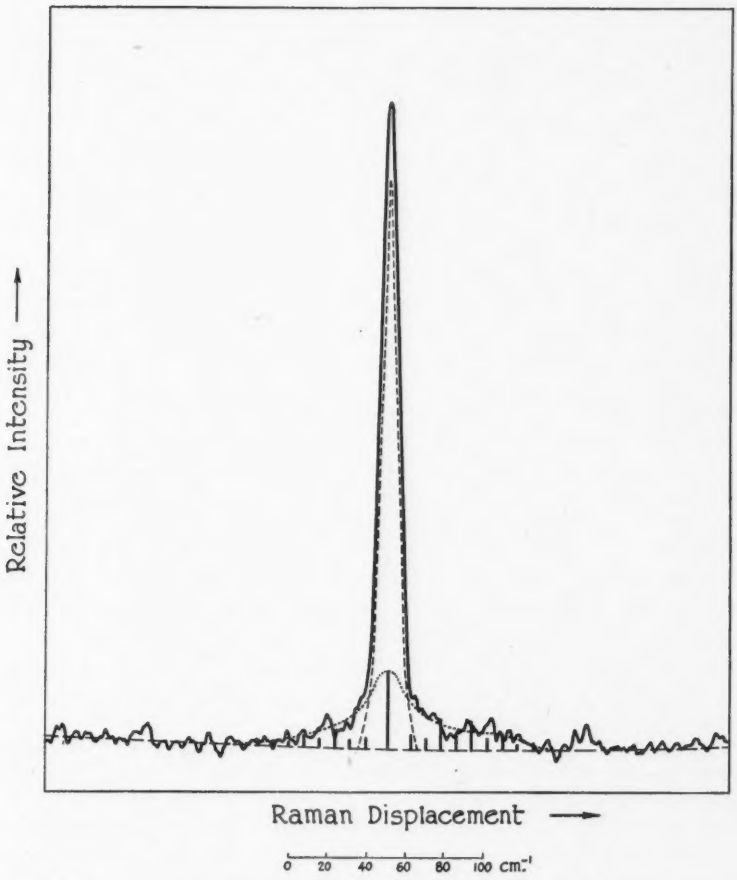

FIG. 6. Intensity distribution in vibrational Raman band of liquid nitrogen.

that there is no distinct division between the base of the Q branch and the wings. The photographic results with narrow slits show that there is no discrete structure in the wings, and that the merging of the base of the Q branch into the wings is real and not simply a consequence of the use of wider slits for photoelectric recording. Thus the Raman band can be considered as a sharp intense line, and an underlying broad band, in which the individual lines are broadened to form a continuum. On the assumption that the sharp line corresponds to isotropic Raman scattering and the broad band to anisotropic scattering, their intensity ratio can be calculated by using the value of ρ for the gas, and the anisotropic scattering separated from the rest of the contour.

The dashed curves in Figs. 5 and 6 indicate the isotropic and anisotropic parts, calculated from the values of ρ measured by Cabannes and Rousset (3) for the gaseous state, 0.26 for oxygen and 0.19 for nitrogen. In each case the isotropic part is drawn with a contour the same as that of a mercury line of equal integrated intensity and recorded with the same slit width. The small half-width found photographically for the Q branch justifies this procedure. The residual intensity of the band is assigned to anisotropic scattering. The vertical lines represent the theoretical intensities of the discrete lines for freely rotating molecules, with the intensity of the anisotropic part of the Q branch matched to the peak intensity of the broad band.

For both oxygen and nitrogen the extent of the rotational wings and the intensity distribution in the entire band are in satisfactory agreement with the theoretical distribution. Thus the result of this analysis shows that the rotation of the molecules is essentially free. It also shows that the perturbations caused by the intermolecular forces in the liquid state broaden only the lines arising from anisotropic scattering. The lack of a division between the base of the Q branch and the wings shows that the anisotropic part of the Q branch is broadened to a half-width of at least 20 cm.$^{-1}$

For liquid oxygen, O_4 aggregates have been postulated to explain certain physical phenomena. From a consideration of the magnetic susceptibility of liquid oxygen Lewis (6) has estimated the concentration of the O_4 aggregates as about 50% by weight. If the concentration were as high as this, the intensity distribution in the vibrational band would have been distinctly different from the theoretical pattern for diatomic molecules. Also, the presence of O_4 aggregates could cause a splitting of the Q branch, but secondary components were not found, although with the E-1 spectrograph any secondary component displaced as little as 1 cm.$^{-1}$ from the main line and with an intensity ratio as low as 1/20 would have been detected.

Liquid Methane

The stronger Raman bands of liquid methane were much more intense than those of liquid oxygen under similar conditions of observation. Thus a tube of Type B, with dimensions as in Fig. 1 (*b*), was satisfactory for photoelectric as well as photographic recording. Fig. 7 shows microphotometer traces of

spectrograms from which the lines and bands were identified. The identification for each frequency shift and other relevant data are listed in Table I, and for comparison the frequency shifts for the gas (4).

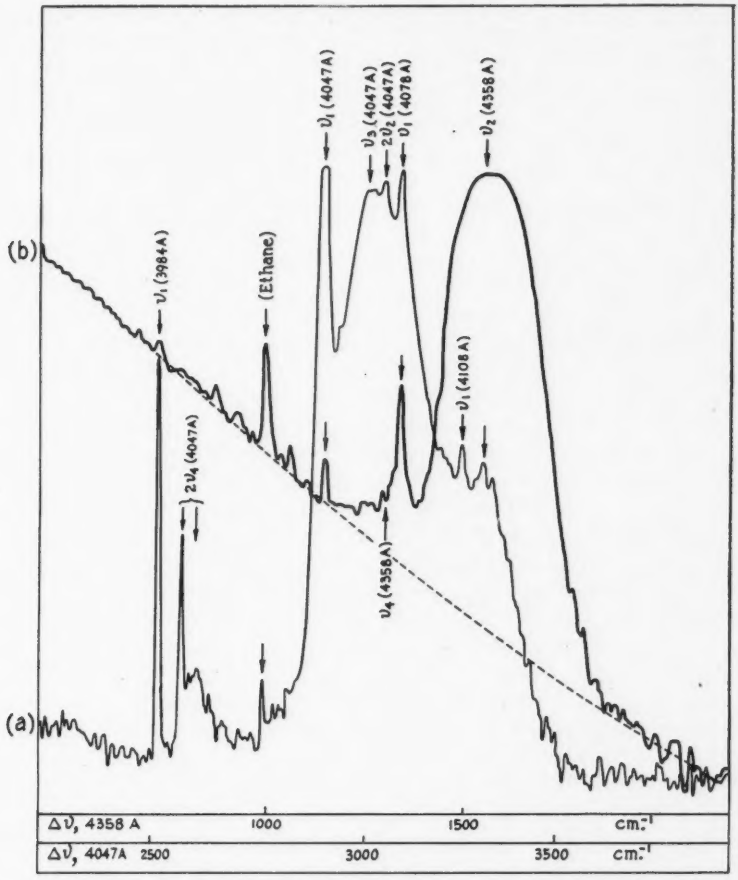

FIG. 7. Raman spectra of liquid methane:
(*a*) Exposure seven hours without filter, *f*/10 camera, slit width 5 cm.$^{-1}$
(*b*) Exposure 12 hr. with filter, *f*/4 camera, slit width 15 cm.$^{-1}$

The relative intensities greater than the value 10 in Table I were determined from photoelectric recordings. The intensities of the weaker lines were determined from the spectrograms of Fig. 7, in which the stronger lines and bands are considerably overexposed, and correlated with those of the stronger lines by measuring the latter on spectrograms taken with shorter

TABLE I

RAMAN SPECTRUM OF LIQUID METHANE

Frequency shift, cm.$^{-1}$		Vibrational assignment	Integrated intensity	Polarization	Structure in liquid
Liquid	Gas				
1300	....	ν_4 (F_2)	4	....	Weak diffuse band
1535	....	ν_2 (E)*	80	depol.	Continuous band
2570	....	$2\nu_4$ (A_1)*	2	....	Sharp line
2600	....	$2\nu_4$ (F_2)	10	....	Continuous band
2906	2914	ν_1 (A_1)*	400	pol.	Strong sharp line
3020	3022	ν_3 (F_2)*	400	depol.	Strong continuous band
3053	3072	$2\nu_2$ (A_1)*	10	pol.	Sharp line

*These vibrations have been previously observed in the Raman spectrum of the liquid (9, 15).

exposures. Plates of the same emulsion number, for which a calibration had been determined, were used for both long and short exposures. This is not the most accurate procedure for the determination of relative intensities, but unquestionably the intensity of the ν_4 fundamental is of the order of 1% of that of the other triply degenerate vibration (ν_3). The faintness of the ν_4 band explains why it has not been previously observed.

The Raman lines for A_1 vibrations noted in Table I (ν_1 and two overtones) are very sharp; the half-widths are equal to those of Rayleigh lines recorded with the same intensity. For these lines the excited states are, like the ground state, spherically symmetrical; as a result these lines do not have associated rotational wings, and are highly polarized.

The Raman bands for the degenerate vibrations (all species other than A_1) are very broad and depolarized. No discrete structure was observed in the bands (Fig. 7) even with a spectral slit width of 5 cm.$^{-1}$ which is much smaller than the line spacing of 21.5 cm.$^{-1}$ found in the ν_3 band of the gas (4). The strong ν_2 and ν_3 bands were traced over a range of 400 cm.$^{-1}$ and the intensity distributions determined (see Fig. 8, which will be discussed in detail below). Subsidiary maxima were not observed in the wings of either of these bands. Rank, Shull, and Axford (15) reported three maxima for the ν_2 band, but our traces at high photographic density give no evidence of their two subsidiary maxima at $\Delta\nu$ = 1513 cm.$^{-1}$ and $\Delta\nu$ = 1547 cm.$^{-1}$ However, in the ν_2 band excited by 4358A there appears a sharp component; it is certainly ν_1 excited by 4108A, because it disappears when the 4047A group of exciting lines is filtered out. This component, which has a displacement of 1509 cm.$^{-1}$ from 4358A, may perhaps correspond to the component, $\Delta\nu$ = 1513 cm.$^{-1}$, reported by Rank *et al.*

The ν_4 and $2\nu_4$ (F_2) bands were weak and could be definitely traced only over a range of 200 cm.$^{-1}$ It is doubtful if greater exposures would bring up the ν_4 band further, because it is partly overlapped by the much stronger ν_2 band. The ν_4 band should not show as pronounced a central peak as the other degenerate bands, because of its large internal Coriolis interaction.

The overtones listed in Table I have anomalously great intensities because of resonance with the stronger fundamentals. The sharp line at $\Delta\nu$ =

3053 cm.$^{-1}$ in the liquid is the A_1 part of $2\nu_2$ in resonance with ν_1, as is verified by its high degree of polarization, equal to that of the ν_1 line. The sharp line at $\Delta\nu = 2570$ cm.$^{-1}$ and the continuous band at $\Delta\nu = 2600$ cm.$^{-1}$ are the A_1 and F_2 parts of $2\nu_4$ in resonance with ν_1 and ν_3, respectively. The intensity of the $2\nu_4$ overtone is actually greater than that of the corresponding fundamental, whereas the intensity of the $2\nu_2$ overtone is about an eighth of that of the fundamental.

In the Raman spectrum, two additional lines were recorded very faintly, $\Delta\nu = 990$ cm.$^{-1}$ and $\Delta\nu = 2940$ cm.$^{-1}$ Their intensity relative to the methane lines varied from sample to sample. These lines are attributed to traces of ethane.

The existence of four fundamental bands in the Raman effect of methane with appropriate rotational wings and polarizations, the lack of a pure rotational Raman effect, combined with infrared data verify completely the assumption of a tetrahedral structure for the methane molecule.

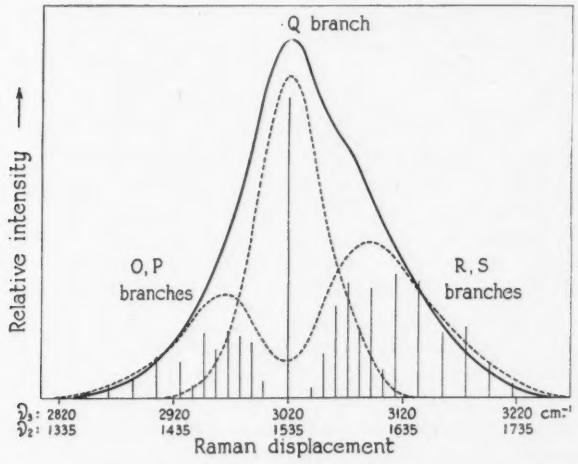

FIG. 8. Intensity distribution in ν_2 and ν_3 Raman bands of liquid methane.

Free Rotation in Liquid Methane

The intensity distributions in the ν_2 and ν_3 bands were determined from several spectrograms and from photoelectric recordings. The distributions obtained by both methods were identical and the same for both bands, and are shown by the continuous curve in Fig. 8. The theoretical intensity distribution (14) expected for freely rotating molecules at the temperature of the liquid is also shown in the figure by the vertical lines. Comparison of the theoretical and observed distributions shows that the extent of the bands is as

great as that for freely rotating molecules. The Q branches are considerably broadened, and the lines of the other branches must also be broadened as no discrete structure is evident in the wings. The absence of maxima in the wings is further evidence of the marked broadening. For these degenerate bands all the intensity of the Q branch as well as that of the rotational wings is due to anisotropic scattering. In the lines for A_1 vibrations (ν_1, etc.) the scattering is entirely isotropic, and these lines remain sharp in the liquid state. Thus for liquid methane, as for liquid oxygen and nitrogen, it is only the anisotropic Raman transitions that are broadened by intermolecular forces.

The dashed curves in Fig. 8 show a division of the observed intensity distribution into the Q branch and the O, P, and R, S branches. This division was made on the assumptions that all lines of the O, P, R, and S branches have their theoretical relative intensities, that all the lines are broadened equally by the intermolecular forces, and that each has a Gaussian distribution of intensity. The division was effected in the following manner: a specific value of the half-width was selected and the intensity contribution, in terms of one arbitrary factor determining the absolute intensity, was computed for each line at intervals of $2B = 10.5$ cm.$^{-1}$ from the theoretical position of the line. The calculated contributions of all the lines were then summed at displacements of $0, \pm 2B, \pm 4B \ldots\ldots \pm 40B$ from the center of the band, taken as the peak of the Q branch. The sums in the regions beyond $\pm 20B$, where the contribution of the Q branch is negligible, were equated to the observed distributions to evaluate the arbitrary factor. Using this value of the factor the envelope of the O, P, R, S branches was plotted, and then subtracted from the observed distribution to obtain the distribution for the Q branch. This procedure was repeated for several half-widths. A half-width of 55 cm.$^{-1}$ gave a fairly unique fit in the wings, and a symmetrical Q branch of only slightly greater half-width, but with an intensity 2.7 times the theoretical value (Fig. 8).

The excess intensity in the Q branch over the theoretical prediction appears at first sight to be large, but is only 24% of the total intensity of the band. The high intensity of the Q branch is probably attributable to the fact that during a small fraction of the time a molecule is in a sufficiently close collision to hinder seriously its rotation and to distort its tetrahedral structure. If one attributes the excess intensity solely to the first factor one concludes that the extent of the hindering of the rotation is equivalent to a molecule being a free rotator during approximately 76% of the time and a nonrotator during the remainder. To be sure, this division of the molecules into free rotators and nonrotators is an oversimplified picture, but it serves to give the order of magnitude of the hindering.

This analysis shows that the observed contour is explicable on the basis of broadened rotational lines, all with half-widths of the order of 55 cm.$^{-1}$ and with relative intensities conforming approximately to those for freely rotating molecules. This conclusion explains the broadness of the infrared bands of liquid methane observed by Holden, Taylor, and Johnston (5).

Solid Methane

Fig. 9 (*b*) shows the Raman spectrum of solid methane, excited by the 4047A group of mercury lines in a 16 cm. column of the solid formed in the vertical Raman tube and recorded photoelectrically. A sharp line corresponding to the totally symmetric vibration, ν_1, at $\Delta\nu = 2906$ cm.$^{-1}$, and a

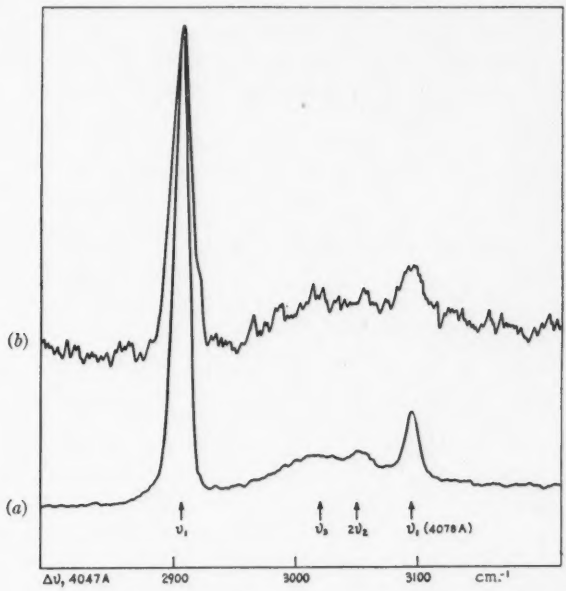

Fig. 9. Raman spectra of methane (photoelectric recording):
(*a*) Liquid, slit widths 10 cm.$^{-1}$
(*b*) Solid, slit widths 15 cm.$^{-1}$

band at least 200 cm.$^{-1}$ wide corresponding to the triply degenerate vibration, ν_3, ($\Delta\nu = 3020$ cm.$^{-1}$ at band center) are clearly evident. The spectrum of the liquid obtained photoelectrically with the Type B tube is shown in Fig. 9 (*a*) with the same output signal strength at ν_1, but with lower gain in the amplifier. The extent of the wings of the ν_3 band is about the same for both liquid and solid, and the ratio of the integrated intensity of ν_3 to that of ν_1 is also the same. Thus the rotation of the molecules in solid methane 12° below its melting point is not appreciably more hindered by intermolecular forces than in the liquid state. Since the molecular rotation is relatively free in both the liquid and the solid state, the order in solid methane crystals just below the melting point must be entirely positional in character. On this interpretation, the infrared bands of solid methane should be very broad, in accordance with recent observations (5).

BROADENING OF RAMAN LINES BY INTERMOLECULAR FORCES

The three substances studied, oxygen, nitrogen, and methane, all have relatively small intermolecular forces in the liquid state (7). The contours of the Raman bands of all of these substances show that there is a marked broadening of the transitions associated with anisotropic scattering, but no detectable broadening of the transitions giving rise to isotropic scattering. The distinction between isotropic and anisotropic scattering must therefore be considered.

In the polarizability theory of Raman scattering (14) the difference between the two types of scattering is associated with the selection rules for J, the rotational quantum number (also the additional quantum number, K, when it is defined), and m, the quantum number specifying the component of J on a spatially fixed direction. Permitted changes in J and m are $0, \pm 1, \pm 2$ independently, depending on the symmetry of the molecule. For isotropic scattering the selection rules are $\Delta J = \Delta m = 0$; for anisotropic scattering one of these quantum numbers must change. If the molecule is unperturbed—not under the influence of an external field—the changes in J determine the positions of the rotational lines (K is not defined for the diatomic and tetrahedral molecules to which this discussion is confined); and for a

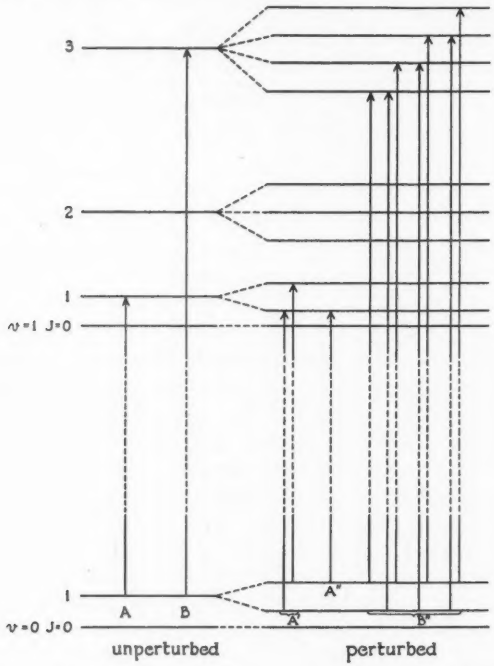

FIG. 10. Rotation-vibrational Raman transitions in unperturbed and perturbed molecules.

given ΔJ, the positions of the lines are independent of Δm. If the m degeneracy is removed by a perturbing field, the positions of the rotational lines will depend on Δm as well as on ΔJ. In the liquid state, each molecule moves in the intermolecular force field of its nearest neighbors. If we assume that the energy of this motion depends on the value of m, the frequencies of the Raman transitions involving changes of J or m will be altered. In the close packing of the liquid state, the force field will be approximately spherically symmetrical and thus m will remain well defined, in contrast to the case of a simple two-body collision.

Fig. 10 illustrates qualitatively the removal of the m degeneracy and the effect on the frequencies of the Raman transitions given by the selection rules of the preceding paragraph. At the left are the rotational energy levels associated with the $v = 0$ and $v = 1$ vibrational energy levels in the field-free state, and at the right are the $J + 1$ sublevels into which each is split (removal of the $\pm m$ degeneracy is not assumed). For simplicity the splitting is shown in Fig. 10 as symmetrical and independent of J and v, but these assumptions are not all necessary. Only the assumption that the displacement of a perturbed level with a given J and m from its unperturbed position is independent of v is essential, and it is justifiable as long as there is no strong coupling of the rotational and vibrational motions. A and B are typical field-free transitions producing respectively lines of the Q and S branches of a fundamental Raman band. A', A'', and B'' are corresponding transitions between m levels when a perturbing field is present. The transitions A' produce isotropic Raman scattering in the Q branch; for these m does not change, and the Raman lines for the transitions A' have the same frequency as for the field-free transition A. The transition A'' produces anisotropic Raman scattering in the Q branch; since m must change, the corresponding Raman line will not have the same frequency as that for the field-free transition A. The transitions B'' all produce anisotropic Raman scattering in a line of the S branch; obviously all of these transitions may, and most of them must, produce Raman lines of frequencies different from that of the field-free transition B.

The magnitude of the splitting of the m levels will have a statistical distribution corresponding to the statistical distribution of the magnitude of the intermolecular force field, which is sharply dependent on the fluctuations (of long period relative to the mean life for Raman transitions) in the distances of nearest neighbors. Therefore the Raman lines for which J or m change (anisotropic scattering) will in the aggregate scattering appear broadened; but those for which J and m do not change (isotropic scattering) should be sharp. Thus the postulate that the m degeneracy is removed by the intermolecular force field explains the experimental results.

It is possible that the splittings of each of the first few rotational levels may be greater than their unperturbed separations, so that J may not be a good quantum number for these. However, the separation of successive rotational levels increases linearly with J, and thus J should retain its significance for the higher and more widely spaced levels; that is, the molecular rotation is

essentially free when the energy is above a certain minimum. All similar substances composed of simple molecules with relatively low interaction energies should likewise possess considerable freedom of molecular rotation in the liquid state, and in some cases, where the symmetry of the molecules is sufficiently high, even in the solid state.

REFERENCES

1. BHAGAVANTAM, S. Nature, 129: 830. 1932.
2. BHAGAVANTAM, S. and RAO, A. V. Phys. Rev. 47: 921. 1935.
3. CABANNES, J. and ROUSSET, A. Compt. rend. 206: 185. 1938.
4. DICKENSON, R. G., DILLON, R. T., and RASETTI, F. Phys. Rev. 34: 583. 1929.
5. HOLDEN, R. B., TAYLOR, W. J., and JOHNSTON, H. L. J. Chem. Phys. 17: 1356. 1949.
6. LEWIS, G. N. J. Am. Chem. Soc. 46: 2027. 1924.
7. LONDON, F. Z. phys. Chem. 11: 222. 1930.
8. MCLENNAN, J. C. and MCLEOD, J. H. Nature, 123: 160. 1929.
9. MCLENNAN, J. C., SMITH, H. D., and WILHELM, J. Trans. Roy. Soc. Can. III, 23: 279. 1929.
10. MACNAUGHTON, E. B. Ph.D. Thesis, University of Toronto. 1948.
11. MAGAT, M. Ann. phys. 6: 108. 1936.
12. MILLER, C. E. J. Chem. Phys. 6: 902. 1938.
13. PAULING, L. Phys. Rev. 36: 430. 1930.
14. PLACZEK, G. and TELLER, E. Z. Physik. 81: 209. 1933.
15. RANK, D. H., SHULL, E. R., and AXFORD, D. W. E. J. Chem. Phys. 18: 116. 1950.
16. SAHA, B. Indian J. Phys. 14: 123. 1940.
17. THOMAS, J. T., ALPERT, N. L., and TORREY, H. C. J. Chem. Phys. 18: 1511. 1950.
18. TRUMPY, B. Z. Physik. 84: 282. 1933.
19. VOLKRINGER, H., FREYMANN, M., and FREYMANN, R. Compt. rend. 208: 1005. 1939.
20. WELSH, H. L., CRAWFORD, M. F., and Scott, G. D. J. Chem. Phys. 16: 97. 1948.

DENSITY EFFECTS IN THE RAMAN SPECTRUM OF CARBON DIOXIDE[1]

By H. L. Welsh, P. E. Pashler,[2] and B. P. Stoicheff[3]

ABSTRACT

Two Raman tubes, one of quartz and one of glass, capable of withstanding pressures up to 75 and 300 atm. respectively, were used to study density effects in the Raman spectrum of carbon dioxide. The components of the ν_1 band show changes in frequency and relative intensity with increasing density. An analysis shows that the frequency changes are due to a lowering of the frequency of $2\nu_2$, in Fermi resonance with ν_1, with increasing density. The intensity effect, however, is not completely explained by the change in the sharpness of the resonance. In the high pressure gas and in the liquid faint bands corresponding to the Raman inactive frequencies, ν_2 and ν_3, are observed. The effect of increasing density on the rotational Raman spectrum can be explained in terms of the broadening of anisotropic scattering by intermolecular forces.

INTRODUCTION

Raman and infrared spectra can be used to study the forces between molecules in their ground electronic state. Investigations on compressed gases are especially useful; changes in the spectrum can be related to the gas density which is continuously variable from low values, where the molecules are essentially free, to values approaching liquid density. Recent experiments on the infrared absorption of compressed gases have yielded new information. For example, it has been found that vibrations which are normally inactive in infrared absorption are rendered active by the distortion of the electron distribution of the molecules during close collisions (6, 24, 7, 25). It has also been shown that the absorption due to infrared active vibrations is enhanced when the absorbing molecule is surrounded by polarizable foreign gas molecules at high densities (26). It is evident that additional information can be gained by experiments on the Raman scattering from high pressure gases. Since the origin of Raman scattering in the polarizability of the molecule is fundamentally different from the origin of infrared absorption, new aspects of the problem of intermolecular forces can be studied.

There have been few investigations on the Raman effect of gases at high pressures. Bhagavantam (2) and Trumpy (22) studied the pressure broadening of the rotational Raman lines of some nonpolar molecules up to 60 atm. Weiler (23) showed that the shape of the rotational Raman band of carbon dioxide undergoes significant changes in the pressure range up to 60 atm. Recently, the effect of increasing density on the Raman spectrum of water vapor up to and beyond the critical point has been investigated by Andrychuk (1).

[1] *Manuscript received November 23, 1951.*
Contribution from the McLennan Laboratory, University of Toronto, Toronto, Ont.
[2] *Present address: General Electric Research Laboratory, The Knolls, Schenectady, N.Y.*
[3] *Holder of a scholarship under the Research Council of Ontario, 1948-49, a Garnet W. McKee scholarship, School of Graduate Studies, University of Toronto, 1949-50, a Garnet W. McKee – Lachlan Gilchrist Postdoctorate Scholarship, 1950-51. Present address: Division of Physics, National Research Council Laboratories, Ottawa, Canada.*

In this paper the construction of Raman tubes for high pressures is discussed, and density effects in the vibrational and rotational Raman spectra of carbon dioxide are described.

RAMAN TUBES FOR COMPRESSED GASES

The designing of Raman tubes for high pressure is complicated by the large window area required for intense irradiation of the scattering medium. Sealed-off capillary tubes of fused quartz have been used up to pressures of 400 atm. for the Raman effect of water (8) and water vapor (1). This method, however, is not easily adapted to substances with low boiling points. The construction of a more generally useful Raman tube for high pressures was therefore undertaken. Descriptions of two tubes are given below; the first of these has been used up to 300 atm., the second up to 75 atm.

Raman Tube for High Pressures

The design of this tube, shown in Fig. 1, was suggested by the construction of transparent liquid-level gauges. The gas chamber is a slot, 9 in. × 1 in. ×

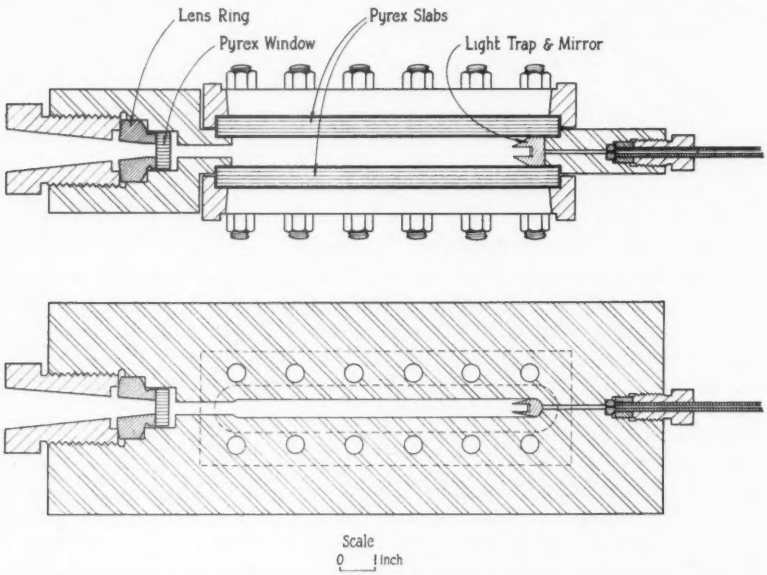

FIG. 1. Raman tube for high pressures: (*a*) horizontal section, (*b*) vertical section.

½ in., machined in a block of high-strength alloy steel, and is closed by slabs of armor plate Pyrex glass, 11/16 in. thick. Slotted steel plates, bolted to the body of the tube, press the windows against lead gaskets to give a high pressure seal. The exit window for the scattered radiation is a Pyrex disk, 1 in. in diameter and ½ in. thick, sealed with an optical cement to a hardened steel "lens-ring", the surfaces in contact being optically flat. The high pressure seal is effected by forcing the lens ring against a shoulder in the body of the

tube by means of a heavy screw. The gas is introduced through a steel capillary attached to the tube by a lens-ring seal. A mirror, placed at the back of the gas chamber and shielded from the irradiating lamps, effectively doubles the length of the tube.

In preliminary experiments it was observed that the cone of observation was distorted by density fluctuations in the compressed gas. The necessary temperature control was obtained by circulating water from a thermostated reservoir through a system of rectangular copper tubes in contact with the Raman tube. To prevent heating by the mercury lamps, the tube was also surrounded by a polished steel box with water-cooled cells as windows.

The required gas pressures were obtained in two ways. In the first method a gas compressor with mercury as the transmitting fluid was used in conjunction with an oil pump capable of generating pressures up to 400 atm. In the second method, a thermal compressor, a thick-walled stainless steel flask, was filled with the substance at liquid air temperature, and the desired pressure obtained by raising the temperature of the flask.

Two mercury lamps with water-cooled electrode pools, operated on 110 v. at a current of 15 amp., were used for irradiation, one lamp on each side of the Raman tube. The lamps, made of Pyrex glass tubing, 1 in. in diameter and 3 ft. long, had the form of a flattened **S** to give maximum illumination of the gas chamber.

The spectrograph used with this Raman tube is a two-prism instrument with an $f/4$ camera lens, giving a reciprocal linear dispersion of 225 cm.$^{-1}$ per mm. at 4358A. A condensing lens was used to focus the exit window of the Raman tube on the collimator lens and the mirror image of the exit window on the slit of the spectrograph.

In practice it was found that a Raman tube of this design has several unsatisfactory features. The tube under pressure is potentially dangerous and safety precautions are imperative. To prevent the development of leaks because of the flow of the lead gaskets, frequent tightening of the bolts holding the windows is necessary. It is difficult to clean the tube well enough to eliminate fluorescence caused by traces of impurities dissolved in the compressed gas. Raman radiation from the thick windows, scattered as Rayleigh light by the substance under study, produces a banded continuum which can obscure faint Raman bands. The irradiation of the gas chamber is not cylindrically symmetrical; thus the theoretical interpretation of intensity ratios of Raman lines with different degrees of depolarization is uncertain. It was impossible to use ultraviolet excitation because fused quartz slabs as windows were found to break when the bolts were tightened to form the high pressure seal.

Raman Tube for Medium Pressures

This tube, designed for use in the ultraviolet, consists of three sections, each 20 cm. long, held together by four rods connecting the stainless steel end sections (Fig. 2). The middle section is a tube of fused quartz, 1 cm. in internal diameter, with a wall thickness of 4 mm. The front section carries the exit

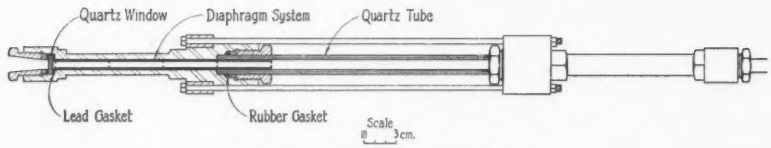

FIG. 2. Raman tube for medium pressures.

window of fused quartz, 5 mm. thick, and a system of bakelite diaphragms. The rear section is connected to the high pressure line and carries an insert of black bakelite, set with its front surface at 45° to the axis of the tube, to give a black background for photographing the scattered light. The pressure seals are made by the deformation of lead or rubber gaskets with heavy retaining screws. A water-jacket made of fused quartz and brass tubing envelops the Raman tube. Two helical mercury lamps of fused quartz with water-cooled mercury pools are used for irradiation (21).

The quartz spectrograph used with this tube is a two-prism instrument of the Littrow type (21), with a reciprocal linear dispersion of 27 cm.$^{-1}$ per mm. at 2537A. A quartz condensing lens is used to focus the front window of the Raman tube on the collimator lens, and the rear diaphragm of the front section on the slit of the spectrograph.

Intensity calibration of the photographic plates was obtained by replacing the spectrograph slit with a stepped slit and photographing the continuous spectrum of a tungsten band lamp or a low-voltage hydrogen arc for work in the visible or ultraviolet, respectively. The spectrum of an iron arc, in juxtaposition with the Raman spectrum, was used for frequency calibration. All the spectra were photographed on Eastman 103*a*-O Spectroscopic plates.

DENSITY EFFECTS IN THE VIBRATIONAL RAMAN SPECTRUM OF CARBON DIOXIDE

Since the free carbon dioxide molecule is linear and symmetric, the totally symmetric frequency ν_1 is active only in Raman effect, whereas the doubly degenerate frequency ν_2 and the antisymmetric frequency ν_3 are active only in infrared absorption. The ν_1 Raman band consists of two intense lines, each accompanied by a faint satellite (11, 16). The strong doublet is due to the transition $(1\ 0^0\ 0)\ (0\ 2^0\ 0) \longleftarrow\!\!\!- (0\ 0^0\ 0)$*, the upper states being in Fermi resonance. The satellite lines correspond to the transition $(1\ 1^1 0)\ (0\ 3^1 0) \longleftarrow\!\!\!- (0\ 1^1\ 0)$; here the separation of the perturbed states is somewhat greater than for the main doublet. For convenience, the Raman shift at 1387.6 cm.$^{-1}$ is referred to as ν_1 and that at 1285.0 cm.$^{-1}$ as $2\ \nu_2$, although this designation is not strictly correct in view of the resonance degeneracy; the satellites are designated as ν_1' and $2\ \nu_2'$.

The ν_1 Band

The frequencies of the ν_1 group of lines were measured for the gas at low and high densities and for the liquid. The most accurate determinations were

* *The vibrational state is designated by the quantum numbers* $(v_1\ v_2{}^l\ v_3)$.

those made for the low pressure gas and the liquid with the medium pressure Raman tube and the high dispersion quartz spectrograph. The spectrum of the gas at 15 atm. and 25° C. was photographed in 12 hr., and that of the liquid at 66 atm. and 25° C. in three hours, with a spectral slit width of 1 cm.$^{-1}$ The half-widths of the lines were approximately 3 cm.$^{-1}$ for both the low pressure gas and the liquid. No rotational wings on the main lines were observed for the gas; however, on heavily exposed spectrograms of the liquid a characteristic intensity distribution, similar to that observed in the rotational Raman effect (see below), was evident, as shown in Fig. 3.

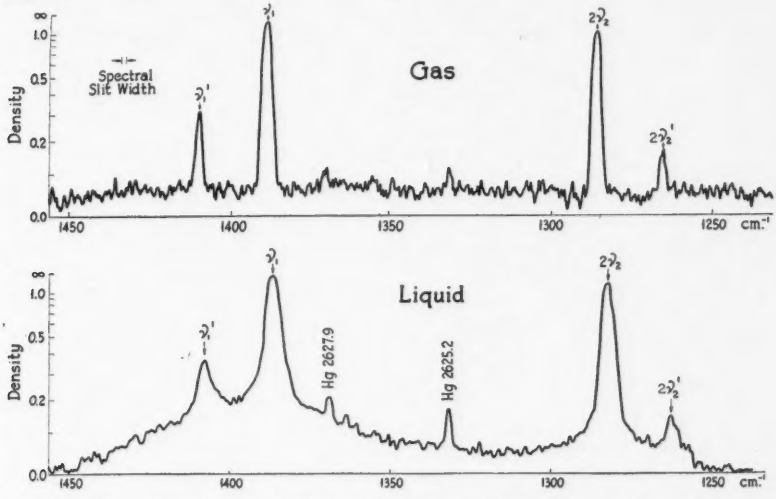

FIG. 3. Microphotometer traces of the ν_1 Raman band of carbon dioxide: (*a*) gas at 15 atm., (*b*) liquid.

The frequencies obtained with ultraviolet excitation, given in Table I, are probably accurate to within 0.2 cm.$^{-1}$ The frequencies for the liquid are all

TABLE I

FREQUENCIES IN THE ν_1 BAND OF CARBON DIOXIDE

Experimental conditions	ν_1, cm.$^{-1}$	$2\nu_2$, cm.$^{-1}$	ν_1', cm.$^{-1}$	$2\nu_2'$, cm.$^{-1}$
Gas (15 atm., 25° C.)	1387.6	1285.0	1408.9	1264.7
Liquid (66 atm., 25° C.)	1386.0	1281.7	1407.8	1262.0

somewhat lower than for the gas, but the change in frequency is not the same for all the lines. The frequencies measured for the gas agree almost exactly with those of Dickinson, Dillon, and Rasetti (11), but are somewhat less than those of Langseth and Nielsen (16). Six additional lines noted by Langseth

and Nielsen in the region $\Delta\nu = 1200$ to 1500 cm.$^{-1}$ were not observed even with very long exposures.

The measured frequencies permit an analysis of the Fermi degeneracy in both the gas and the liquid. According to the theory of Placzek (19), the separations of the main components and of the satellites are $X_1 = \sqrt{\delta^2 + 4W^2}$ and $X_2 = \sqrt{\delta^2 + 8W^2}$, respectively. In these expressions δ is the separation of the unperturbed levels, and $W = W_{100,02^00}$ is the matrix element of the cubic term in the potential energy which gives rise to the perturbation. The values of δ and W can be obtained from the experimental values of X_1 and X_2. Also, since the sum of the unperturbed levels is the same as the sum of the perturbed levels, the unperturbed values of ν_1 and $2\nu_2$ can be calculated. The results are given in Table II.

TABLE II

DERIVED CONSTANTS FOR THE ν_1 BAND OF CARBON DIOXIDE

Constant	Low pressure gas	Liquid
δ	16.1 cm.$^{-1}$	22.3 cm.$^{-1}$
$W_{100,020}$	50.7 "	50.9 "
ν_1 (unperturbed)	1344.4 "	1345.0 "
$2\nu_2$ (unperturbed)	1328.3 "	1322.7 "

The values of δ and W obtained from the Raman spectrum of the low pressure gas agree very well with the values, 16.7 cm.$^{-1}$ and 50.4 cm.$^{-1}$, respectively, calculated by Dennison (10) using infrared absorption data. The value of W is nearly the same in the low pressure gas and in the liquid, showing that there is little change in this cubic term of the potential energy with increasing density. The unperturbed frequency ν_1 remains practically constant with increasing density, but the unperturbed frequency $2\nu_2$ shifts to a definitely lower value. Thus the alteration in frequency in the whole group of lines is due almost entirely to a lowering of $2\nu_2$ with increasing density. The observed change of 5.6 cm.$^{-1}$ in $2\nu_2$ corresponds to a change of about 1% in the potential energy constant for the doubly degenerate vibration. It might be noted that Dahlke (9) found a decrease of 11 cm.$^{-1}$ in the infrared frequency ν_2 in solid carbon dioxide.

Spectrograms of the high pressure gas could be obtained only with the high pressure Raman tube and excitation by Hg4358; the accuracy of frequency measurements was therefore limited by the small dispersion of the glass spectrograph. However, it was established that the frequencies in the ν_1 band for the gas at a density of 430 Amagat units (220 atm. at 40° C.) were identical within the error of measurement with those for the liquid at a density of 500 Amagat units.

The relative intensities in the ν_1 band were measured for the low and high pressure gas and for the liquid, with both visible and ultraviolet excitation. The results for the high pressure gas and the liquid in the visible region were

obtained with the high pressure Raman tube with exposure times ranging from 5 to 60 min. For the low pressure gas in the visible region, a Pyrex tube, 120 cm. long, suitably diaphragmed and symmetrically illuminated over 60 cm. of its length, was used. The results are summarized in Table III,

TABLE III

RELATIVE INTENSITIES IN THE ν_1 BAND OF CARBON DIOXIDE

Experimental conditions	Density (Amagat units)	Exciting line	I_{ν_1}	$I_{2\nu_2}$	I_{ν_3}	$I_{2\nu_2}$
Gas (15 atm., 25° C.)	15	Hg2537	1.0	0.54	0.064	0.023
Gas (6 atm., −−) (13)	(6)*	"	1.0	0.57	....	....
Liquid (66 atm., 25°C.)	360	"	1.0	0.40	0.047	0.020
Gas (3 atm., 20° C.)	2	Hg4358	1.0	0.72	....	....
Gas (15 atm., −−) (17)	(15)	"	1.0	0.61	....	....
Gas (220 atm., 40° C.)	430	"	1.0	0.61	....	....
Liquid (55 atm., 1° C.)	(500)	"	1.0	0.55	....	....

**Values of density in brackets are approximate only.*

along with earlier measurements by Hanson (13) and Langseth and Nielsen (17).

The intensity ratio, $I_{2\nu_2}/I_{\nu_1} = 0.54$, obtained with ultraviolet excitation in the low pressure gas shows fair agreement with the value, 0.57, of Hanson. In the liquid this ratio is 26% lower. The same relative change in the ratio between the low pressure gas and the liquid is also found with visible excitation. However, the values of the ratios in the visible region are consistently higher than those in the ultraviolet. No satisfactory explanation of this discrepancy in the measurements can be given. In all cases the values quoted for $I_{2\nu_2}/I_{\nu_1}$ were confirmed from several spectrograms. The different spectral slit widths used, 1 cm.$^{-1}$ in the ultraviolet and 10 cm.$^{-1}$ in the visible, should not cause a difference in the intensity measurements.

According to the theory of resonance degeneracy the ratio of the intensities of the main components is given by:

$$\frac{I_{2\nu_2}}{I_{\nu_1}} = \left\{\frac{\sqrt{X_1 - \delta}\, a_1 - \sqrt{X_1 + \delta}\, a_2}{\sqrt{X_1 + \delta}\, a_1 + \sqrt{X_1 - \delta}\, a_2}\right\}^2,$$

where a_1 and a_2 are the matrix elements of the polarizability for the transitions $(1\ 0^0\ 0) \longleftarrow (0\ 0^0\ 0)$ and $(0\ 2^0\ 0) \longleftarrow (0\ 0^0\ 0)$, respectively. From the observed value of $I_{2\nu_2}/I_{\nu_1}$, the ratio a_1/a_2 can be calculated since the values of X_1 and δ are known from the frequency analysis. The intensity ratio measured for the low pressure gas in the ultraviolet gives $a_1/a_2 = 14.1$, which can now be used with the appropriate value of X_1 to calculate $I_{2\nu_2}/I_{\nu_1}$ for the liquid. The calculated ratio is 0.48 as compared with the measured ratio, 0.40. Thus, the change in the sharpness of the resonance in going to the liquid is not sufficient to explain the change in the intensity ratio. It therefore appears that a_1/a_2 is also dependent on the density; using $I_{2\nu_2}/I_{\nu_1} = 0.40$, the calculated value of a_1/a_2 for the liquid is 8.9. When the intensity ratio obtained for the low pressure gas in the visible is used, it is found that a_2 is negligibly small

compared with a_1; this does not seem a very probable result. However, a considerable decrease in a_1/a_2 with increasing density is again indicated.

The ν_2 and ν_3 Bands

In long exposures with the high pressure gas and the liquid two additional bands were observed at 4490A and 4853A. Because of their extremely low intensities, subsidiary experiments were necessary to establish unequivocally their origin in carbon dioxide. It was found that the bands were not present in the spectrum of the irradiating lamps, and also that they were not due to secondary scattering from the thick Pyrex windows of the high pressure tube. The use of a Noviol-*A* glass filter showed that the exciting line was Hg4358; the measured frequency shifts of the centers of the bands were 670 ± 10 and 2340 ± 20 cm.$^{-1}$. The bands can therefore be assigned to the Raman inactive frequencies ν_2 and ν_3, respectively, since the infrared frequencies observed in gaseous carbon dioxide are 667.3 and 2349.3 cm.$^{-1}$ (10). A strongly overexposed spectrogram of the low pressure gas gave no evidence of the new bands.

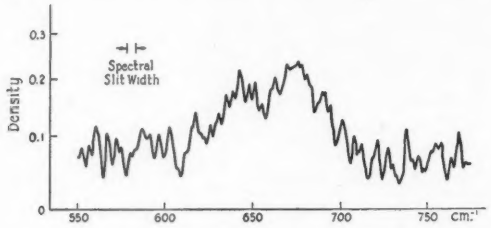

FIG. 4. Microphotometer trace of the ν_2 Raman band of liquid carbon dioxide.

The ν_2 band, a microphotometer trace of which is shown in Fig. 4, has a double maximum. The fainter ν_3 band is narrow, indicating a strong Q branch with rotational wings of low intensity. These characteristics of the observed bands can be used to deduce the general nature of the molecular distortion which gives rise to the forbidden transitions. In the linear unsymmetric molecule (point group $C_{\infty v}$), ν_2 has the species π, and ν_3 the species σ^+. According to Placzek and Teller (20) the Raman band corresponding to the π vibration has a weak Q branch, and hence the two maxima in the wings are the outstanding features of the contour; the band corresponding to the σ^+ vibration has a Q branch and weak rotational wings. The appearance of the forbidden bands is therefore probably caused by a lengthwise distortion of the molecule, since other possible models do not reproduce the observed characteristics. The distortion of the molecule can be due to collisions, as in induced infrared absorption, or, more probably, to the formation of dimers. Because of the weakness of the bands and the strong continuum which appears in long exposures, it has not yet been possible to find out how the intensity of the forbidden bands varies with the density of the gas.

EFFECT OF INCREASING DENSITY ON THE ROTATIONAL RAMAN SPECTRUM OF CARBON DIOXIDE

The intensity distribution in rotational and rotation-vibrational Raman bands of gases at low density is characteristic of freely rotating molecules; with increasing distance from the center of the band the intensity in each wing rises to a maximum and then decreases slowly. In some liquefied gases with low boiling points, such as hydrogen (18), nitrogen, oxygen, and methane (5), this contour is more or less preserved, indicating that molecular rotation remains practically unhindered. In most liquids, however, no maxima are observed in the wings, and the intensity decreases rapidly with increasing distance from the center of the band. The origin of this anomalous intensity distribution has been discussed in terms of hindered rotation (3), formation of molecular complexes (4), quasicrystalline structure (12), and collision broadening (2).

Weiler (23) investigated the changes in the rotational spectrum of gaseous carbon dioxide up to pressures of 60 atm. as a function of density. He found a considerable departure from the theoretical intensity contour even at these relatively low pressures, but he was unable to offer a plausible explanation of the effect. Bhagavantam and Rao (4) also studied this problem but in less detail. These experiments were inadequate in one respect; since the spectro-

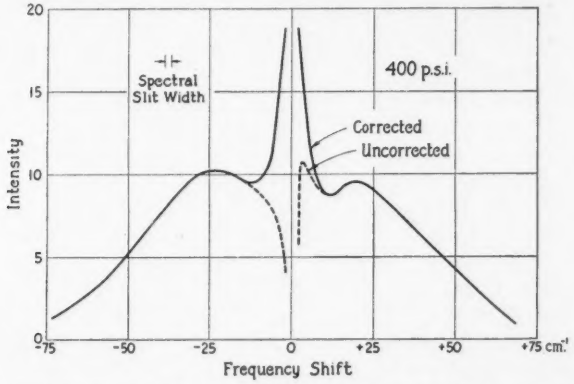

FIG. 5. Intensity contour of the rotational Raman spectrum of gaseous carbon dioxide, showing the correction for the absorption of the exciting radiation, 2537A, by mercury vapor in the spectrograph.

grams were obtained with Hg4046 excitation and at comparatively low dispersion, the strong Rayleigh line interfered with the intensity measurements in the rotation band, especially at small frequency shifts.

In view of the limitations of the previous work, rotational Raman spectra of gaseous and liquid carbon dioxide were obtained using Hg2537 excitation and the high dispersion quartz spectrograph with a spectral slit width of 2 cm.$^{-1}$ The medium pressure tube was used with the gas in the pressure range 200–700 p.s.i. at 25° C. and the liquid at 1000 p.s.i. and 25° C. Mercury

vapor was introduced into the spectrograph to reduce the intensity of the Rayleigh line. Since the absorption line of the vapor was broadened by the atmospheric pressure it was necessary to apply a correction to the intensity contour of the Raman spectrum in the region of small frequency shifts. The percentage transmission of the vapor in the neighborhood of 2537A was therefore measured using the continuous spectrum of a hydrogen arc. The broadening of the line is asymmetric, the absorption extending to about 15 cm.$^{-1}$ on the low-frequency side and 10 cm.$^{-1}$ on the high-frequency side. Corrections for this effect were applied, as in Fig. 5, to all the Raman spectra; at frequency shifts less than 3 cm.$^{-1}$, the absorption was so great that no satisfactory correction could be made.

The corrected contours for a series of gas densities, reproduced in Fig. 6, were adjusted to fit the Stokes side of the theoretical intensity curve at a

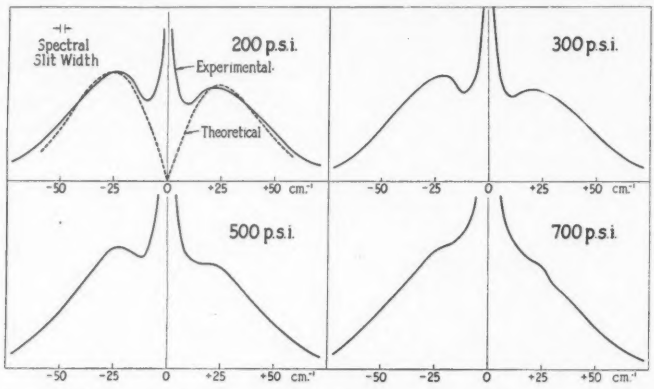

FIG. 6. Intensity contours of the rotational Raman spectrum of carbon dioxide at various gas pressures.

frequency shift of 40 cm.$^{-1}$ In all cases the ratio of anti-Stokes to Stokes intensity approximates the theoretical value, thus indicating that vignetting in the spectrograph had only a small effect on the intensity measurements over the wave length region of the pattern. The maxima, evident in the rotational wings of all the contours, show some displacement towards the center of the band with increasing density. Most outstanding, however, is the rise in intensity at small frequency shifts, which becomes more pronounced as the density increases. This feature was obscured to a great extent in Weiler's work since it occurs so close to the exciting line.

An adequate explanation of the intensity distribution in the curves of Fig. 6 can be given in terms of the pressure broadening of the Raman and Rayleigh lines. It is well known that the isotropic or polarized part of the Rayleigh scattering is contained in the unshifted line, and that the anisotropic or depolarized part gives rise to the rotational Raman effect and also to a depolarized component in the unshifted line (Q branch). For a linear symmetric

molecule such as carbon dioxide one-quarter of the total anisotropic scattering is contained in the Q branch (20). In recent experiments on the Raman effect in liquefied gases it was found that Raman lines corresponding to isotropic scattering are sharp in the liquid, whereas lines corresponding to anisotropic scattering are broad (5). This means that pressure broadening is very small for isotropic scattering and large for anisotropic scattering. This conclusion is confirmed by experiments on the pressure broadening of the Raman lines of compressed gases. It therefore appears that the observed changes in the rotational Raman effect of carbon dioxide can be explained by the broadening of the anisotropic Rayleigh scattering with increasing density. The increased intensity at small frequency shifts is the broadened Q branch of the anisotropic scattering. This component overlaps the rotational wings and causes an *apparent* shift of the maxima towards the center of the pattern with increasing density.

It should be noted that the above explanation was not overlooked by Weiler, but was rejected by him on both experimental and theoretical grounds. Kappler and Weiler (15) were unable to detect any broadening of either the isotropic or anisotropic parts of the Q branch; however, their conclusion concerning the anisotropic scattering is probably vitiated by convergence errors in their experimental arrangement. Kappler (14) attempted to show theoretically by classical concepts that, although the rotational Raman lines can be broadened by collisions, neither the isotropic nor the anisotropic part of the Rayleigh scattering can be broadened. However, Crawford, Welsh, and Harrold (5) have shown by arguments based on quantum principles that the intermolecular fields in substances at high density can broaden all anisotropic scattering.

The intensity distribution for liquid carbon dioxide at 25° C. and 360 Amagat units of density is shown in Fig. 7, along with the contour for the gas at 70 Amagat units. The intensity scales are not the same for the two curves

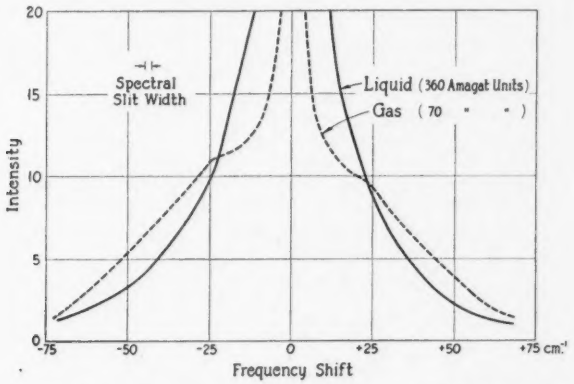

FIG. 7. Comparison of the intensity contours of the rotational Raman spectra of gaseous and liquid carbon dioxide.

so that only the shapes can be compared. The characteristic appearance of the rotational wings has disappeared entirely in the liquid, and all the anisotropic intensity seems to be concentrated in a greatly broadened Q branch. This distribution of intensity might be expected if all molecular rotation ceases in the liquid state. However, it is unwise to assume that the contour can be explained by hindering of rotation and line broadening alone, since other factors, such as the formation of molecular complexes, can be involved. It is unfortunate that gas densities of the order of 400 Amagat units cannot be reached with the present quartz Raman tube, since an accurate intensity investigation of the rotational contours over a wide range of densities could contribute much to the elucidation of the problem.

ACKNOWLEDGMENTS

The work in high pressures at Toronto has been made possible by the generous support of the National Research Council of Canada. The authors are also greatly indebted to Prof. A. Michels of the Van der Waals Laboratory, University of Amsterdam, for his continued interest and advice.

REFERENCES

1. ANDRYCHUK, D. Ph.D. Thesis, University of Toronto. 1948.
2. BHAGAVANTAM, S. Indian J. Phys. 6: 319. 1931.
3. BHAGAVANTAM, S. Proc. Indian Acad. Sci., A, 2: 63. 1935.
4. BHAGAVANTAM, S. and RAO, A. V. Proc. Indian Acad. Sci., A, 1: 419. 1935.
5. CRAWFORD, M. F., WELSH, H. L., and HARROLD, J. H. Can. J. Phys. 30: 81. 1952.
6. CRAWFORD, M. F., WELSH, H. L., and LOCKE, J. L. Phys. Rev. 75: 1607. 1949.
7. CRAWFORD, M. F., WELSH, H. L., MACDONALD, J. C. F., and LOCKE, J. L. Phys. Rev. 80: 469. 1950.
8. CROSS, P. C., BURNHAM, J., and LEIGHTON, P. A. J. Am. Chem. Soc. 59: 1134. 1937.
9. DAHLKE, W. Z. Physik, 102: 360. 1936.
10. DENNISON, D. M. Revs. Modern Phys. 12: 175. 1940.
11. DICKINSON, R. G., DILLON, R. T., and RASETTI, F. Phys. Rev. 34: 582. 1929.
12. GROSS, E. and VUKS, M. Nature, 135: 100, 431. 1935.
13. HANSON, I. Phys. Rev. 46: 122. 1934.
14. KAPPLER, E. Ann. Physik, 5: 272. 1936.
15. KAPPLER, E. and WEILER, J. Ann. Physik, 5: 279. 1936.
16. LANGSETH, A. and NIELSEN, J. R. Z. physik Chem., B, 19: 427. 1932.
17. LANGSETH, A. and NIELSEN, J. R. Phys. Rev. 46: 1057. 1934.
18. MCLENNAN, J. C. and MCLEOD, J. H. Nature, 123: 160. 1929.
19. PLACZEK, G. Marx, Handbuch der Radiologie. Vol. 6 (2) Akademische Verlagsgesellschaft m.b.H., Leipzig. 1934. p. 205.
20. PLACZEK, G. and TELLER, E. Z. Physik, 81: 209. 1933.
21. STOICHEFF, B. P., CUMMING, C., ST. JOHN, G. E., and WELSH, H. L. J. Chem. Phys. In press. 1951.
22. TRUMPY, B. Z. Physik, 84: 282. 1933.
23. WEILER, J. Ann. Physik, 23: 493. 1935.
24. WELSH, H. L., CRAWFORD, M. F., and LOCKE, J. L. Phys. Rev. 76: 580. 1949.
25. WELSH, H. L., CRAWFORD, M. F., MACDONALD, J. C. F., and CHISHOLM, D. A. Phys. Rev. 83: 1264. 1951.
26. WELSH, H. L., PASHLER, P. E., and DUNN, A. F. J. Chem. Phys. 19: 340. 1951.

RADIOACTIVE DEPOSITS FOUND AT OTTAWA AFTER THE ATOMIC EXPLOSIONS OF JANUARY AND FEBRUARY 1951[1]

By D. C. Rose and J. Katzman

ABSTRACT

Gamma-ray counter equipment, in continuous operation at Ottawa, Canada, indicated that considerable radioactive matter fell on January 29 and again on February 7. The decay period of this material was measured and is consistent with the assumption that the material consisted mainly of products of fission. The fall on January 29 came from an explosion on January 27 and the February 7 material appeared to be three to five days old. The quantity can be estimated only very roughly and is thought to be of the order of one microgram radium equivalent per square meter.

I. OBSERVATIONS ON THE FALL OF RADIOACTIVE DUST

At the time of the atomic explosions in Nevada during the latter part of January and first part of February 1951 continuous recordings of cosmic ray intensity were being taken with various arrangements of Geiger–Mueller counters, singly and in coincidence. The objective of the experimental arrangement was to maintain a continuous watch for sudden increases associated with solar phenomena (2) and at the same time carry out some experiments on the meson spectrum.

At approximately 1000 G.M.T. on Monday, January 29, the intensity in lightly shielded counters (less than 8 gm. per cm.^{2} of low atomic weight material) started to increase rapidly. Within two hours the counting rate was 45% above background and the decay rate was sufficiently long that it precluded the possibility of this being due to the radioactivity normally brought down by rain or snow. Very light snow was falling at the time though it seemed uncertain whether this had any connection with the deposit of radioactive material.

Preliminary tests were made which showed that the radioactive matter was a dust rather than a gas and that it was distributed over the snow cover in the neighborhood of Ottawa. The substance was also shown to be beta and gamma active (1). Lacking evidence to the contrary it is assumed that this radioactive material came from the atomic explosions in Nevada which were announced in the press a day or two before.

The arrangement of apparatus is shown in Fig. 1. The counters were arranged in a small penthouse, about 5 ft. square and 6 ft. high, on the roof of the cosmic ray observatory at the Montreal Road Laboratory of the National Research Council of Canada. The top counter tray was about 50 cm. from the outer surface of the roof of the penthouse. Fig. 2 (upper curve) shows the increase and its decay plotted as a percentage of the background for two hours before it started. The rate did not return to normal until five days later.

[1] *Manuscript received October 15, 1951.*
Contribution from the Division of Physics, National Research Laboratories, Ottawa, Canada. Issued as N.R.C. 2663.

A second fall of radioactive material similar to this occurred on February 7. At about 0800 G.M.T. the intensity started to increase rapidly, rising to 35% above the background in about four hours. This increase and its decay over

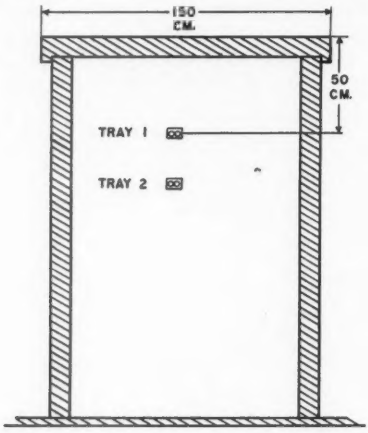

FIG. 1. Arrangement of counter trays under the roof of the penthouse.

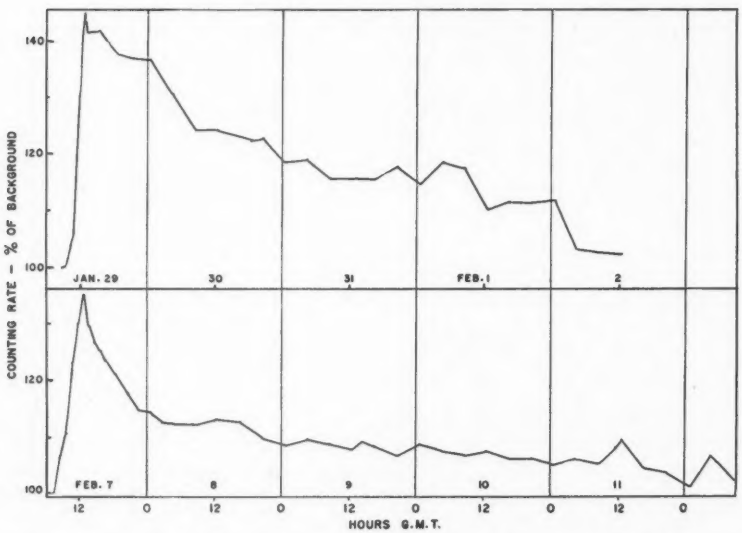

FIG. 2. The increase and decay in the counting rate of Tray 1 on January 29 and February 7.

six days is shown in the lower curve in Fig. 2. Snow was falling lightly during the early morning of February 7, changing to rain and stopping about noon local time (1700 G.M.T.).

The decline in intensity shown by the curves in Fig. 2 does not represent the true decay rates. This is partly because the weathering of the snow on the roof over the counters may change the geometry, or winds blow off some of the dust. Further, fresh snow will also contain radioactive matter normally brought down with precipitation (3, 4). Such radioactive matter is observed on the present recording apparatus with almost every fall of rain or snow. Its decay period is short since it usually has disappeared by the time the precipitation has stopped. Experiments by Stefanizzi (3) have identified this radioactive matter regularly found in precipitation as products of disintegration of radon and thoron, the latter representing only a very small percentage of the activity. The half life of the radon products is about half an hour while that of the thoron at about 12 to 24 hr. after collection is 10 to 11 hr. With the present apparatus the activity usually found in heavy precipitation represents less than 15% of the cosmic ray background but in one extreme case of heavy wet snow it was as high as 35%.

The decay of the activity recorded on January 29 and February 7 was so much slower that there is no difficulty in making a separation between that and the activity normally expected with precipitation. An example of the latter appears in Fig. 2. The upper curve shows an increase during the early hours of February 1. It was snowing heavily during that morning and this increase would be considered about normal. The early part of the fall on February 7 also showed evidence of the short period products mixed with the dust which presumably came from the atomic explosions. Snow or rain continued to fall that morning until about 1700 G.M.T. Immediately after the increase and during the latter part of fall of precipitation the decay rate was very rapid. The maximum is about 35% above background of which about 15% is considered to be the short period products that would be expected with the snow and rain.

The background in Fig. 2 has been corrected for meteorological variations in cosmic ray intensity as observed by coincidence counts in two trays in Fig. 1. Both were similarly shielded.

II. DECAY RATE OF MATERIAL COLLECTED IN SNOW

Samples of snow were collected on January 29 and February 7 to test the decay rate. The snow was melted and the liquid and sediment placed in a flat tray made of about 16 gauge sheet steel. This tray containing the liquid and sediment was placed immediately beside a counter tray. This counter tray was the top tray of a telescope used for studying directional effects of mesons, and had no other shielding around it except lead plates underneath, between it and the next tray of the telescope. It was located in the center of the laboratory some distance from the walls and roof and hence was only slightly affected by radioactive material in falling precipitation. The dimensions of the tray containing the liquid and sediment were $14\frac{7}{8}$ in. by $10\frac{3}{4}$ in. and the liquid was about 2 in. deep. This makeshift arrangement was used because no preparation had been made for the study of such products, and a

measure of the decay rate had to be started without delay. The counting rate was about twice the background in the case of the January 29 fall and about 50% above background in that of the February 7 fall. The background was observed for a period of about one hour each day by removing the tray to a remote corner of the laboratory. This was not a completely satisfactory method because, even though precautions were taken, the movement of the tray may have disturbed the sediment and there was no certainty that the geometry would be identical when it was returned.

In spite of this a good decay curve was obtained for the first fall (January 29) but the results for the February 7 fall were rather irregular. Fig. 3 shows a

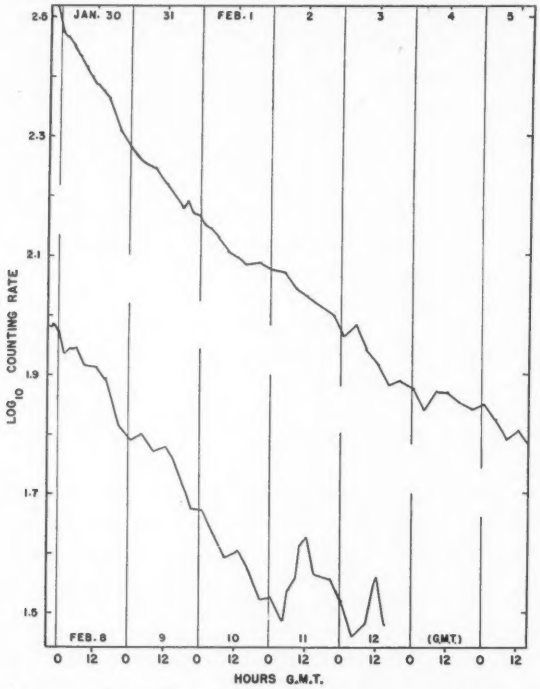

FIG. 3. Decay curves of radioactive material found in sample of snow. Upper curve, January 29 fall; lower curve, February 7 fall.

plot of log counting rate *vs.* time. The decay curves indicate that several radioactive products are present such as are found in products of fission. Assuming that each fall of radioactive material came from one atomic explosion an attempt was made to identify the time of the explosion by its decay rate. Way and Wigner (5) have calculated the decay rate of β-activity and of total energy of the radiation from fission products. They indicate an inverse power law of activity of the form k/t^{α} where α is about 1.2 for long

periods after the explosion. Experimental curves (included in Ref. 5) indicate that α may be a little higher than 1.2. The present measurements are based on gamma rays but assuming that the number of gammas is proportional to the number of beta rays the same law should hold. For softer rays there will be some loss by absorption therefore too close an agreement cannot be expected.

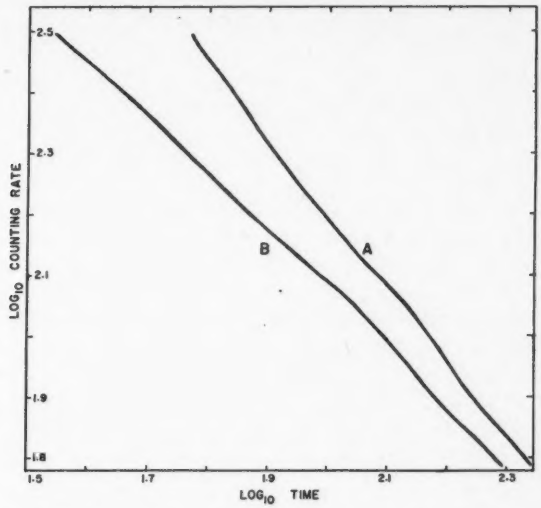

FIG. 4. Decay law for the January fall of radioactive material,—log counting rate *vs.* log time. Zero time for Curve *A* is 1300 hours on January 27 and for Curve *B* 1300 hours on January 28.

Fig. 4 shows a plot of log counting rate against log time for the January 29 fall. The counting rate was taken from a smoothed curve using the points in Fig. 3. Two zeros of time were chosen in accord with newspaper reports of the times of firing the atomic explosions. The reports indicate that the explosions usually occurred at an early hour in the morning by local time. Therefore, zero times were assumed at 1300 G.M.T. on January 27 (Curve *A* in Fig. 4) and January 28 (Curve *B* in Fig. 4). The slope of Curve *A* is very close to 1.3 and it does not change appreciably during the five days of observation. The slope of Curve *B* is about 0.9. The discrimination therefore is such that if this inverse power index should be near 1.3 the radioactive material which was deposited in Ottawa on January 29 came from the explosion on January 27.

The decay curve for the February 7 fall is not nearly so good. The plot of log counting rate against log time using various periods back to zero time did not produce nearly as straight lines as in the earlier case. To make the results fit even roughly a power law with $\alpha = 1.3$ it would have to be assumed that the material, if it is fission products, was from three to five days old. It could of course be a mixture of dusts from more than one explosion.

III. QUANTITY OF MATERIAL

Only a rough estimate of the quantity of material can be made. The counter nearest the roof of the penthouse showed an increase of 45% over the cosmic ray background in the case of the fall on January 29. Previous tests with a radium source had been made using counters similarly situated in the penthouse. Inverse square law calculations indicate this 45% represents approximately 10^{-6} gm. of radium in equilibrium with its products placed on the roof immediately above the counter. Assuming that the effective area exposed to the counter is of the order of 1 sq. meter the intensity of the fall of radioactive matter is of the order of 1 μgm. of radium equivalent per square meter. This is subject to considerable error and should only be considered as a measure of the order of magnitude of the quantity present.

IV. SUMMARY OF CONCLUSIONS

Radioactive matter presumably from the Nevada atomic explosion fell in Ottawa on January 29 and again on February 7. The decay period indicates that it could have been products of fission. The January 29 fall very probably came from an explosion on January 27, but the time of the February 7 fall is less definite, the material appearing to be three to five days old. It could, of course, be a mixture of materials of different ages or contain unusual products of fission. The quantity is estimated to be equivalent in gamma radiation, with the shielding used, to 1 μgm. of radium per square meter. This estimation is, however, not accurate and represents only the order of magnitude.

REFERENCES

1. MORRISON, A. Private communication.
2. ROSE, D. C. Phys. Rev. 78: 181. 1950.
3. STEFANIZZI, A. J. Geophys. Research, 55: 373. 1950.
4. WAIT, G. R. and MCNISH, A. G. Monthly Weather Rev. 62: 1. 1934.
5. WAY, K. and WIGNER, E. P. Phys. Rev. 73: 1318. 1948.

ON THE THERMODYNAMICS OF WAVE FIELDS[1]

By A. E. Scheidegger and C. D. McKay[2]

ABSTRACT

It is shown that the thermodynamic functions cannot be defined for a nonquantized field theory in the usual way; i.e., if there exists a partition function in Gibbs' sense at all, $Z = \int \exp(-\vartheta H)\, d^{2N}\Omega$ is certainly not the correct one.

The authors have recently developed a theory of the thermodynamics of wave fields (2). In that paper (2) the quantum theoretical method of Klein (1) was used. One might expect that similar results could have been obtained by using the classical formalism of Gibbs' instead.

However, this is not the case. It has long been known that the thermodynamic functions cannot be defined for the nonquantized electromagnetic field. As a matter of fact, this was the very reason why quantum theory was discovered. The fact that the thermodynamic functions cannot be defined in the nonquantized Maxwell field, expresses itself in many ways. In Gibbs' formalism it effects the divergence of the integrals in the partition function.

In this connection one may wonder whether this breakdown of Gibbs' formalism is a peculiar feature of electrodynamics or rather a fault in the theory of Gibbs. We are undertaking to show that the breakdown is essentially due to the fact that one has an infinite number of co-ordinates. Thus no thermodynamics can be defined in any of the usual field theories if they are not quantized.

In order to show this we write the field theory in canonical form. Denoting the field variables by ψ, the field equations are given by the variational principle

$$\delta \int_{t_1}^{t_2} L\, dt = 0 \tag{1}$$

$$L = \int \mathscr{L}\, d^3x.$$

The lagrangian density $\mathscr{L}$ is a function of ψ, grad ψ, and $\partial\psi/\partial t = \dot{\psi}$. Introducing as usual the momenta π leads to the hamiltonian formulation with

$$H = \int \mathscr{H}\, d^3x\,; \tag{2}$$

$\mathscr{H}$ is a function of ψ, grad ψ, and π.

Next we have to set up the partition function Z; in a nonquantized theory the expression for the latter corresponding to Gibbs' theory is

$$Z = \int \exp(-\vartheta H)\, d^{2N}\Omega \tag{3}$$

where $\vartheta = 1/kT$, N denotes the number of degrees of freedom and Ω the phase space. The difficulty is that for a field theory N is infinite. As a first

[1] *Manuscript received October 9, 1951.*
Contribution from the Department of Physics, Queen's University, Kingston, Ont.
[2] *Now at Department of Applied Mathematics, Physical Sciences Centre, McGill University, Montreal, P.Q.*

approach, therefore, we take only a finite volume wherein our field equations be defined, and, in addition, split that volume into a finite number of small cells of size $\Delta^3 x$. Thus N will be finite. Equation (3) then becomes

$$Z = \lim_{N\to\infty} \int \ldots \int_{2N} \exp\left(-\vartheta \sum_{N} \mathscr{H}_i \Delta^3 x_i\right) d\psi_1 \ldots d\psi_N \, d\pi_1 \ldots d\pi_N. \tag{4}$$

A difficulty is immediately apparent here in the occurrence of the derivatives of ψ in $\mathscr{H}$ and hence the process indicated by the integral sign is actually to be interpreted as the inverse operation to the variational derivative. Fortunately, it is not necessary to actually perform this operation. One can get a sufficient estimate of Z in the following way. Noting that in all field theories $\mathscr{H}$ is a homogeneous quadratic function in the field variables and their space derivatives, we can perform the following substitution

$$p_i = \sqrt{\vartheta}\, \pi_i; \qquad q_i = \sqrt{\vartheta}\, \psi_i. \tag{5}$$

Thus Equation (4) becomes

$$\left\{ \begin{array}{l} Z = \lim \dfrac{1}{\vartheta^N} \int \ldots \int_{2N} \exp\left(-\sum_{N} \mathscr{H}_i \Delta^3 x_i\right) dp_1 \ldots dp_N \, dq_1 \ldots dq_N, \\ \Delta p_i \to 0 \\ \Delta q_i \to 0 \\ N \to \infty \end{array} \right. \tag{6}$$

which obviously can be written as follows

$$Z = \lim_{N\to\infty} \frac{1}{\vartheta^N} \phi\,(N) \tag{7}$$

since the "integrals" in (6) do not depend on the temperature. The expression of $\phi\,(N)$ is very complicated and it would be difficult to evaluate it, but whatever it is, there is at most *one* value of ϑ which possibly could make the partition function Z finite.

This proves our proposition, namely that the thermodynamic functions cannot be defined for a nonquantized field theory with a homogeneous quadratic hamiltonian.

REFERENCES

1. KLEIN, O. Z. Physik, 72: 767. 1931.
2. SCHEIDEGGER, A. E. and MCKAY, C. D. Phys. Rev. 83: 125. 1951.

THE ACOUSTICAL FIELD NEAR A CIRCULAR TRANSDUCER[1]

By E. W. Guptill and A. D. MacDonald

ABSTRACT

An approximate solution for the near field of a circular transducer is given. The results indicate that, if a similar transducer is used as a receiver, the measured particle velocity is equal to $1 + (2.70/(ka)^2)$ times the plane wave velocity, where ka is the number of wave lengths in the perimeter of the transducer.

The acoustical field from a piston source has received attention from several writers (1, 2, 3, 4, 6), but a solution for the near field has not, to the writers' knowledge, been published. While the piston source has a relatively simple boundary condition to be fulfilled yet the solution for the near field is, apparently, more difficult than that for a circular diaphragm clamped around its edge. It is the purpose of this paper to give an approximate solution for the latter case.

The velocity potential, ϕ, for an acoustical wave with a sinusoidal time variation and no attenuation is a solution of:

$$\nabla^2 \phi + k^2 \phi = 0, \text{ where } k = \frac{2\pi}{\lambda}.$$

Unfortunately none of the known general solutions of this equation allow the boundary conditions for a vibrating diaphragm to be completely fulfilled. However an integral solution in cylindrical coordinates is possible (3, 5):

$$\phi = \sum_{n=-\infty}^{\infty} e^{in\theta} \int_0^{\infty} \frac{g_n(\alpha)\, J_n(\alpha\rho)\, e^{-i\mu z}}{i\mu} \alpha\, d\alpha$$

where

$$\mu = \sqrt{k^2 - \alpha^2}$$

and ρ, θ, and z are the parameters of the cylindrical coordinate system. In case of circular symmetry ϕ is not a function of θ and the integral reduces to

$$\phi = \int_0^{\infty} \frac{g(\alpha)\, J_0(\alpha\rho)\, e^{-i\mu z}}{i\mu} \alpha\, d\alpha. \tag{1}$$

The particle velocity, $V(\rho)$, at $z = 0$ becomes:

$$-V(\rho) = \left(\frac{\partial \phi}{\partial z}\right)_{z=0} = -\int_0^{\infty} g(\alpha)\, J_0(\alpha\rho)\, \alpha\, d\alpha$$

[1] *Manuscript received September 17, 1951.*
Contribution from the Department of Physics, Dalhousie University, Halifax, N.S.

which is a Fourier–Bessel transform of

$$g(\alpha) = \int_0^\infty V(\rho)\, J_0(\alpha\rho)\, \rho\, d\rho; \tag{2}$$

$g(\alpha)$ may now be evaluated by (2) and $\frac{\partial\phi}{\partial z}$ in (1) will reduce to the proper boundary value, $(V(\rho))$, in the plane $z = 0$.

A case of practical interest is that of a uniform circular diaphragm clamped at the periphery and driven by a force uniform over the area of the diaphragm. A possible mode of its motion gives as the velocity in the $z = 0$ plane:

$$\begin{aligned} V(\rho) &= V_0\, J_0(\gamma\rho) \qquad 0 < \rho < a \\ &= 0 \qquad\qquad\quad a < \rho < \infty \end{aligned} \tag{3}$$

where "a" is the radius of the diaphragm and γa is the first root of the zero-order Bessel function. The actual motion of the face of a piezoelectric transducer clamped at the edge may be complicated but preliminary experiments indicate that the amplitude varies smoothly from a maximum at the center to zero at the edges when a nonresonant frequency is applied. $g(\alpha)$ now becomes:

$$\begin{aligned} g(\alpha) &= \int_0^a V_0\, J_0(\gamma\rho)\, J_0(\alpha\rho)\, \rho\, d\rho \\ &= Q\frac{J_0(\alpha a)}{\alpha^2 - \gamma^2} \end{aligned}$$

where Q is a constant and equal to $V_0\ \gamma a\ J_1(\gamma a)$. Replacing $g(\alpha)$ by $Q\, J_0(\alpha a)/(\alpha^2 - \gamma^2)$ in Equation (1), the velocity potential for any z is:

$$\phi = Q \int_0^\infty \frac{e^{-i\mu z}\, J_0(\alpha\rho)\, J_0(\alpha a)}{i\mu(\alpha^2 - \gamma^2)}\, \alpha\, d\alpha.$$

In measuring the velocity of sound in liquids a receiving transducer which may have the same diameter as the transmitter is frequently used. Consequently, the value of ϕ, averaged over a surface of radius a, is of interest. If the receiver is coaxial with the transmitter the average value of ϕ, using the notation of Williams (6), is:

$$\begin{aligned} \langle\phi\rangle &= \frac{Q}{\pi a^2} \int_0^\infty \frac{e^{-i\mu z}\, J_0(\alpha a)\, \alpha\, d\alpha}{i\mu(\alpha^2 - \gamma^2)} \int_0^a 2\pi\, J_0(\alpha\rho)\, J_0(\gamma\rho)\, \rho d\rho \\ &= \frac{2Q^2}{a^2 V_0} \int_0^\infty \frac{e^{-i\mu z}\, J_0^2(\alpha a)\, \alpha\, d\alpha}{i\mu(\alpha^2 - \gamma^2)^2}. \end{aligned}$$

A weighing factor $J_0(\gamma\rho)$ is inserted in the integral for the average value of ϕ. It has been observed experimentally that at nonresonant frequencies the electrical signal generated by a crystal when excited by an acoustic wave over

a small fraction of its area is a maximum when excited at the center and varies smoothly to zero at the periphery. The weighing factor is an attempt to take account of this fact.

The average velocity, $\langle V \rangle$, in the z direction becomes

$$\langle V \rangle = \frac{2Q^2}{a^2 V_0} \int_0^\infty \frac{e^{-i\mu z} J_0^2(\alpha a)\ \alpha\, d\alpha}{(\alpha^2 - \gamma^2)^2}$$

$$(4) \qquad = \frac{2Q^2}{V_0}\left[\int_0^{ka} \cos \mu z\, f(x)\, dx - i \int_0^{ka} \sin \mu z\, f(x)\, dx + \int_{ka}^\infty e^{-\mu z} f(x)\, dx \right.$$

where $x = \alpha a$ and $f(x) = J_0^2(x)\, x/(x^2 - 2.40^2)^2$. The third integral of Equation (4) can be neglected for large values of ka. In fact, for $ka = 50$ and $z = 0$ it is smaller than the first integral by a factor of 10^4.

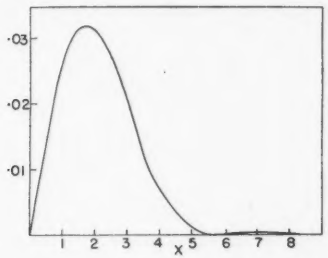

FIG. 1. A plot of $f(x) = \dfrac{J_0^2(x)\, x}{(x^2 - 2.40^2)^2}$.

A plot of $f(x)$ is shown in Fig. 1 and it suggests that an approximate solution for the real and imaginary part of $\langle V \rangle$ may be obtained by expanding $\cos \mu z$ and $\sin \mu z$ about the point $x = 0$. This expansion yields for the real part of $\langle V \rangle$:

$$Re\ \langle V \rangle = \frac{2Q^2}{V_0} \int_0^{ka} \left[\cos kz + u \sin kz - \frac{u^2}{2!} \cos kz + \ldots . \right] f(x)\, dx$$

$$= \frac{2Q^2}{V_0}\left[\cos kz \int_0^{ka} f(x)\, dx + \sin kz \int_0^{ka} u\, f(x)\, dx + \ldots . \right]$$

where $u = \dfrac{z}{a}\left[\dfrac{1}{2}\dfrac{x^2}{ka} + \dfrac{1}{4.2!}\dfrac{x^4}{(ka)^3} + \ldots . \right]$.

The integral of the form $\displaystyle\int_0^{ka} x^n f(x)\, dx$ may be computed graphically and if the constant, $.0858 \left(\dfrac{2Q^2}{V_0}\right)$, is omitted $Re\ \langle V \rangle$ becomes:

$$Re\,\langle V\rangle = \cos kz + \frac{z}{a}\left[\frac{2.70}{ka} + \frac{.465}{(ka)^2} + \ldots\right]\sin kz$$
$$-\left(\frac{z}{a}\right)^2\left[\frac{.465}{(ka)^2} + \frac{3.50}{(ka)^3} + \ldots\right]\cos kz$$

and

$$Im\,\langle V\rangle = \sin kz - \frac{z}{a}\left[\frac{2.70}{ka} + \frac{.465}{(ka)^2} + \ldots\right]\cos kz$$
$$-\left(\frac{z}{a}\right)^2\left[\frac{.465}{ka} + \frac{3.50}{(ka)^2} + \ldots.\right]\sin kz\,.$$

It is now a simple matter to compute the phase velocity when z/a is less than 1, for if z_1 and z_2 are two consecutive values for which $Re\,\langle V\rangle$ or $Im\,\langle V\rangle$ is zero, then $z_1 - z_2$ is the measured wave length. In either case,

$$\frac{z_1 - z_2}{\lambda} \simeq 1 + \frac{2.70}{(ka)^2}$$

indicating that the velocity in the near field is greater than that for a plane wave. For $ka = 50$, which would correspond, for example, to a crystal in water of 1 cm. radius and a frequency of about 1 mc., this difference is approximately 0.1%. It should be noted that the above theory is strictly applicable only if the energy incident on the receiving transducer is totally absorbed.

ACKNOWLEDGMENT

The authors wish to express their thanks to the Defence Research Board of Canada which has given financial support to the work in acoustics at Dalhousie, and to Mr. F. A. Fergusson who has assisted us in the numerical integrations.

REFERENCES

1. Bouwkamp, C. J. Philips Research Repts. 1: 251. 1946.
2. Carter, A. H. and Williams, A. O. J. Acoust. Soc. Am. 23: 179. 1951.
3. King, L. V. Can. J. Research, 11: 135. 1934.
4. Pachner, J. J. Acoust. Soc. Am. 23: 185. 1951.
5. Stratton, J. A. Electromagnetic theory. McGraw-Hill Book Co., Inc., New York and London. 1941. p. 369.
6. Williams, A. O. J. Acoust. Soc. Am. 23: 1. 1951.

ELECTROMAGNETIC ENERGY DENSITY AND FLUX[1]

By C. O. Hines[2]

ABSTRACT

Although Poynting's theorem receives general acceptance in the treatment of electromagnetic energy, an alternative theorem, Macdonald's, has equal claim to validity at the present state of our knowledge. In a comparison of many results derived from the two, Macdonald's theorem exhibits sufficient superiority to warrant its consideration more generally in electromagnetics.

1. INTRODUCTION

We shall use the common notation of electromagnetic theory, including Φ and $\mathbf{A}$ for the potentials, dots for partial time derivatives, and $\mathbf{C}$ for Maxwell's "total current" ($= \dot{\mathbf{D}} + \mathbf{J}$). We shall treat nonmagnetic media only, although it seems likely that this restriction is unnecessary. Heaviside–Lorentz units will be used throughout.

In this paper, we shall take as Poynting's theorem the statement that energy has a density which increases at the rate

$$\dot{\mathfrak{E}} = \mathbf{E} \cdot \mathbf{C} + \mathbf{H} \cdot \dot{\mathbf{H}} \tag{1}$$

and a flux (or more properly, a flux density) given by

$$\mathbf{S} = c\mathbf{E} \times \mathbf{H} . \tag{2}$$

These quantities are related by the continuity–conservation equation

$$\int_V \dot{\mathfrak{E}}\, dv = -\int_\Sigma S_n \, d\sigma \tag{3}$$

in keeping with our ideas of energy. (Σ is the closed surface bounding the volume V.)

Opposed to this, Macdonald (Reference 7) proposed the theorem, which we shall name after him, that the proper expressions are

$$\dot{\mathfrak{D}} = \mathbf{E} \cdot \mathbf{C} + \frac{1}{2c} \frac{\partial}{\partial t} (\mathbf{A} \cdot \mathbf{C}) \tag{4}$$

and

$$\mathbf{R} = c \left[\mathbf{E} \times \mathbf{H} + \frac{1}{2c} \frac{\partial}{\partial t} (\mathbf{A} \times \mathbf{H}) \right] \tag{5}$$

which are related by the similar, and equally valid, equation

$$\int_V \dot{\mathfrak{D}}\, dv = -\int_\Sigma R_n \, d\sigma . \tag{6}$$

[1] *Manuscript received July 10, 1951.*
Contribution from Radio Physics Laboratory, Defence Research Board of Canada, Ottawa.
[2] *Now at the Department of Mathematics, University of Cambridge, Cambridge, England.*

Each theorem was originally based on the density expression which its author accepted, together with the conservation condition. By different formulations of the aether theory, either expression could be justified. Maxwell himself considered $\mathfrak{E}$ to be more appropriate to the near-action treatment he preferred (Reference 8, Chap. XI), and apparently Poynting agreed with him in this. The expression $\mathfrak{D}$, however, appeared to be more natural on a dynamical theory of the aether, and it was on this basis that Macdonald supported it. Livens has since developed an alternative dynamical theory in which $\mathfrak{E}$ appears as the density (Reference 4), but his treatment is open to an objection which Macdonald had raised earlier: integrals over a surface at infinity are rejected although they are not generally negligible.

Livens has gone on (5) to attack Macdonald's theorem on various counts. One of these involves the arbitrariness usually associated with the potentials but, as he admits in his text (Reference 6, p. 244), "it is not *a priori* impossible that one of the sets of potentials does in fact represent some physical quantity so that this difficulty may not prove to be so serious as it seems at first sight." In actual fact, the retarded potentials of L. Lorenz provide an admirable basis for a fundamental nonaether theory—a theory which leads to $\mathfrak{D}$ as the density. (See O'Rahilly, Reference 9.)

Other objections raised by Livens in (5) are based on a presumed knowledge of the workings of the aether, a basis which we no longer accept and which he himself doubted. Still others are based on results he found for specific applications but, as we shall see, his treatment was inaccurate; corrected and extended results for these problems are simpler, and in the author's opinion more satisfactory, on Macdonald's theorem than on Poynting's.

2. INFINITE PLANE WAVES

We shall first treat infinite plane waves derived from a vector potential having complex components proportional to $\exp ik(nz-ct)$, where n is the refractive index for waves having frequency $kc/2\pi$ and phase normals in the z direction.

For isotropic nonabsorbing media, Livens found that both $\mathfrak{D}$ and $\mathbf{R}$ vanished, and hence found Macdonald's theorem unsatisfactory. This result is faulty, however; it was obtained by the multiplication of complex vectors where real ones should have been used. The correct calculation shows that $\mathfrak{D}$ and $\mathbf{R}$ are constants, equal to the mean values of $\mathfrak{E}$ and $\mathbf{S}$. If the medium absorbs, one finds that $\dot{\mathfrak{D}}$ is constant in time and equal to the time mean of $\dot{\mathfrak{E}}$, so that the two theorems agree on the mean rate of absorption. Even in anisotropic absorbing media $\dot{\mathfrak{D}}$ and $\mathbf{R}$ are constant in time and space, except for an exponential damping. They are equal to the time means of $\dot{\mathfrak{E}}$ and $\mathbf{S}$, which are quite involved functions. (See the appendix and Reference (3).)

These results appear preferable, to the present author at least. We now have constant energy density, or a constant rate of absorption, and constant energy flux everywhere (cf. water waves). As this is only a personal opinion, however, the point will not be labored. Instead, we shall pass on to a consideration of the velocity with which the energy moves.

3. ENERGY VELOCITY

We shall confine our attention for the moment to nonabsorbing media. In these, Poynting's density is a function of the phase, $k(nz\text{-}ct)$. This suggests a flow having a speed in the z direction equal to the phase speed, c/n — a result which is at variance with the generally accepted group speed, $c/(dkn/dk)$, if the medium is dispersive. On the other hand, Macdonald's density is a constant and so can give no information, by itself, as to the speed of the energy.

The velocity of energy flow is often taken as that suggested by a fluid analogy, namely, the quotient flux/density. Using the $\mathfrak{E}$ and $\mathbf{S}$ commonly given in texts, this method, too, gives c/n as the z component of the energy velocity. (See Stratton, Reference 11, p. 342, Prob. 8.) This unwanted result is often explained away by the excuse that, when treating the energy in infinite waves, it is impossible for us to label and follow individual bits. That is, the analogy is handy but fails if we try to apply it. It will shortly appear that, though the excuse may be valid, no excuse is necessary if Macdonald's expressions are used.

It is possible to obtain the group speed from Poynting's theorem and the fluid analogy, for an isotropic Lorentz-dispersive medium, by a method equivalent to the following: in deriving $\mathfrak{E}$ from $\dot{\mathfrak{E}}$, add a suitable constant of integration to the usual expression. The value used can be justified on the electron theory. Now, on dividing the result into S and averaging, the group speed is obtained. (See Havelock (1) or White (12).) This is a complicated function of the physical quantities involved, and its derivation by such a method must be considered as being of great importance. However there is one drawback to the new picture: in obtaining the correct speed of the energy we have destroyed the uniformity of its flow. The z speed is no longer constant; it equals the group speed only on the average. The peculiarity of the flow is increased if anisotropic media are considered. (See Reference (3).)

These objections do not arise if Macdonald's theorem is used. The integral of $\dot{\mathfrak{D}}$ is simply an arbitrary constant which we may take as the average of the $\mathfrak{E}$ just used, again with justification on the electron theory. Further, $\mathbf{R}$ is the average of $\mathbf{S}$. Hence the ratio $R/\mathfrak{D}$ is always the group speed; the fluid analogy is completely vindicated. The extension to anisotropic media is equally satisfying: $\mathbf{R}/\mathfrak{D}$ is a constant vector having the direction of the mean Poynting vector, which is also the direction of packet velocity (Reference (2)), and having magnitude equal to that of the packet velocity if $\mathfrak{D}$ is properly chosen.

The expressions for $\mathfrak{E}$ and $\mathfrak{D}$ which we have been using here differ from those employed by Maxwell, Poynting, Macdonald, and Livens, by an added constant. Its addition is in no way in conflict with the theories on which their expressions were based, but is more in accord with the electron theory.

The flow of energy within a packet, as distinct from these infinite waves, also becomes simplified if Macdonald's theorem is accepted. (The method is outlined in Reference (3).) Poynting's theorem leads to a very disturbed

flow of energy inside the packet envelope whereas Macdonald's gives an even flow, each bit of energy always moving with the velocity of the packet.

The fluid analogy has been generalized and treated in some detail for anisotropic absorbing media in Reference (3). Similar results are obtained there. Poynting's theorem leads to an unusual picture—almost unacceptable if the constant of integration is not taken sufficiently large — whereas Macdonald's theorem results in a perfectly orderly flow with constant velocity. It would be very surprising to the author if anyone who had worked on this particular application of the two theorems could still agree with Stratton (p. 134) that Macdonald's has not "the advantage of . . . . . greater simplicity to recommend it." In fact, it was the difficulty encountered in the use of Poynting's theorem in this problem that led to the present investigation.

4. DIPOLE RADIATION

Livens apparently considered Macdonald's theorem to be unsatisfactory for the problem of a dipole radiating into free space (Reference 5). The fields here may be derived from potentials given in polar form by

$$\Phi = -\cos\theta \frac{\partial}{\partial r}\frac{f}{r} \tag{7}$$

$$A_r = \cos\theta f'/r \tag{8}$$

$$A_\theta = -\sin\theta f'/r \tag{9}$$

$$A_\phi = 0 \tag{10}$$

where f is some function of $(ct\text{-}r)$, and $'$ denotes differentiation with respect to this argument. The dipole lies along the z axis at $r = 0$, and its method of varying in time determines the form of f. Incidentally, many of Livens' formulae are in error owing to the improper use of a " + " instead of the " − " in Equation (9), in conflict with the expressions he gives for **E**, **H**, and **C**.

Retaining only the terms of lowest order in $1/r$, and using the original expressions for $\mathfrak{E}$ and $\mathfrak{D}$, we obtain in the distant field

$$c\mathfrak{E} = c\sin^2\theta\,(f''^2 + f''^2)/2r^2 = S_r \tag{11}$$

and

$$c\mathfrak{D} = c\sin^2\theta\,(f''^2 - f'f''')/2r^2 = R_r. \tag{12}$$

Livens complains of this result since, on Poynting's theorem, the "kinetic energy density in the distant radiation field is equal to the potential energy density, but on Macdonald's own form of his theory these are not equal except in the case of simple harmonic oscillation." We might note that it is only in cases of simple harmonic oscillation that we find such a result in mechanics, and even then the two energies are not equal instantaneously but only on the average; at any given time they add up to a constant value. This result corresponds to Macdonald's theorem, not Poynting's.

Two objections to Macdonald's expressions do appear, however. If we consider nonsinusoidal variation of the dipole, we find that the $\mathfrak{D}$ given above can become negative, owing to the $f' f'''$ term. Even for sinusoidal motion there is the surprising result that R_θ does not vanish except on the average (or on the z axis or in the x-y plane), and we even find that $(R_\theta/\mathfrak{D}) \to \infty$ as we approach the z axis. These difficulties will have to be reexamined on the basis of the electron theory, but this requires a more detailed treatment of dipoles than we are undertaking at present. However, it might be well to point out here that the embarrassing term in $f' f'''$ appears, on the electron theory, to be necessary if we are to retain our usual concepts of relativistic mass. (See Schott, Reference 10, Sections 5, 145, and 146; his $\mathbf{v}$ and β correspond to our f.)

5. MODIFICATION OF MACDONALD'S THEOREM

We may now turn to an objection to Poynting's theorem which is sometimes raised in text books: when nonparallel static electric and magnetic fields exist together, as when a magnet lies near a charged body, a flow of energy is indicated where none would be expected. The same objection would apply to Macdonald's theorem. Some authors deny that there is any cause for wonder in such a flow, it being solenoidal and therefore, we are to believe, physically irrelevant. Here again, the excuse may be valid but it is unnecessary if we properly choose our energy equation.

We may alter Macdonald's theorem while retaining its original bases, the density $\mathfrak{D}$ and the conservation condition, by taking the flux of energy to be

$$\mathbf{Q} = (\mathbf{A} \times \dot{\mathbf{H}} - \dot{\mathbf{A}} \times \mathbf{H})/2 + \Phi \mathbf{C} \tag{13}$$

rather than $\mathbf{R}$. We readily obtain

$$\int_V \dot{\mathfrak{D}}\, dv = -\int_\Sigma Q_n\, d\sigma \tag{14}$$

since $\mathbf{R}$ and $\mathbf{Q}$ differ only by a solenoidal vector, c curl $\Phi \mathbf{H}$. All the results given in previous sections for the original theorem continue to hold for the modified form, as may be verified easily. However, in the case of the static fields just mentioned, $\mathbf{Q}$ vanishes. This is the physically acceptable result which the modification was designed to yield.

The new expression $\mathbf{Q}$ has another advantage, at least in the eyes of practical physicists. When a constant current flows through a wire, Poynting's theorem gives the picture of energy flowing through the surrounding medium and then entering the wire where it is converted to heat. This idea has been forced on experimenters, over their objections, by field theorists for some time now. The picture given by the modified theorem is the one maintained by the man in the laboratory all along: the energy flows at the rate ΦJ through the wire, and no flow takes place outside.

6. CONCLUSION

It is common practice today to present Poynting's theorem simply as a hypothesis or as a definition, based primarily on the $\mathbf{E} \cdot \mathbf{J}$ term which it contains and on the conservation condition. But Macdonald's theorem, and any number of others, can be presented on these same bases. So long as $\mathbf{E} \cdot \mathbf{J}$ is the only observationally relevant term, there can be no question of any "clash with new experimental evidence" (Stratton, p. 135) to affect our opinion of any one of them; any preference we may have must be of a conceptual, not an observational, nature.

Stratton, to take one example, justifies the choice of Poynting's theorem by noting that the "hypothesis of an energy density in the electromagnetic field and a flow of intensity $\mathbf{S} = [c]\,\mathbf{E} \times \mathbf{H}$ has . . . . . proved extraordinarily fruitful." Macdonald's, as we have seen, can lead to results which can be at least equally fruitful (Sections 2 and 4) and, in conjunction with the fluid analogy, even more so (Section 3). In its modified form it even removes some complications which Poynting's theorem introduced (Section 5).

It would seem that Macdonald's theorem has shown sufficient merit in the problems discussed here to warrant its further consideration.

This work was carried out at the Radio Physics Laboratory, Defence Research Board, Ottawa. The investigation is being continued at the Department of Mathematics, University of Cambridge.

REFERENCES

1. HAVELOCK, T. H. The propagation of disturbances in dispersive media. Cambridge Tracts in Mathematical Physics. 1914.
2. HINES, C. O. J. Geophys. Research, 56: 63. 1951.
3. HINES, C. O. J. Geophys. Research, 56: 535. 1951.
4. LIVENS, G. H. Phil. Mag. 32: 195. 1916.
5. LIVENS, G. H. Phil. Mag. 34: 385. 1918.
6. LIVENS, G. H. The theory of electricity. 2nd ed. Cambridge University Press. 1926.
7. MACDONALD, H. M. Electric waves. Cambridge University Press. 1902.
8. MAXWELL, J. C. Treatise on electricity and magnetism. 3rd ed. The Clarendon Press, Oxford. 1904.
9. O'RAHILLY, A. Electromagnetics. Longmans, Green and Co., Inc., London, etc. 1938.
10. SCHOTT, G. A. Electromagnetic radiation. Cambridge University Press. 1912.
11. STRATTON, J. A. Electromagnetic theory. McGraw-Hill Book Co., Inc., New York and London. 1941.
12. WHITE, F. W. G. Electromagnetic waves. Methuen & Co. Ltd., London. 1950.

APPENDIX

The field vectors are to be obtained from the potentials by the relations $\mathbf{E} = -\operatorname{grad} \Phi - \partial\mathbf{A}/c\partial t$, $\mathbf{H} = \operatorname{curl} \mathbf{A}$, and $\mathbf{C} = c \operatorname{curl} \mathbf{H}$.

For the plane waves of Sections 2 and 3, where $\Phi = 0$, we find

$$\dot{\mathfrak{D}} = (\mathbf{A} \cdot \dot{\mathbf{C}} - \dot{\mathbf{A}} \cdot \mathbf{C})/2c \tag{15}$$

$$\mathbf{R} = (\mathbf{A} \times \dot{\mathbf{H}} - \dot{\mathbf{A}} \times \mathbf{H})/2\,. \tag{16}$$

If we now use $\mathbf{A}$, $\mathbf{H}$, and $\mathbf{C}$ as the corresponding complex vectors, proportional to ϵ^{-ikct}, and signify complex conjugates by $^-$, these expressions become

$$\dot{\mathfrak{D}} = (ik/4)\,(\mathbf{A}\cdot\tilde{\mathbf{C}} - \tilde{\mathbf{A}}\cdot\mathbf{C}) \tag{15'}$$

$$\mathbf{R} = (ikc/4)\,(\mathbf{A}\times\tilde{\mathbf{H}} - \tilde{\mathbf{A}}\times\mathbf{H}) \tag{16'}$$

after reduction. Now t enters each of these products only through $\epsilon^{-ikct}\epsilon^{ikct} = 1$; that is, t does not enter at all. Thus $\dot{\mathfrak{D}}$ and $\mathbf{R}$ are constant in time. The same is true of space in a nonabsorbing medium, while a factor ϵ^{-2kn_2z} enters each expression if the medium absorbs (n_2 being the imaginary part of n). If the effective dielectric matrix is Hermitian (see Reference 2), that is, if the medium is nonabsorbing, it may be shown that $\mathbf{A}\cdot\tilde{\mathbf{C}}$ is real, so $\dot{\mathfrak{D}}$ vanishes.

For nonabsorbing isotropic media, $\mathfrak{D}$ is given by $k^2n^2A\tilde{A}/2$ in terms of the complex amplitude of $\mathbf{A}$. This expression equals the time mean of $\mathfrak{E}$, not zero as found by Livens. (These are the $\mathfrak{D}$ and $\mathfrak{E}$ of the original theories; no integration constant has been added.)

It may be noted that in all cases of periodic variation, sinusoidal or not, the time means of $\dot{\mathfrak{D}}$ and $\mathbf{R}$ will equal those of $\dot{\mathfrak{E}}$ and $\mathbf{S}$ since the various expressions differ only by time derivatives.

SOME DIRECTIONAL CORRELATION FUNCTIONS FOR SUCCESSIVE NUCLEAR RADIATIONS[1]

By F. G. Hess[2]

ABSTRACT

A method of evaluating the sums of angular momentum coefficients appearing in the directional correlation function for successive nuclear radiations is presented. The sums are evaluated for the simplest cases and alpha–gamma and gamma–gamma correlation functions are calculated for these cases—the angular momentum quantum number of one of the emitted particles being arbitrary and that of the other being 1 or 2.

INTRODUCTION

The theory of the directional correlation of successively emitted nuclear gamma rays has been treated in detail by Hamilton (5) and Goertzel (4). The case in which a photon emitted corresponds to mixed 2^J electric and 2^{J-1} magnetic multipole radiation is treated by Ling and Falkoff (6). The theory of the directional correlation for the general case of any particles or photons was first given by Falkoff and Uhlenbeck (3).

An explicit computation of directional correlation functions involves the problem of evaluating certain sums. After some introductory considerations in Section I, a general method of treating this problem is presented in Section II. The method has some advantages although the computations remain, in general, cumbersome. It is applied in Section III to certain cases ("special transitions") which are characterized by special relations which the angular momenta of the particles and nuclei have to satisfy. For these cases the method is easiest to apply. The results obtained are used to calculate alpha–gamma and gamma-gamma correlation functions for the case that the angular momentum quantum number of one of the emitted particles is arbitrary and that of the other 1 or 2 (only one angular momentum being carried off by the emitted particle or photon in each transition). These results partly overlap the results of Falkoff (2) and Lloyd (7). The method can also be used to compute mixture correlation functions.

It is felt that some of the summation formulae, in particular Formulae (22), (23), and (24), may be found useful independently of the theory of directional correlation.

I. BASIC FORMULAE FOR CALCULATIONS OF DIRECTIONAL CORRELATION FUNCTIONS

The following notation is used throughout this paper: $J'm'$, Jm, $J''m''$, J_1m_1, J_2m_2 are the quantum numbers for the total angular momentum and its z component for the initial, intermediate, and final states of the nucleus and the

[1] *Manuscript received September 17, 1951.*
Contribution from the Department of Physics, University of British Columbia, Vancouver, B.C. This work was carried out in partial fulfillment of the requirements for an M.A. degree. During these investigations the author was a holder of a Bursary and Studentship from the National Research Council of Canada.

[2] *Present address: Depatment of Physics, University of Illinois, Urbana, Ill., U.S.A.*

total angular momentum (intrinsic plus orbital) and its z component for the first and second emitted particles respectively.

The types of correlation between particles and photons with given angular momenta will be denoted as follows: alpha(J_1)–gamma(J_2) means that an alpha particle with angular momentum J_1 is emitted in the first transition and a photon with angular momentum J_2 corresponding to a 2^{J_2} multipole is emitted in the second.

Using the above notation, one can write the expression for the directional correlation function, $W(\theta)$, between a particle (J_1) or a photon (J_1) and a particle (J_2) or photon (J_2), as obtained by Falkoff and Uhlenbeck (3), in the form:

$$(1) \qquad W(\theta) = \sum_{m_1 m_2} \Bigg[\sum_{m} (JJ_1 mm_1 | JJ_1 J' m + m_1)^2 \, (J'' J_2 m - m_2 m_2 | J'' J_2 Jm)^2 \Bigg] F_{J_1}^{m_1}(0) F_{J_2}^{m_2}(\theta).$$

Here the round bracketed expressions are the well-known angular momentum coefficients as defined by Condon and Shortley (1); $F_J^m(\theta)$ is a polynomial in $\cos^2\theta$ of degree at most equal to J, the coefficients of the polynomial varying with the type of particles emitted. The $F_J^m(\theta)$'s used in this paper can be found in References (3) and (6). $W(\theta)$ remains unchanged if the angles 0 and θ are interchanged.

Since only the relative variation of $W(\theta)$ with θ is of interest experimentally, factors appearing in (1) which are independent of the summation dummies m_1, m_2, and m, may be omitted from the expression. For this reason, we may write

$$(2) \quad (J'' J_2 m'' m_2 | J'' J_2 Jm) = \left[\frac{(2J+1)(2J''-\lambda_2)!(2J_2-\lambda_2)!\lambda_2!}{(2J+\lambda_2+1)!} \right]^{\frac{1}{2}} C^{Jm\lambda_2}_{J'' m'' J_2 m_2}$$

where λ_2 is defined by $J = J'' + J_2 - \lambda_2$, i.e. $0 \leqslant \lambda_2 \leqslant$ minimum of $2J''$, $2J_2$; $m = m'' + m_2$. Substituting (2) in (1) gives

$$(3) \qquad W(\theta) = \sum_{m_1 m_2} \Bigg[\sum_{m} (C^{J'm+m_1\lambda_1}_{Jm J_1 m_1})^2 (C^{Jm\lambda_2}_{J'' m-m_2 J_2 m_2})^2 \Bigg] F_{J_1}^{m_1}(0) F_{J_2}^{m_2}(\theta),$$

omitting the square root factors.

Racah (8) has shown that

$$C^{Jm\lambda_2}_{J'' m'' J_2 m_2}$$

may be expressed by the formula

$$C^{Jm\lambda_2}_{J'' m'' J_2 m_2} = \frac{1}{\lambda_2!} \left[\frac{(J+m)!(J-m)!}{(J''+m'')!(J''-m'')!(J_2+m_2)!(J_2-m_2)!} \right]^{\frac{1}{2}}$$

$$(4) \qquad \cdot \sum_{\alpha=0}^{\lambda_2} (-1)^{\alpha} \left[\frac{(J''+m'')!(J''-m'')!}{(J''+m''-\lambda_2+\alpha)!(J''-m''-\alpha)!} \right.$$

$$\left. \frac{(J_2+m_2)!(J_2-m_2)!}{(J_2+m_2-\alpha)!(J_2-m_2-\lambda_2+\alpha)!} \right] \binom{\lambda_2}{\alpha},$$

where

$$\binom{\lambda_2}{\alpha} = \frac{\lambda_2!}{\alpha!(\lambda_2 - \alpha)!}.$$

The summation over α is carried out with the understanding that each fraction $A!/(A-\beta)!$, $(A \geqslant 0, \beta \geqslant 0)$, appearing in the summand is to be written identically as $A(A-1)\ldots(A-\beta+1)$. Then, if $A - \beta < 0$, the term containing the fraction $A!/(A-\beta)!$ will vanish. Using the equations $J = J'' + J_2 - \lambda_2$ and $m = m'' + m_2$, it is easily shown that each axial quantum number appearing in $C^{Jm\lambda_2}_{J''m''J_2m_2}$ must lie within the smallest range given by the following conditions:

$$\begin{aligned} &-J \leqslant m \leqslant J, \quad -J'' \leqslant m'' \leqslant J'', \quad -J_2 \leqslant m_2 \leqslant J_2, \\ &-(J'' + J_2 - \lambda_2) \leqslant m'' + m_2 \leqslant J'' + J_2 - \lambda_2, \\ &-(J - J_2 + \lambda_2) \leqslant m - m_2 \leqslant J - J_2 + \lambda_2, \\ &-(J - J'' + \lambda_2) \leqslant m - m'' \leqslant J - J'' + \lambda_2. \end{aligned} \tag{5}$$

The C's defined by (4) have the following symmetry properties:

$$C^{Jm\lambda_2}_{J''m''J_2m_2} = (-1)^{\lambda_2} C^{J-m\lambda_2}_{J''-m''J_2-m_2} \tag{6a}$$

$$C^{Jm\lambda_2}_{J''m''J_2m_2} = (-1)^{\lambda_2} C^{Jm\lambda_2}_{J_2m_2J''m''} \tag{6b}$$

$$C^{Jm2J_2-\lambda_2}_{J''m''J_2m_2} = (-1)^{J_2+m_2+\lambda_2} C^{J''m''\lambda_2}_{JmJ_2-m_2} \tag{6c}$$

$$C^{Jm2J''-\lambda_2}_{J''m''J_2m_2} = (-1)^{J''+m''} C^{J_2m_2\lambda_2}_{JmJ''-m''} \tag{6d}$$

These symmetry relations are also given in Reference (8).

The summation over m appearing in the square brackets of Equation (3) is independent of the type of particles emitted. Once evaluated, the result may be used to calculate correlation functions for any type of particles emitted provided the angular momenta involved are the same.

Before a method of evaluating this summation is presented, let us first see how the calculation of correlation functions may be simplified by making use of the symmetry property (6a). In particular, the formulae for correlation functions in which an alpha particle or photon is emitted in the first transition are obtained for later use. The mixture correlation functions of Reference (3) can be simplified in a similar manner.

Applying (6a) to the summation

$$\sum_m (C^{J'm+m_1\lambda_1}_{JmJ_1m_1})^2 (C^{Jm\lambda_2}_{J''m-m_2J_2m_2})^2 \tag{7}$$

appearing in (3), and changing the summation over m to one over $-m$, one can show that (7) is equal to

$$\sum_m (C^{J'm-m_1\lambda_1}_{JmJ_1-m_1})^2 (C^{Jm\lambda_1}_{J''m+m_2J_2-m_2})^2. \tag{8}$$

As soon as the types of particles emitted are given, the formula (3) can be simplified since the $F^{m_1}_{J_1}(0)$ will vanish but for certain values of m_1.

If an alpha particle is emitted in the first transition then $m_1 = 0$ since $F^{m_1}_{J_1}(0) = 0$ unless $m_1 = 0$ for an alpha particle. Using this result and applying the relations (7) = (8) and $F^{m_2}_{J_2}(\theta) = F^{-m_2}_{J_2}(\theta)$ to (3) one obtains

$$(9) \qquad W(\theta) = \Big[\sum_m (C^{J'm\lambda_1}_{JmJ_1 0})^2 (C^{Jm\lambda_2}_{J''mJ_2 0})^2\Big] F^0_{J_2}(\theta) + 2\sum_{m_2=1}^{J_2}\Big[\sum_m (C^{J'm\lambda_1}_{JmJ_1 0})^2 (C^{Jm\lambda_2}_{J''m-m_2 J_2 m_2})^2\Big] F^{m_2}_{J_2}(\theta)$$

for the alpha(J_1)–particle(J_2) or alpha(J_1)–gamma(J_2) correlation function. The common factor $F^0_{J_1}(0)$ is omitted.

The emission of a photon in the first transition along the axis of quantization requires that $m_1 = \pm 1$ in (3) since $F^{m_1}_{J_1}(0) = 0$ unless $m_1 = \pm 1$ for a photon. Applying the relation (7) = (8) and setting $m_1 = \pm 1$ in (3), one obtains

$$(10) \qquad W(\theta) = \sum_{m_2=-J_2}^{J_2}\Big[\sum_m (C^{J'm+1\lambda_1}_{JmJ_1 1})^2 (C^{Jm\lambda_2}_{J''m-m_2 J_2 m_2})^2\Big] F^{m_2}_{J_2}(\theta)$$

for gamma(J_1)–particle(J_2) or gamma(J_1)–gamma(J_2) correlation functions. The common factor $2F^1_{J_1}(0)$ is omitted.

It has been shown by Falkoff and Uhlenbeck (3) that $W(\theta)$, as given by (3), is also the correlation function for the reverse transition scheme,

$$J'' \xrightarrow[J_2]{} J \xrightarrow[J_1]{} J'$$

with the emission of the particles or photons occurring in the reverse order. If also $J_1 = J_2$, then $W(\theta)$ in (3) further represents the directional correlation function for the reverse transition scheme,

$$J'' \xrightarrow[J_1]{} J \xrightarrow[J_2]{} J',$$

but with the emission of the particles or photons occurring in the given order. These results may be shown by applying the symmetry property (6*c*), the relation $F^m_J(\theta) = F^{-m}_J(\theta)$, to (3) with simple changes in the summation dummies m_1, m_2.

If for some transition $W(\theta) = 0$ then that transition can not occur, i.e. the angular momentum selection rules are not satisfied. Such cases are illustrated in the "special transitions" (iii) and (iv) of Section III.

II. A GENERAL METHOD FOR COMPUTATION OF SUMS GIVEN BY EQUATION (7)

As seen from the expression for $W(\theta)$, Equation (3), or from the expressions (9) and (10), the problem of computing $W(\theta)$ consists of finding a closed expression for the sum (7) which, as mentioned previously, is independent of the types of particles emitted. A method of evaluating such sums is given

below. The results can also be applied to sums appearing in mixture correlation functions.

A very direct method of evaluating (7) is as follows. It can be shown that the $(C)^2$ appearing in (7) are polynomials in m and hence the summand of (7) is a polynomial in m. Thus one can perform the indicated summation over m directly by using the known results for the sums $\sum_{m=J}^{J} m^k$, where k is a positive integer. If the numerical values of m_1 and m_2 are also prescribed, then the final result is a polynomial in J. It is not too difficult to find the rational roots of a polynomial. By finding the rational roots of this polynomial in J, one can express it in a partially factored form and some of the factors can be factored out of $W(\theta)$ and omitted, thus simplifying the final expression for $W(\theta)$. However, for J_1 and $J_2 \geqslant 2$, the summand in (7) is a polynomial in m of degree $\geqslant 8$ and so the direct procedure of evaluating (7) and then calculating $W(\theta)$ becomes clumsy.

In the method presented here one does not have to expand the complete summand into a polynomial in m but only part of it. Furthermore, the final result is automatically factored in terms of some of the rational roots (e.g. the factor $\binom{2J'+1}{2J''}$ in (28) is factored out of $W(\theta)$). These features make the calculation of correlation functions by this method simpler and easier than by the direct method.

The method is based on the fact that (7) can be reduced to the problem of summing either

$$S^r_{pnq} \equiv \sum_{v=0}^{n} \binom{p+v}{p}\binom{n+q-v}{q}(A_r v^r + A_{r-1}v^{r-1} + \ldots + A_0) \tag{11}$$

or

$$R^t_{PNQ} \equiv \sum_{v} \binom{P}{v}\binom{Q}{N-v}(B_t v^t + B_{t-1}v^{t-1} + \ldots + B_0) \tag{12}$$

after substituting explicit expressions for the C's and translating the sum over m to one over v. In (11) and (12), v takes on all those values for which the binomial coefficients do not vanish, i.e., it has the range defined by $0 \leqslant v \leqslant n$ in (11) and by $N-Q \leqslant v \leqslant N$ and $0 \leqslant v \leqslant P$ in (12).

In view of the form of Equations (11) and (12), the problem of evaluating (7) reduces to that of evaluating sums of the type

$$\sum_{v=0}^{n} \binom{p+v}{p}\binom{n+q-v}{q} v^k$$

and

$$\sum_{v} \binom{P}{v}\binom{Q}{N-v} v^k.$$

We first show the equivalence of (7) to (11) and (12) and then derive the formulae required to evaluate the above sums.

In the proof of the equivalence of (7) to (11) and (12), some expressions for the parameters appearing in (11) and (12) can be found. Further expressions can be found in Sections III and IV.

(*a*) To express (7) in the form (11):

From the definition (4) of $C^{Jm\lambda_2}_{J'm'' J_2 m_2}$ we may write

$$C^{J'm+m_1\lambda_1}_{JmJ_1m_1} = \left[\frac{(J'+m_1+m)!(J'-m_1-m)!}{(J+m)!(J-m)!(J_1+m_1)!(J_1-m_1)!}\right]^{\frac{1}{2}} P_1(m) \tag{13}$$

$$C^{Jm\lambda_2}_{J''m-m_2\ J_2m_2} = \left[\frac{(J+m)!(J-m)!}{(J''-m_2+m)!(J''+m_2-m)!(J_2+m_2)!(J_2-m_2)!}\right]^{\frac{1}{2}} P_2(m) \tag{14}$$

where $P_1(m)$ and $P_2(m)$ are polynomials in m, their explicit expressions being obtained from the definition.

The proof of (*a*) is divided into two cases, depending on whether the quantity $J_1 + J_2 - \lambda_1 - \lambda_2$ is $\geqslant 0$ or $\leqslant 0$.

(i) $J_1 + J_2 - \lambda_1 - \lambda_2 \geqslant 0$.

Substituting (13) and (14) into (7) one obtains

$$\sum_m (C^{J'm+m_1\lambda_1}_{JmJ_1m_1})^2 (C^{Jm\lambda_2}_{J''m-m_2J_2m_2})^2$$

$$= \sum_m \frac{(J'+m_1+m)!(J'-m_1-m)!}{(J''-m_2+m)!(J''+m_2-m)!} \tag{15}$$

$$\frac{[P_1(m)P_2(m)]^2}{(J_1+m_1)!(J_1-m_1)!(J_2+m_2)!(J_2-m_2)!}$$

$$= K\sum_m \binom{J'+m_1+m}{J''-m_2+m}\binom{J'-m_1-m}{J''+m_2-m}[P_1(m)P_2(m)]^2 \tag{16}$$

where

$$K = \frac{(J'-J''+m_1+m_2)!(J'-J''-m_1-m_2)!}{(J_1+m_1)!(J_1-m_1)!(J_2+m_2)!(J_2-m_2)!}.$$

In the binomial coefficients, it is required that

$$J'+m_1+m \geqslant J''-m_2+m \tag{17}$$

and

$$J'-m_1-m \geqslant J''+m_2-m \tag{18}$$

or $J' \geqslant J''$ and $m_1 + m_2 \geqslant 0$ (adding and subtracting (17) and (18)) or $J_1 + J_2 - \lambda_1 - \lambda_2 \geqslant 0$ and $m_1 + m_2 \geqslant 0$ (substituting for J' in terms of J''). Now since the summation (7) is equal to the summation (8), and by the last conditions (8) can be put in the form (16) if $J_1 + J_2 - \lambda_1 - \lambda_2 \geqslant 0$ and $-(m_1 + m_2) \geqslant 0$ or $m_1 + m_2 \leqslant 0$, it is seen that the condition $m_1 + m_2 \geqslant 0$ is irrelevant and hence can be discarded. We are then left with condition (i) which is satisfied for this case.

In order to have nonvanishing binomial coefficients in the summand of (16), m must take on values in the range

$$-J'' + m_2 \leqslant m \leqslant J'' + m_2 \tag{19}$$

which becomes

$$-J + J_2 + m_2 - \lambda_2 \leqslant m \leqslant J - J_2 + m_2 + \lambda_2 \tag{20}$$

upon substituting for J'' in terms of J. Using the upper and lower limits on m given by (19) and performing the translation $m = v - J'' + m_2$ on (16) one can show that (16) becomes

$$K\sum_{v=0}^{2J''}\binom{J' - J'' + m_1 + m_2 + v}{J' - J'' + m_1 + m_2}\binom{2J'' + J' - J'' - m_1 - m_2 - v}{J' - J'' - m_1 - m_2}P(v) \tag{21}$$

where $P(v)$ is a polynomial in v. This result is of the form (11). However, from the range on m as given by (20), it is seen that if $J_2 + m_2 - \lambda_2 < 0$ or $J_2 - m_2 - \lambda_2 > 0$ then m will take on values outside of its natural range $-J \leqslant m \leqslant J$. If the summand of (16) does not vanish for such values of m then the summation limits given by (19) must not be used and the result (21) does not follow. It is easily shown, however, that it does vanish owing to the vanishing of $[P_1(m)\ P_2(m)]^2$ for such values of m.

(ii) $J_1 + J_2 - \lambda_1 - \lambda_2 \leqslant 0$

For this case, we have

$$\sum_m (C^{J'm+m_1\lambda_1}_{Jm J_1 m_1})^2 (C^{Jm\lambda_2}_{J''m-m_2 J_2 m_2})^2 = \sum_m (C^{Jm2J_1-\lambda_1}_{J'm+m_1 J_1-m_1})^2 (C^{J''m-m_2 2J_2-\lambda_2}_{Jm J_2-m_2})^2$$

using the symmetry property (6c). Again, from the definition (4), expressions similar to those in (13) and (14) may be obtained for the C's appearing in the last summation. The remainder of the proof runs parallel to that given for (i).

(b) To express (7) in the form (12).

Here, the proof is very similar (although not identical) to the proof in Case (a), so that it may be omitted.

The formulae (11) and (12) are evaluated by the use of the formulae:

$$\sum_{v=0}^{n}\binom{p+v}{p}\binom{n+q-v}{q}v^k = \begin{cases}\binom{n+p+q+1}{n} & \text{for } k = 0\\ \sum_{\alpha=1}^{k} a_{k\alpha}\dfrac{(p+\alpha)!}{p!}\binom{n+p+q+1}{n-\alpha} & \text{for } k \geqslant 1\end{cases} \tag{22}$$

$$\sum_v \binom{P}{v}\binom{Q}{N-v}v^k = \begin{cases}\binom{P+Q}{N} & \text{for } k = 0\\ \sum_{\alpha=1}^{k} a_{k\alpha}\dfrac{P!}{(P-\alpha)!}\binom{P+Q-\alpha}{N-\alpha} & \text{for } k \geqslant 1,\end{cases} \tag{23}$$

where the coefficients $a_{k\alpha}$, listed in Table I, are obtained from the induction formula

TABLE I

A TABULATION OF THE COEFFICIENTS $a_{k\alpha}$ DEFINED BY EQUATION (24)

k	α									
	1	2	3	4	5	6	7	8	9	10
1	1	.	.	.	.	.	.	.	.	.
2	1	1	.	.	.	.	.	.	.	.
3	1	3	1	.	.	.	.	.	.	.
4	1	7	6	1	.	.	.	.	.	.
5	1	15	25	10	1	.	.	.	.	.
6	1	31	90	65	15	1	.	.	.	.
7	1	63	301	350	140	21	1	.	.	.
8	1	127	966	1701	1050	266	28	1	.	.
9	1	255	3025	7770	6951	2646	462	36	1	.
10	1	511	9330	34105	42525	22827	5880	750	45	1

$$(24)\qquad a_{k\alpha} = \begin{cases} 1 & \text{for } k \geqslant 1,\ \alpha = 1 \\ \sum_{\beta=1}^{k-\alpha+1} a_{k-\beta,\alpha-1}\binom{k-1}{\beta-1} & \text{for } k \geqslant 2,\ \alpha \geqslant 2. \end{cases}$$

If p and q are set equal to zero in (22), the binomial coefficients on the left hand side of the equation become unity and the summation reduces to the sum of the k^{th} power of the positive integers. The formulae (22) and (24) constitute an induction method of evaluating such summations. As mentioned previously, these sums are used in the direct method of evaluating (7).

The derivation of the formulae (22), (23), and (24) is given in the Appendix.

By substituting the summation formulae (22) and (23) into (11) and (12), the final forms,

$$(25)\quad S^r_{pnq} \equiv \sum_{\alpha=1}^{r}\left[\sum_{\beta=\alpha}^{r} A_\beta a_{\beta\alpha}\right]\frac{(p+\alpha)!}{p!}\binom{n+p+q+1}{n-\alpha} + A_0\binom{n+p+q+1}{n}$$

$$(26)\quad R^t_{PNQ} \equiv \sum_{\alpha=1}^{t}\left[\sum_{\beta=\alpha}^{t} B_\beta a_{\beta\alpha}\right]\frac{P!}{(P-\alpha)!}\binom{P+Q-\alpha}{N-\alpha} + B_0\binom{P+Q}{N},$$

for evaluating (11) and (12) are obtained. Only the terms containing A_0 and B_0 appear in each formula for the cases $r = 0$ and $t = 0$ respectively. In evaluating (7), the formula (25) or (26) is used depending on whether r or t has the smallest integral value i.e. for the smallest polynomial appearing in (11) or (12).

III. THE CASE OF "SPECIAL TRANSITIONS"

The transitions for which r and t are zero in the formulae (11) and (12) or (25) and (26) respectively will henceforth be called "special transitions." For these transitions the simplest summation formulae are used. These transitions are determined as follows.

The expressions for $C^{Jm\lambda_2}_{J''m''J_2m_2}$ are the simplest, for any m, m'', or m_2, when $\lambda_2 = 0, 2J_2, 2J''$. From the definition (4),

$$(27) \qquad C^{Jm0}_{J''m''J_2m_2} = \left[\frac{(J+m)!(J-m)!}{(J''+m'')!(J''-m'')!(J_2+m_2)!(J_2-m_2)!}\right]^{\frac{1}{2}},$$

the expressions for the other two values of λ_2 being obtained from (27) and the symmetry properties (6*c*), (6*d*). In each of the $(C)^2$'s in the summand of (7) the factor $(J+m)!\ (J-m)!$ will appear, either in the numerator or denominator, if the values of λ_1 and λ_2 are chosen from the set $0, 2J_1, 2J$, and the set $0, 2J_2, 2J''$ respectively. The simplest summand in (7) is obtained when a combination of λ_1 and λ_2 is chosen from the above values in such a way that the factor $(J+m)!\ (J-m)!$ will be cancelled out. Of the combinations possible only four permit such a cancellation. These are:

(i) $\lambda_1 = 0, \quad \lambda_2 = 0.$
(ii) $\lambda_1 = 2J_1, \quad \lambda_2 = 2J_2.$
(iii) $\lambda_1 = 2J, \quad \lambda_2 = 0.$
(iv) $\lambda_1 = 2J_1, \quad \lambda_2 = 2J''.$

The summations (7) for these four cases are evaluated below. The results may be used to calculate any correlation functions for the special transitions. In particular, some alpha–gamma and gamma–gamma correlation functions are given.

(i) $\lambda_1 = 0, \ \lambda_2 = 0$ or $J' = J + J_1, \ J = J'' + J_2.$

For this case the total angular momenta of the particles and nuclei resulting from each transition are parallel to one another. It is seen from condition (i) that J_1 and J_2 are the smallest angular momenta that can be emitted compatible with the angular momenta of the nuclear levels J', J, J''. The summation (7) is evaluated as follows:

$$\sum_m (C^{J'm+m_1 0}_{Jm J_1 m_1})^2 (C^{Jm0}_{J''m-m_2 J_2 m_2})^2$$

$$= \sum_m \frac{(J'+m_1+m)!}{(J_1+m_1)!(J_1-m_1)!(J''-m_2+m)!} \frac{(J'-m_1-m)!}{(J'+m_2-m)!(J_2+m_2)!(J_2-m_2)!}$$

(from (27))

$$= \binom{J_1+J_2+m_1+m_2}{J_1+m_1}\binom{J_1+J_2-m_1-m_2}{J_1-m_1} \sum_{m=-J+J_2+m_2}^{J-J_2+m_2} \binom{J'+m_1+m}{J_1+J_2+m_1+m_2}\binom{J'-m_1-m}{J_1+J_2-m_1-m_2}$$

(from (5))

$$= \binom{J_1+J_2+m_1+m_2}{J_1+m_1}\binom{J_1+J_2-m_1-m_2}{J_1-m_1} \sum_{v=0}^{2(J-J_2)} \binom{J_1+J_2+m_1+m_2+v}{J_1+J_2+m_1+m_2}\binom{2(J-J_2)+J_1+J_2-m_1-m_2-v}{J_1+J_2-m_1-m_2}$$

(using $m = v - J + J_2 + m_2$)

$$= \binom{J_1+J_2+m_1+m_2}{J_1+m_1}\binom{J_1+J_2-m_1-m_2}{J_1-m_1}\binom{2J'+1}{2J''}, \tag{28}$$

using the summation formula (22).

One can substitute this result into (3) to obtain the correlation function between a particle (J_1) or photon (J_1) and a particle (J_2) or photon (J_2), subject to the condition (i) on the angular momenta. If an alpha particle or photon is emitted along the axis of quantization in the first transition, the correlation functions are obtained by substituting (28) into (9) and (10). The results are:

$\alpha(J_1)$ − particle (J_2) or $\alpha(J_1)-\gamma(J_2)$:

$$W(\theta) = \binom{J_1+J_2}{J_1}^2 F^0_{J_2}(\theta) + 2\sum_{m_2=1}^{J_2}\binom{J_1+J_2+m_2}{J_1}\binom{J_1+J_2-m_2}{J_1}F^{m_2}_{J_2}(\theta) \tag{29}$$

$\gamma(J_1)$ − particle (J_2) or $\gamma(J_1)-\gamma(J_2)$:

$$W(\theta) = \sum_{m_2=-J_2}^{J_2}\binom{J_1+J_2+1+m_2}{J_1+1}\binom{J_1+J_2-1-m_2}{J_1-1}F^{m_2}_{J_2}(\theta) \tag{30}$$

where the factor $\binom{2J'+1}{2J''}$ has been omitted. In the case that a photon is emitted in the second transition with angular momentum $J_2=1$ (dipole) or $J_2=2$ (quadrupole) one obtains the correlation functions:

$\alpha(J_1)-\gamma(1)$:

$$W(\theta) = 1 - \frac{J_1}{3J_1+4}\cos^2\theta$$

$\alpha(J_1)-\gamma(2)$:

$$W(\theta) = 1 + \frac{6J_1(J_1+1)}{(J_1+3)(5J_1+8)}\cos^2\theta - \frac{3J_1(J_1-1)}{(J_1+3)(5J_1+8)}\cos^4\theta$$

$\gamma(J_1)-\gamma(1)$:

$$W(\theta) = 1 - \frac{J_1^2+J_1-3}{3J_1^2+7J_1+3}\cos^2\theta$$

$\gamma(J_1)-\gamma(2)$:

$$W(\theta) = 1 + \frac{6J_1(J_1^2+2J_1-5)}{(J_1+1)(5J_1^2+23J_1+30)}\cos^2\theta - \frac{3(J_1-1)(J_1^2+J_1-10)}{(J_1+1)(5J_1^2+23J_1+30)}\cos^4\theta. \tag{31}$$

Common factors have been omitted from these formulae.

(ii) $\lambda_1 = 2J_1$, $\lambda_2 = 2J_2$ or $J' = J - J_1$, $J = J'' - J_2$.

By using the third symmetry property (6c) together with (27) one can sum (7) as in Part (i) to get

$$(32)\qquad \sum_m (C^{J'm+m_1 2J_1}_{JmJ_1m_1})^2 (C^{Jm2J_2}_{J''m-m_2J_2m_2})^2$$
$$= \binom{J_1+J_2+m_1+m_2}{J_1+m_1}\binom{J_1+J_2-m_1-m_2}{J_1-m_1}\binom{2J''+1}{2J'}.$$

Since $\binom{2J''+1}{2J'}$ can be factored out of $W(\theta)$ just as $\binom{2J'+1}{2J''}$ was in Part (i), then, comparing the results (28) and (32), one can see that the correlation functions for this transition scheme are the same as those given in Part (i) i.e. the same as Equations (29), (30), and (31).

(iii) $\lambda_1 = 2J,\ \lambda_2 = 0$ or $J' = J_1 - J,\ J = J'' + J_2$.

From this condition it is evident that $J_1 \geqslant J$ — in fact, J_1 is here the largest angular momentum which can be emitted compatible with the angular momenta J', J. The calculation of correlation functions for this transition requires the use of the summation formula (23). Thus, (7) becomes

$$\sum_m (C^{J'm+m_1 2J}_{JmJ_1m_1})^2 (C^{Jm0}_{J''m-m_2J_2m_2})^2$$
$$= \sum_m \frac{(J_1+m_1)!}{(J'+m_1+m)!(J'-m_1-m)!(J''-m_2+m)!} \cdot \frac{(J_1-m_1)!}{(J''+m_2-m)!(J_2+m_2)!(J_2-m_2)!}$$

(from (27))

$$= \binom{J_1+m_1}{J_2-m_2}\binom{J_1-m_1}{J_2+m_2}\sum_m \binom{J'+J''+m_1+m_2}{J'+m_1+m}\binom{J'+J''-m_1-m_2}{J'-m_1-m}$$
$$= \binom{J_1+m_1}{J_2-m_2}\binom{J_1-m_1}{J_2+m_2}\sum_v \binom{J'+J''+m_1+m_2}{v}\binom{J'+J''-m_1-m_2}{2J'-v}$$
$$(33)\qquad = \binom{J_1+m_1}{J_2-m_2}\binom{J_1-m_1}{J_2+m_2}\binom{2J'+2J''}{2J'},$$

from (23). This result with (3) gives the correlation function between particles or photons subject to condition (iii). If an alpha particle is emitted in the first transition, then the correlation function is obtained from (33) and (9) i.e.

$$(34)\qquad W(\theta) = \binom{J_1}{J_2}^2 F^0_{J_2}(\theta) + 2\sum_{m_2=1}^{J_2}\binom{J_1}{J_2-m_2}\binom{J_1}{J_2+m_2}F^{m_2}_{J_2}(\theta).$$

If a photon is emitted in the first transition, then from (33) and (10),

$$(35)\qquad W(\theta) = \sum_{m_2=-J_2}^{J_2}\binom{J_1+1}{J_2-m_2}\binom{J_1-1}{J_2+m_2}F^{m_2}_{J_2}(\theta).$$

If a photon is also emitted in the second transition with angular momentum $J_2 = 1$, or 2 then, as in (i), one obtains the following correlation functions:

$\alpha(J_1) - \gamma(1)$: $$W(\theta) = J_1\left[1 - \frac{J_1 - 1}{3J_1 - 1}\cos^2\theta\right]$$

$\alpha(J_1) - \gamma(2)$:

$$W(\theta) = J_1(J_1 - 1)\left[(J_1 - 2) + \frac{6J_1(J_1 + 1)}{5J_1 - 3}\cos^2\theta - \frac{3(J_1 + 1)(J_1 + 2)}{5J_1 - 3}\cos^4\theta\right]$$

(36) $$\gamma(J_1) - \gamma(1): W(\theta) = 1 - \frac{J_1^2 + J_1 - 3}{3J_1^2 - J_1 - 1}\cos^2\theta$$

$\gamma(J_1) - \gamma(2)$:

$$W(\theta) = (J_1 - 1)\left[J_1 + \frac{6(J_1 + 1)(J_1^2 - 6)}{5J_1^2 - 13J_1 + 12}\cos^2\theta - \frac{3(J_1 + 2)(J_1^2 + J_1 - 10)}{5J_1^2 - 13J_1 + 12}\cos^4\theta\right],$$

from (34) and (35). Common factors have been omitted from the formulae (36). For those values of J_1 which make the factors appearing outside the square brackets vanish the transition can not take place. For, using the condition (iii), it is seen that $J_1 = J' + J'' + J_2$ i.e. the equation $J_1 \geqslant J_2$ must be satisfied if a transition occurs. Thus, for $0 \leqslant J_1 < J_2$ no transition producing an alpha (J_1) particle can occur, and for $1 \leqslant J_1 < J_2$ no transition producing a photon (J_1) can occur.

(iv) $\lambda_1 = 2J_1$, $\lambda_2 = 2J''$ or $J' = J - J_1$, $J = J_2 - J''$.

Here $J_2 = J'' + J' + J_1$ and so it is larger than any of the other angular momenta. It would be difficult to calculate correlation functions in terms of $\cos^2\theta$ for this case with arbitrary J_1 since by the last equation J_2 must also be arbitrary. However, correlation functions can be calculated with J_2 arbitrary and J_1 having some small value. Such correlation functions are given below.

To evaluate (7) for this case the summation formula (23) is used with (27) and the symmetry properties (6*c*) and (6*d*). Following the method employed in (iii) one can show that

(37) $$\sum_m (C^{J'm+m_1 2J_1}_{Jm J_1 m_1})^2 (C^{Jm2J''}_{J''m-m_2 J_2 m_2})^2 = \binom{J_2 + m_2}{J_1 - m_1}\binom{J_2 - m_2}{J_1 + m_1}\binom{2J' + 2J''}{2J'}.$$

If a photon is emitted along the axis of quantization in the second transition, then, omitting the factor $2F^1_{J_2}(0)\binom{2J' + 2J''}{2J'}$, the correlation function will be

(38) $$W(\theta) = \sum_{m_1 = -J_1}^{J_1}\binom{J_2 + 1}{J_1 - m_1}\binom{J_2 - 1}{J_1 + m_1}F^{m_1}_{J_1}(\theta)$$

from (6*a*). Comparing (38) and (35), one observes that the gamma(1)–gamma(J_2) and gamma(2)–gamma(J_2) correlation functions for this case are

the same as the gamma(J_1)–gamma(1) and gamma(J_1)–gamma(2) correlation functions respectively in (36) with J_1 replaced by J_2. The corresponding alpha–gamma correlations are calculated from (38). The results are:

$$\alpha(1) - \gamma(J_2): \qquad W(\theta) = 1 + \frac{J_2^2 + J_2 - 3}{J_2^2 - J_2 + 1}\cos^2\theta$$

$\alpha(2) - \gamma(J_2)$:

$$W(\theta) = (J_2 - 1)\Bigg[(J_2 - 2) + \frac{2(J_2^3 - 5J_2^2 + 36)}{3J_2^2 - J_2 + 6}\cos^2\theta + \frac{3(J_2 + 2)(J_2^2 + J_2 - 10)}{3J_2^2 - J_2 + 6}\cos^4\theta\Bigg]$$

(39) $$\gamma(1) - \gamma(J_2): \qquad W(\theta) = 1 - \frac{J_2^2 + J_2 - 3}{3J_2^2 - J_2 - 1}\cos^2\theta$$

$\gamma(2) - \gamma(J_2)$:

$$W(\theta) = (J_2 - 1)\Bigg[J_2 + \frac{6(J_2 + 1)(J_2^2 - 6)}{5J_2^2 - 13J_2 + 12}\cos^2\theta - \frac{3(J_2 + 2)(J_2^2 + J_2 - 10)}{5J_2^2 - 13J_2 + 12}\cos^4\theta\Bigg],$$

omitting common factors. By the same reasoning as that in (iii), one can show that no transition occurs for $J_2 = 1$ in the alpha(2)–gamma(J_2) and gamma(2)–gamma(J_2) correlation functions of (39).

IV. OTHER CASES

For a transition scheme next to a special one, i.e. a transition scheme characterized by λ_1, λ_2 for which the quantity $\lambda_1 + \lambda_2$ differs from that for a special transition by 1, the evaluation of the summation (7) is a little more difficult than for the special case. As an example, take the transition scheme $\lambda_1 = 0$, $\lambda_2 = 1$ or $J' = J + J_1$, $J = J'' + J_2 - 1$ (next to the special transition (i) in Section III) and evaluate (7) as follows:

From the definition (4), we have

$$C^{Jm1}_{J''m-m_2J_2m_2} = 2\Bigg[\frac{(J + m)!(J - m)!}{(J'' - m_2 + m)!(J'' + m_2 - m)!(J_2 + m_2)!(J_2 - m_2)!}\Bigg]^{\frac{1}{2}} \cdot [mJ_2 - m_2(J'' + J_2)],$$

and hence

$$\sum_m (C^{J'm+m_1 0}_{JmJ_1m_1})^2 (C^{Jm1}_{J''m-m_2J_2m_2})^2$$

$$= \sum_m \frac{(J' + m_1 + m)!(J' - m_1 - m)!}{(J_1 + m_1)!(J_1 - m_1)!(J'' - m_2 + m)!}$$

$$\frac{4[mJ_2 - m_2(J'' + J_2)]^2}{(J'' + m_2 - m)!(J_2 + m_2)!(J_2 - m_2)!}$$

$$= K \sum_m \binom{J' + m_1 + m}{J_1 + J_2 - 1 + m_1 + m_2} \binom{J' - m_1 - m}{J_1 + J_2 - 1 - m_1 - m_2}$$

$$\cdot [mJ_2 - m_2(J'' + J_2)]^2$$

$$= K \sum_{v=0}^{2J''} \binom{J_1 + J_2 - 1 + m_1 + m_2 + v}{J_1 + J_2 - 1 + m_1 + m_2} \binom{2J'' + J_1 + J_2 - 1 - m_1 - m_2 - v}{J_1 + J_2 - 1 - m_1 - m_2 \quad !}$$

$$\cdot [J_2 v - J''(J_2 + m_2)]^2$$

(using $m = v - J'' + m_2$)

$$= K \Big[J_2^2 (J_1 + J_2 + m_1 + m_2 + 1)(J_1 + J_2 + m_1 + m_2) \binom{2J' + 1}{2J'' - 2}$$

(40) $$+ (J_2^2 - 2J_2 J''(J_2 + m_2))(J_1 + J_2 + m_1 + m_2) \binom{2J' + 1}{2J'' - 1}$$

$$+ J''^2 (J_2 + m_2)^2 \binom{2J' + 1}{2J''} \Big]$$

(using (22)). Here

$$K = \frac{4}{(J_1 + J_2)^2 - (m_1 + m_2)^2} \binom{J_1 + J_2 + m_1 + m_2}{J_1 + m_1} \binom{J_1 + J_2 - m_1 - m_2}{J_1 - m_1}.$$

From (5), $-(J_1 + J_2 - 1) \leqslant m_1 + m_2 \leqslant J_1 + J_2 - 1$ hence the denominator of K does not vanish. The result (40) is awkward to use unless numerical values of the angular momenta are given. As the values of λ_1, λ_2 get farther away from those of the special transitions the summation results will become more awkward.

ACKNOWLEDGMENT

I wish to thank Prof. W. Opechowski for suggesting the research problem and for his advice and encouragement throughout the performance of the research.

This work was generously supported by a grant from the National Research Council of Canada.

APPENDIX

To derive the formulae (22) and (24);

The result (22) with $k = 0$ and 1 is first obtained. The formulae (22) and (24) then follow by induction.

To prove (22) for $k = 0$, one forms

$$(1 - x)^{-p-1}(1 - x)^{-q-1} = (1 - x)^{-p-q-2}$$

and expands each binomial to get

$$\sum_{v=0}^{\infty}\binom{p+v}{p}x^v\sum_{w=0}^{\infty}\binom{q+w}{q}x^w = \sum_{n=0}^{\infty}\binom{n+p+q+1}{n}x^n.$$

Collecting the coefficient of x^n on both sides of this equation one arrives at the result (22) for $k = 0$.

If $k = 1$, then

$$\begin{aligned}\sum_{v=0}^{n}\binom{p+v}{p}\binom{n+q-v}{q}v &= \sum_{v=1}^{n}\frac{(p+v)!}{(v-1)!\,p!}\binom{n+q-v}{q}\\ &= (p+1)\sum_{w=0}^{n-1}\binom{p+1+w}{p+1}\binom{n-1+q-w}{q}\\ &= (p+1)\binom{n+p+q+1}{n-1}\end{aligned}$$

using (22) with $k = 0$.

Now assume (22) is true for all values of k up to $k = r - 1$ ($r \geqslant 2$). Then

$$\begin{aligned}&\sum_{v=0}^{n}\binom{p+v}{p}\binom{n+q-v}{q}v^r\\ &\quad= \sum_{v=1}^{n}\frac{(p+v)!}{(v-1)!\,p!}\binom{n+q-v}{q}v^{r-1}\\ &\quad= (p+1)\sum_{w=0}^{n-1}\binom{p+1+w}{p+1}\binom{n-1+q-w}{q}(w+1)^{r-1}\\ &\quad= (p+1)\sum_{w=0}^{n-1}\binom{p+1+w}{p+1}\binom{n-1+q-w}{q}\left[\sum_{\gamma=1}^{r-1}\binom{r-1}{\gamma}w^\gamma + 1\right]\\ &\quad= (p+1)\sum_{\gamma=1}^{r-1}\binom{r-1}{\gamma}\sum_{\lambda=1}^{\gamma}a_{\gamma\lambda}\frac{(p+1+\lambda)!}{(p+1)!}\binom{n+p+q+1}{n-\lambda-1}\\ &\qquad\qquad + (p+1)\binom{n+p+q+1}{n-1}\end{aligned}$$

(using the induction assumption)

$$\begin{aligned}&= (p+1)\sum_{\lambda=1}^{r-1}\left[\sum_{\gamma=\lambda}^{r-1}a_{\gamma\lambda}\binom{r-1}{\gamma}\right]\frac{(p+1+\lambda)!}{(p+1)!}\binom{n+p+q+1}{n-\lambda-1}\\ &\qquad\qquad + (p+1)\binom{n+p+q+1}{n-1}\end{aligned}$$

$$= \sum_{\alpha=2}^{r}\left[\sum_{\gamma=\alpha-1}^{r-1} a_{\gamma,\alpha-1}\binom{r-1}{\gamma}\right]\frac{(p+\alpha)!}{p!}\binom{n+p+q+1}{n-\alpha} + (p+1)\binom{n+p+q+1}{n-1}$$

$$= \sum_{\alpha=2}^{r}\left[\sum_{\beta=1}^{r-\alpha+1} a_{r-\beta,\alpha-1}\binom{r-1}{r-\beta}\right]\frac{(p+\alpha)!}{p!}\binom{n+p+q+1}{n-\alpha} + (p+1)\binom{n+p+q+1}{n-1}$$

$$= \sum_{\alpha=1}^{r} a_{r\alpha}\frac{(p+\alpha)!}{p!}\binom{n+p+q+1}{n-\alpha}$$

where

$$a_{r\alpha} = \begin{cases} 1 & \text{for } r \geqslant 1,\ \alpha = 1 \\ \sum_{\beta=1}^{r-\alpha+1} a_{r-\beta,\alpha-1}\binom{r-1}{\beta-1} & \text{for } r \geqslant 2,\ \alpha \geqslant 2. \end{cases}$$

This completes the proof of (22) and (24).

To derive the formula (23);

The formula (23) may be derived by using the same method as that already given for the formulae (22) and (24) starting with the equation

$$(1-x)^{P}(1-x)^{Q} = (1-x)^{P+Q}$$

instead of

$$(1-x)^{-p-1}(1-x)^{-q-1} = (1-x)^{-p-q-2}$$

and expanding the binomials using the formula

$$(1-x)^{P} = \sum_{v=0}^{P}\binom{P}{v}(-x)^{v}$$

instead of

$$(1-x)^{-P} = \left[\sum_{v=0}^{\infty}\binom{-P}{v}(-x)^{v}\right] = \sum_{v=0}^{\infty}(-1)^{v}\binom{P-1+v}{v}(-x)^{v}.$$

However, the relation

$$\binom{-P}{v} = (-1)^{v}\binom{P-1+v}{v}$$

is all that is needed to get (23) from (22). If one sets $-p-1=P$ and $-q-1=Q$ in (22) then (23) can be obtained using this relation. The limits for the summations are determined from the range for which the binomial coefficients appearing in the summand do not vanish.

REFERENCES

1. CONDON, E. U. and SHORTLEY, G. H. Theory of atomic spectra. Cambridge University Press, London. 1935. P. 73.
2. FALKOFF, D. L. Phys. Rev. 82: 98. 1951.
3. FALKOFF, D. L. and UHLENBECK, G. E. Phys. Rev. 79: 323. 1950. Compare also LLOYD, S. P. Phys. Rev. 80: 118. 1950; and SPIERS, J. A. Phys. Rev. 80: 491. 1950.
4. GOERTZEL, G. Phys. Rev. 70: 897. 1946.
5. HAMILTON, D. R. Phys. Rev. 58: 122. 1940.
6. LING, D. S. and FALKOFF, D. L. Phys. Rev. 76: 1639. 1949.
7. LLOYD, S. P. Phys. Rev. 83: 716. 1951.
8. RACAH, G. Phys. Rev. 62: 438. 1942.

SUR QUELQUES PROBLÈMES POSÉS PAR LES MÉTHODES D'ANALYSE DES GRAPHIQUES PAR LE CALCUL[1]

PAR M. LEVY

I. RÉSUMÉ

Les méthodes d'analyse des graphiques par le calcul ont posé de nombreux problèmes dont les solutions paraissent très difficiles à trouver:

(1) Est-il possible de trouver des combinaisons* dont la sélectivité est en forme de bande passante et qui n'exigent pas trop d'opérations?

(2) Le résultat des analyses est-il unique? C'est à dire que si on arrive à des résultats par des combinaisons de natures différentes, ces résultats devront-ils être les mêmes?

Ces problèmes ont été étudiés très longuement dans un grand nombre de publications mais il ne semble pas qu'ils aient été réellement résolus. Dans ce travail nous montrons comment on peut résoudre simplement ces questions en considérant d'abord des opérations continues et en passant ensuite aux opérations discontinues. Cela revient à considérer des intégrales d'abord et à passer ensuite aux combinaisons de sommes et différences. Nous montrons comment ce passage peut se faire simplement et nous montrons que le résultat des analyses est unique, quel que soit le procédé utilisé pourvu que certaines règles soient respectées. Nous montrons aussi qu'il existe des combinaisons pratiques donnant une sélectivité en forme de bande passante. Nous démontrons aussi une propriété nouvelle et intéressante des transformantes (réponses impulsiales) des filtres électriques à dephasage linéaire.

II. INTRODUCTION

Les méthodes d'analyse des graphiques par le calcul ont été étudiées depuis le temps de Lagrange et des méthodes remarquablement simples ont été proposées (23, 3) du genre utilisé plus tard par le Professeur Labrouste (5, 6, 7).

Le principe fondamental utilisé dans ces méthodes est le suivant:

Considérons une sinusoide d'amplitude unité par example, et faisons sur cette courbe la transformation suivante: traçons deux ordonnées d'abscisses t et $t + t_0$, t_0 étant une constante; multiplions l'amplitude de la première ordonnée par λ_1 et celle de la seconde par λ_2, λ_1 et λ_2 étant des paramètres de valeurs arbitraires; prenons maintenant la somme:

$$Y = \lambda_1 Y_1 + \lambda_2 Y_2 = \lambda_1 \cos \omega t + \lambda_2 \cos \omega (t + t_0)$$

comme ordonnée d'abscisse t. Lorsque t varie, les trois ordonnées Y, Y_1, et Y_2 se déplacent et le point de coordonnées (Y, t) décrit une courbe. On a:

$$Y = \sqrt{\lambda_1^2 + \lambda_2^2 + 2\lambda_1\lambda_2 \cos \omega t_0} \cos (\omega t + \phi_0) \tag{1}$$

avec

$$\sin \phi_0 = \lambda_2 \sin \omega t_0 / \sqrt{\lambda_1^2 + \lambda_2^2 + 2\lambda_1\lambda_2 \cos \omega t_0}.$$

[1] *Manuscrit original reçu le 6 janvier, 1951, et sous forme revisée le 11 Octobre, 1951. Contribution de l'Établissement des Télécommunications du Conseil des Recherches pour la Défense.*

* *L'analyse des graphiques par le calcul consiste à faire des combinaisons d'opérations arithmétiques sur les ordonnées successives de la courbe à analyse. On démontre que ces combinaisons sont sélectives, c'est à dire favorisent certaines fréquences et éliminent d'autres.*

On voit que quand on transforme une sinusoide par une opération du genre indiqué plus haut, on obtient une sinusoide de même fréquence, l'amplitude et la phase étant seules fonctions des paramètres λ_1, λ_2 et t_0 de la transformation.

D'autre part la relation (1) montre que l'amplitude de la transformée est

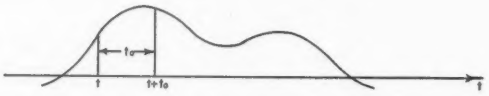

FIG. 1. Principe de la méthode d'analyse des graphiques par le calcul.

fonction de la fréquence de la sinusoide à transformer; quand celle-ci varie, l'amplitude varie également, passant par des maxima et minima successifs. Ceci montre que les transformations définies plus haut sont *sélectives*, la sélectivité étant fonction des paramètres de la transformation.

De ces propriétés on déduit une méthode d'analyse par le calcul; il suffit pour cela de choisir convenablement les paramètres de la transformation pour éliminer les transformations gênantes et amplifier celles que l'on désire isoler. Mais en général une transformation du genre indiqué plus haut ne suffit pas pour éliminer les composantes gênantes; il faut choisir des transformations plus complexes, realisées en prenant plusieurs ordonnées au lieu de deux seulement. Les propriétés énoncées plus haut restent applicables dans ce cas puisque la relation (1) peut se généraliser et s'ecrire

$$\sum_i \lambda_i \cos \omega(t + t_i) = Y \cos \omega(t + t_i) \tag{3}$$

avec

$$Y = f(\lambda_i, t_i, \omega) \tag{4}$$

$$\phi = g(\lambda_i, t_i, \omega). \tag{5}$$

M. et Mme Labrouste ont etudié systématiquement des transformations de ce genre, et dans une série de publications échelonnées entre 1927 et 1933 et dans un ouvrage d'ensemble (5, 6, 7 et 8) ils ont donné les resultats de leurs études. Ils ont montré en particulier que par un choix convenable des combinaisons (coéfficients λ_i), on pouvait obtenir des courbes de sélectivité avec une pointe prédominante. Toutefois le choix des combinaisons se fait plus ou moins par tâtonnements et est extrêmement laborieux.

Dans un mémoire publié en 1934 (14), j'ai proposé de remplacer les sommes par des intégrales. De cette facon on peut généraliser les résultats précédants et les appliquer à de nombreux phénomènes en apparence indépendant les uns des autres (15, 16).

Considérons une courbe $y = f_{(t)}$; tracée sur un graphique et rapportée à deux axes fixes *oy* et *ot* (Fig. 2). Soit, d'autre part, $Y = F_{(T)}$ une seconde courbe mobile par rapport à la première (tracée par example sur une feuille transparente posée sur le graphique) et définie par rapport au trièdre de Galilée

YOT. Nous supposerons que les mouvements de la courbe Y sont des translations telles que l'axe OT glisse toujours sur l'axe ot. A l'aide de cette courbe mobile nous transformons la courbe du graphique de la façon suivante: la courbe Y étant dans une position bien déterminée ($oO = \tau$) nous ferons, pour chaque abscisse t, le produit Yy des ordonnées correspondantes des deux courbes et nous intégrerons pour toutes valeurs de t. Nous marquerons ensuite sur la graphique un point dont l'abscisse est τ et dont l'ordonnée est égale à l'intégrale en question. Nous obtiendrons aussi une nouvelle courbe $y = \mathfrak{F}_{(\tau)}$.

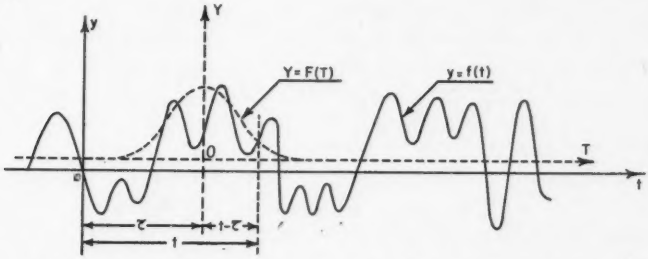

FIG. 2. Transformation d'une courbe. $y = f_{(t)}$ est la courbe à transformer: $Y = F_{(\tau)}$ est la transformante. *YOT* est un trièdre de galilée se deplaçant par translation parallele à *ot*.

La courbe initiale étant la *courbe à transformer* $y = f_{(t)}$ nous appellerons *courbe de transformation* ou *transformante* la courbe $Y = F_{(T)}$ et *transformée* la courbe résultante $y = \mathfrak{F}_{(\tau)}$.

On peut démontrer très facilement que cette transformation est sélective et que la courbe de sélectivité et la courbe de phase sont identiques aux courbes de fréquence et de phase de la transformante. On obtient ces courbes par les intégrales réciproques de Fourier (14, 16). Inversement les intégrales de Fourier permettront de déterminer la forme de la transformante correspondant à une courbe de sélectivité et une courbe de phase données. On peut démontrer facilement que la transformante est la réponse impulsiale (réponse à l'impulsion de Dirac) (20) d'un filtre ayant les courbes de sélectivité et de phase considerées. En particulier à une courbe de sélectivité en forme de bande passante correspondra une transformante en forme de "groupe", c'est à dire en forme de battement entre deux oscillations de fréquences voisines. Des lors l'idée vient de calculer d'abord les transformantes continues correspondant aux courbes de sélectivité voulues et de ces courbes déduire les combinaisons disconnues qui seules peuvent être utilisées dans les calculs. La difficulté naturellement est dans le passage des courbes continues aux courbes discontinues. M. et Mme Labrouste cherchèrent à convertir leurs sommes en intégrales et publièrent les résultats de leurs études dans une série de mémoires et dans un ouvrage d'ensemble paru de 1935 à 1943 (9, 10, 11 et 12). La façon dont ils traitent le problème ne leur permet pas d'aller trop loin. Par example ils cherchent à utiliser une transformante correspondant à une courbe de sélectivité du genre passe-bande, mais ils remarquent que les groupes d'oscil-

lations s'amortissent très lentement, comme $1/t$ et en déduisent que ce genre de transformante n'est pas très utile pour les applications pratiques. Si on néglige les groupes secondaires à partir d'un certain rang, des oscillations apparaissent au sommet de la courbe de sélectivité et rendent ces courbes peu utiles (10). D'autre part la façon de passer des sommes aux intégrales ne nous parait pas très féconde en ce qu'elle manque de généralité et ne permet pas de résoudre le problème de l'unicité d'une façon simple.

Dans cette note nous nous proposons de montrer qu'au lieu de passer des sommes aux intégrales il vaut mieux passer des intégrales aux sommes, comme nous l'avons signalé plus haut, et nous montrons comment ce passage des courbes continues aux courbes discontinues peut se faire d'une façon très simple qui permet de donner un sens très précis aux problèmes d'unicité. D'autre part nous montrons que l'on peut réaliser des courbes de sélectivité du genre passe-bande avec une approximation raisonable et un nombre de groupes d'oscillations secondaires limité.

Nous commencerons d'abord par l'étude du genre de filtre passe-bande à utiliser. Nous passerons ensuite à l'étude du passage des transformantes continues aux transformantes discontinues.

III. TYPES DE FILTRES ET TRANSFORMANTES À UTILISER

Nous supposerons que le graphique est un mélange d'une série d'ondes sinusoidales ou entretenues ou amorties. Le spectre est alors formé par une série de paquets ou groupes de fréquences qui dans les cas les plus simples sont séparés les uns des autres. C'est ce que nous supposerons être le cas pour simplifier l'analyse. L'extension au cas général ne présente aucune difficulté.

Considérons par example le cas de la fig. 3 où six groupes sont représentés. Pour séparer ces groupes sans distortion, il faut utiliser des filtres du genre

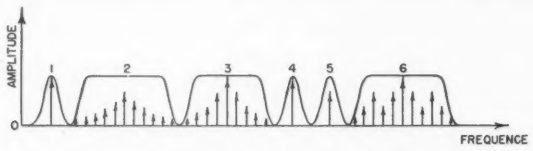

FIG. 3. Spectre d'une courbe complexe formée par trois composantes sinusoidales 1, 4 et 5 et 3 signaux de "groupe" 2, 3 et 6.

représenté en pointillé. Pour des oscillations amorties (groupes No. 2, 3 et 6) ces filtres doivent être du type passe-bande à sommet plat sur toute la region où les composantes de fréquence ont une amplitude appréciable. (Dans le cas où les groupes ont des composantes entrelacées, il faut utiliser des filtres en "peigne" (19) à bande passante dont la forme présente des maxima équidistants et coincidant avec les composantes à isoler, les maxima étant localisés dans une bande passante). D'autre part la courbe de phase doit être linéaire, c'est à dire que le retard introduit par le filtre doit être le même pour toutes les fréquences de la bande passante.

Pour réaliser ce genre de filtre considérons d'abord un filtre idéal passe-bande, c'est à dire un filtre à déphasage linéaire et à coupures brusques, ne laissant passer que les fréquences comprises entre les fréquences de coupures f_1 et f_2 (ou les pulsations comprises entre les pulsations de coupure ω_{c1} et ω_{c2}).* La transformante (ou réponse impulsiale) de ce filtre s'obtient à l'aide de l'intégrale de Fourier (22).

$$T_{B(t)} = \frac{1}{\pi}\int_{\omega c1}^{\omega c2} \cos \omega(t - t_0)d\omega$$

$$= \frac{\omega_{c2}}{\pi}\frac{\sin \omega_{c2}(t - t_0)}{\omega_{c2}(t - t_0)} - \frac{\omega_{c1}}{\pi}\frac{\sin \omega_{c1}(t - t_0)}{\omega_{c1}(t - t_0)} \tag{6}$$

Sous cette forme on voit que la transformante du filtre passe-bande est la différence des réponses impulsiales de deux filtres passe-bas de coupure respectives ω_{c1} et ω_{c2} ce qui est évident. On peut aussi écrire:

$$T_{B(t)} = \frac{\Delta\omega}{\pi}\frac{\sin \frac{1}{2}[\Delta\omega(t - t_0)]}{\frac{1}{2}\Delta\omega(t - t_0)} \cos \omega_0 t. \tag{7}$$

Cette courbe est representée en figure 4. Elle comprend un groupe central d'oscillations précedé et suivi par une série de groupes d'oscillations secon-

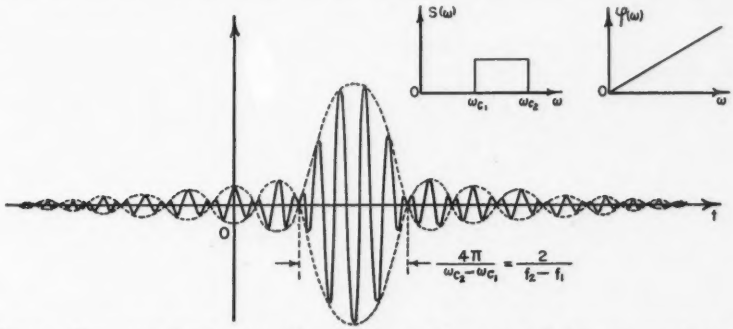

FIG. 4. Filtre passe-bande idéal et transformante (réponse impulsiale) correspondante.

daires, dont l'amplitude maximum s'amortit lentement en raison inverse de l'éloignement.

Le Professeur et Mme Labrouste ont essayé de négliger les oscillations secondaires à partir d'un certain rang, mais ils ont remarqué que cela entraîne des oscillations appréciables de la partie plate de la bande passante. Ils concluent que les filtres passe-bande ne peuvent pas être utilisés en pratique.

En réalité les auteurs n'ont pas remarqué que ce qu'ils ont observé est analogue au phénomène bien connu de Gibbs; si on supprime des oscillations secondaires qui s'amortissent en raison inverse du temps, des oscillations apparaissent sur la courbe de filtrage. Dès lors l'idée vient de réaliser des filtres passe-bande dont la transformante présente des oscillations secondaires

* *Dans cet article, lire* ω_{c_1} *au lieu de* ω_{c1} *et* $\omega c1$. *Pareillement lire* ω_{c_2} *au lieu de* ω_{c2} *et* $\omega c2$.

qui s'amortissent très rapidement. Nous avons déjà démontré que pour obtenir ce résultat il suffit de considérer des filtres à coupure progressive linéaire. Nous allons maintenant généraliser ce résultat et démontrer que pour les filtres a déphasage linéaire:

(1) Si la courbe de filtrage présente des discontinuités, les oscillations secondaires s'amortissent comme $1/t$;

(2) Si la courbe de filtrage est continue et si la dérivée première présente des discontinuités, les oscillations secondaires s'amortissent comme $1/t^2$;

(3) Si la courbe de filtrage et les $(n-1)$ premières dérivées sont continues et si la n^{me} dérivée est discontinue, les oscillations secondaires de la transformante s'attenuent comme $1/t^{n+1}$.

Pour le démontrer supposons que la courbe de fréquence du filtre est $S_{(\omega)}$ et la courbe de phase $\phi_{(\omega)}$. La transformante est donnée par l'intégrale de Fourier (20):

$$T_{(t)} = \frac{1}{\pi}\int_0^\infty S_{(\omega)} \cos\left[\omega t + \phi_{(\omega)}\right] d\omega. \tag{8}$$

$T_{(t)}$ est la partie réelle de

$$\tau_{(t)} = \frac{1}{\pi}\int_0^\infty S_{(\omega)} e^{i[\omega t + \phi(\omega)]} d\omega. \tag{9}$$

Dans tous les filtres utilisés pour l'analyse des graphiques, les transformantes correspondantes sont symétriques de sorte que la courbe de phase est zéro. Nous considérerons le cas des filtres à déphasage linéaire, le déphasage zéro étant un cas particulier. Nous avons, avec cette hypothèse:

$$\phi_{(\omega)} = (\omega - \omega_0)t_0 \tag{10}$$

où t_0 et ω_0 sont des constants. Pour un filtre passe-bande à courbe symétrique autour d'un axe vertical, ω_0 est l'abscisse de cet axe. Remplaçant $\phi_{(\omega)}$ dans (9) par sa valeur donnée par (10), il vient:

$$\tau_{(t)} = \frac{e^{-i\omega 0\, t0}}{\pi}\int_0^\infty S_{(\omega)} e^{i\omega(t-t0)} d\omega. \tag{11}^*$$

Si nous intégrons par parties, nous obtenons:

$$\tau_{(t)} = \frac{e^{-i\omega 0\, t0}}{i\pi(t-t_0)}\left[S_{(\omega)} e^{i\omega(t-t0)}\right]_0^\infty - \frac{e^{-i\omega 0\, t0}}{i\pi(t-t_0)}\int_0^\infty S'_{(\omega)} e^{i\omega(t-t0)} d\omega. \tag{12}$$

Pour aller plus loin nous devrons considérer les discontinuités de la fonction $S_{(w)}$. Appelons S_j la discontinuité de $S_{(w)}$ pour $\omega = \omega_j$. Par définition nous avons:

$$S_j = S_{(\omega j+0)} - S_{(\omega j-0)} \tag{13}^{**}$$

où 0 est la valeur limite d'une quantité infiniment petite $d\omega$ (12) s'écrit alors:

$$\tau_{(t)} = \frac{-e^{-i\omega 0\, t0}}{i\pi(t-t_0)}\sum_{j=0}^{\infty} S_j e^{i\omega j(t-t0)} - \frac{e^{-i\omega 0\, t0}}{i\pi(t-t_0)}\int_0^\infty S'_{(\omega)} e^{i\omega(t-t0)} d\omega. \tag{14}$$

* *Dans cet article, lire* ω_0 *et* t_0 *au lieu de* $\omega 0$ *et* $t0$.
** *Dans cet article, lire* $\omega_j, \omega_k, \omega_l, \omega_m, \omega_a$ *au lieu de* $\omega j, \omega k, \omega l, \omega m, \omega a$.

On peut répéter la même opération indéfiniment. Si les discontinuités des dérivées $S'(w)$, $S''(w)$, ... sont S_k', S_l'' ...., par intégration par parties successives on obtient:

$$\begin{aligned}\pi e^{i\omega_0 t_0}\tau_{(t)} &= \frac{i}{t-t_0}\sum S_j e^{i\omega_j(t-t_0)} + \frac{i}{t-t_0}\int_0^\infty S_{(\omega)} e^{i\omega(t-t_0)} d\omega \\ &= \frac{i}{t-t_0}\sum_j S_j e^{i\omega_j(t-t_0)} - \frac{i}{(t-t_0)^2}\sum_k S_k' e^{i\omega_k(t-t_0)} d\omega \\ &- \frac{i}{(t-t_0)^3}\sum_l S_l'' e^{i\omega_l(t-t_0)} + \frac{1}{(t-t_0)^4}\sum_m S_m''' e^{i\omega_m(t-t_0)} \\ &+ \ldots .\end{aligned} \tag{15A}$$

La partie réelle donne $T_{(t)}$:

$$\begin{aligned}\pi e^{i\omega_0 t_0} T_{(t)} = &- \frac{1}{t-t_0}\sum_j S_j \sin\omega_j(t-t_0) - \frac{1}{(t-t_0)^2}\sum_k S_k' \cos\omega_k(t-t_0) \\ &+ \frac{1}{(t-t_0)^3}\sum_l S_l'' \sin\omega_l(t-t_0) \\ &+ \frac{1}{(t-t_0)^4}\sum_m S_m''' \cos\omega_m(t-t_0) \\ &- \ldots .\end{aligned} \tag{15B}$$

De cette équation on déduit facilement les propriétés enoncées plus haut.

Pour se rendre compte de l'amplitude des oscillations secondaires calculons la forme de la transformante pour un filtre passe-bande à coupure progressive linéaire, c'est à dire un filtre à réponse plate de ω_1 à ω_2 et à coupure progressive

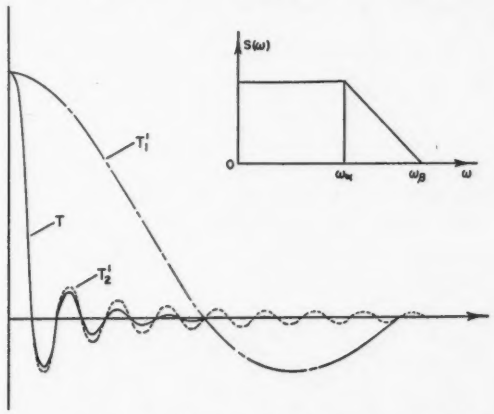

FIG. 5. Transformante d'un filtre idéal passe-bas à coupure progressive. T'_1 et T'_2 sont les transformantes respectives de filtres idéaux passe-bas à coupure brusque à $(\omega_\beta + \omega_\alpha)/2$ et $(\omega_\beta - \omega_\alpha)/2$. T est la résultante.

linéaire à gauche de ω_1 et à droite de ω_2 (fig. 6). Nous supposerons pour simplifier que la courbe de phase est linéaire et que la courbe de fréquence est

symétrique par rapport à la fréquence moyenne $\omega_0 = \frac{\omega_1 + \omega_2}{2}$. On peut démontrer que la transformante d'un filtre passe-bande à courbes de fréquences et de phases symétriques s'obtient en multipliant par $\cos\frac{\omega_1 + \omega_2}{2}t$ la transformante du filtre passe-bas correspondant, c'est à dire celui obtenu en posant $\omega_0 = 0$. La transformante du filtre passe-bas s'obtient très facilement par intégration directe. On remarquera que l'on peut intégrer d'abord sur la partie plate $0 - \left(\frac{\omega_2 - \omega_1}{2}\right)$ et ensuite sur la partie en pente. Sur la partie plate le résultat est le même que pour un filtre passe-bas à coupure brusque à la fréquence $\frac{\omega_2 - \omega_1}{2} = \omega_2$. On a:

$$T_{1(t)} = \frac{1}{2\pi}\int_{-\omega_a}^{+\omega_a} e^{i\omega t} e^{i\phi(\omega)} d\omega$$

où l'intégration est étendue aux fréquences négatives pour permettre d'utiliser la forme complexe des intégrales de Fourier (22). Comme $\phi_{(\omega)}$ est une courbe linéaire, nous pouvons poser:

$$\phi_{(\omega)} = -\omega t_0 \pm 2k\pi$$

d'où:

$$T_{1(t)} = \frac{1}{2\pi}\int_{-\omega_a}^{+\omega_a} e^{i\omega(t-t0)} d\omega.$$

On trouve, tous calculs faits:

$$T_{1(t)} = \frac{\omega_a}{\pi}\frac{\sin\omega_a(t - t_0)}{\omega_a(t - t_0)}.$$

Sur la partie en pente il est plus facile d'utiliser la forme trigonométrique des intégrales de Fourier pour éviter l'intégration dans la région des fréquences négatives. On a:

$$T_{2(t)} = \frac{1}{\pi}\int_{\omega_a}^{\omega_\beta}\frac{\omega_\beta - \omega}{\omega_\beta - \omega_a}\cos\omega t\, d\omega$$

$$= \frac{1}{\pi(\omega_\beta - \omega_a)t}\left[(\omega_\beta - \omega_a)\sin\omega_a t + \frac{1}{t}(\cos\omega_\beta t - \cos\omega_a t)\right].$$

D'où, tous calculs faits:

$$T_{(t)} = T_{1(t)} + T_{2(t)} = \frac{\omega_\beta + \omega_a}{2}\frac{\sin\frac{\omega_\beta - \omega_a}{2} + \sin\frac{\omega_\beta + \omega_a}{2}t}{\frac{\omega_\beta - \omega_a}{2}t\ \frac{\omega_\beta + \omega_a}{2}t}.$$

On voit que la transformante est le produit de la transformante d'un filtre passe-bas à coupure brusque à $\frac{\omega_\beta + \omega_\alpha}{2}$ et d'un autre à coupure brusque à $\frac{\omega_\beta - \omega_\alpha}{2}$. Les deux composantes et la résultante sont representées sur la figure 5. En moyenne, les oscillations secondaires décroissent comme $1/t^2$. La figure 6 donne la courbe résultante pour un cas typique, celui pour lequel

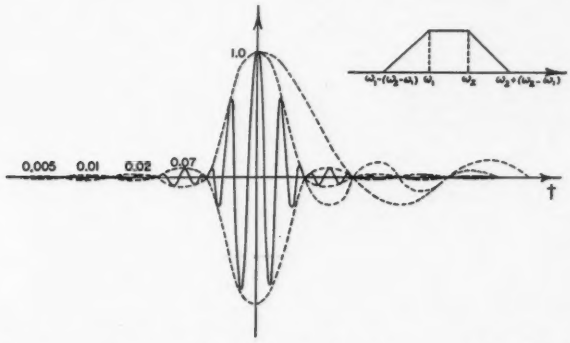

FIG. 6. Transformante d'un filtre passe-bande idéal à coupure progressive montrant une seule oscillation secondaire d'amplitude non négligeable.

chaque partie du filtre à atténuation linéaire progressive occupe une bande de fréquence égale à celle de la partie plate du filtre. On voit que l'on peut négliger tous les groupes secondaires en dehors du premier ou des deux premiers sans déformer la courbe filtrante d'une façon appréciable. Le groupe à filtrer peut occuper environ $(4/6)^{me}$ de la bande sans déformation appréciable. On voit que le Professeur et Mme Labrouste n'ont pu obtenir ces resultats parce qu'ils n'ont examiné que le cas des filtres à coupure brusque.

IV. PASSAGE DES TRANSFORMANTES CONTINUES AUX TRANSFORMANTES DISCONTINUES

Jusqu'ici nous n'avons considéré que *des transformantes continues*. Une fois que l'on décide à peu près le genre de filtre que l'on désire utiliser, un calcul très simple donne en général la transformante voulue (fig. 3 et 5). Comment maintenant passer aux transformantes discontinues? Ici encore nous allons opérer d'une façon tout a fait différente de celle du Professeur Labrouste, plus générale et plus féconde. Considérons un train $I_{(t)}$ d'impulsions de Dirac périodiques (fig. 7) dont la fréquence de répétition est f_r. Le spectre de ce train est une série de composantes de même amplitude C et de fréquences 0, f_r, $2f_r$, $3f_r$, ... On peut écrire:

$$I_{(t)} = C[1 + \sum_n \cos n\omega_r t].$$

Multiplions ce train par la transformante $T_{(t)}$. *On obtient la transformante discontinue voulue.* On a:

$$I_{(t)}T_{(t)} = C[T_{(t)} + \sum_n T_{(t)} \cos n\omega_r t].$$

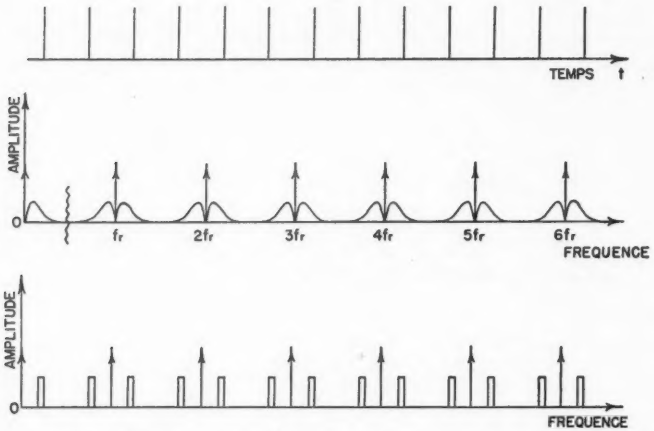

FIG. 7. (*a*) Transformante $I_{(t)}$.
(*b*) Spectre d'une transformante discontinue.
(*c*) Spectre d'une transformante type passe-bande discontinue.

Si on remplace $T_{(t)}$ par son spectre de fréquences, on obtient une série de spectres comme représenté en figure 7*b*. Chaque porteur de fréquence nf_r est entouré par deux bandes latérales dont la forme est identique à celle du spectre de $T_{(t)}$. Ceci est facile à démontrer par des méthodes classiques. *L'ensemble représente le spectre de la transformante discontinue.* On voit que la discontinuité a pour effet de multiplier les spectres comme dans deux miroirs parallèles.

Nous pouvons maintenant dire comment choisir la périodicité. Si le graphique ne présente pas de composantes d'amplitude non négligeables pour les fréquences supérieures à une fréquence f_c, dite fréquence de coupure du graphique, on choisit f_r de façon que la bande latérale à gauche de f_r soit à droite de f_c. *Dans ce cas le résultat est exactement le même que si on choisit une transformante continue.* En figure 7*c*, j'ai montré le spectre d'une transformante type bande-passante discontinue. *Il faut s'arranger pour qu'aucune partie du spectre du graphique ayant une amplitude appréciable ne soit sous une des bandes passantes en dehors de la toute première.* La règle s'applique facilement.

V. LE PROBLÈME D'UNICITÉ

On peut traiter le problème d'unicité sous la forme suivante: à la suite d'une série de transformations élémentaires on a obtenu une transformée. La transformée ne dépend que de la forme résultante (amplitude et phase) de

toutes les transformations élémentaires. Deux transformations différentes filtrant la même partie du spectre du graphique et de la même façon donneront un résultat identique.

La figure 8 montre un example typique: on utilise la même transformante continue et deux transformantes discontinues avec fréquence de répétition

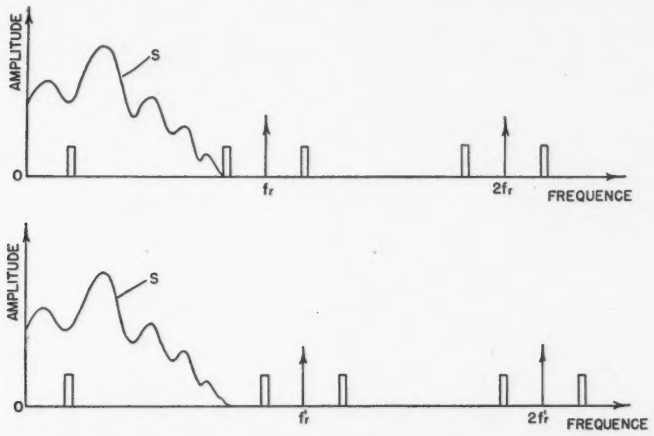

FIG. 8. Illustrant le problème d'unicité. Une courbe de spectre S analysée avec une transformante bande-passante continue et des transformantes bande-passante discontinues, fournit le même résultat si la première bande-passante seulement est à l'intérieur du spectre à analyser.

f_r et f'_r. Le spectre du graphique est montré à gauche. Dans les trois cas on obtient exactement le même résultat, c'est à dire des points sur la même courbe transformée.

Il en résulte en particulier que toutes les methodes d'analyse ayant mêmes courbes de sélectivité et de phase donneront les mêmes résultats. Par exemple, au moins en principe, les résultats obtenus par les méthodes de calcul peuvent être obtenus par des méthodes électro-optiques ou électroniques (14). Nous donnerons dans une autre étude un exposé de ces méthodes et nous ferons une étude comparée des possibilités pratiques des méthodes de calcul et des méthodes à intégration automatique.

BIBLIOGRAPHIE

1. COULOMB, J. 68^{ieme} Congrès des Sociétés Savantes, p. 215. 1935.
2. COULOMB, J. Analyse des graphiques. Presses Universitaires de France. 1943. p. 78.
3. EAGLE, A. A practical treatise on Fourier's theorem. Longmans Green and Co., London, etc. 1925. Chap. 8.
4. FAYARD, J. Compt. rend. 209: 746. 1939.
5. LABROUSTE, H. Compt. rend. 184: 259. 1927.
6. LABROUSTE, H. Ann. inst. phys. globe, Univ. Paris, bur. central magnétisme terrestre. 7. 1929.
7. LABROUSTE, H. Tables numériques pour l'analyse des graphiques. Henry Dévé, Editeur. 1930.
8. LABROUSTE, H. Ann. inst. phys. globe, Univ. Paris, bur. central magnétisme terrestre. 11. 1933.

9. LABROUSTE, M. et MME. 68ième Congrès des Sociétés Savantes, p. 119. 1935.
10. LABROUSTE, M. et MME. 69ième Congrès des Sociétés Savantes, p. 205. 1935.
11. LABROUSTE, M. et MME. 70ième Congrès des Sociétés Savantes, p. 93. 1937.
12. LABROUSTE, M. et MME. Analyse des graphiques. Presses Universitaires de France. 1943.
13. LEVY, M. Extension de la théorie de Fourier à l'analyse des courbes non périodiques. Rapport au Service des Recherches de l'Aeronautique, Ministère de l'Air, Paris, avril 1933.
14. LEVY, M. Compt. rend. 198: 2222. 1934.
15. LEVY, M. Compt. rend. 199: 1031. 1934.
16. LEVY, M. Compt. rend. 200: 646. 1935.
17. LEVY, M. Séries de Fourier et analyse des fonctions par le calcul. Conférence faite au Collège de France en 1935.
18. LEVY, M. Théorie des transformations sélectives. Rapport Technique des Laboratoires L.M.T., juillet 1937.
19. LEVY, M. Brevet Anglais. No. 581, 683, 6 juin. 1941.
20. LEVY, M. J. Inst. Elec. Engrs. (London), 90: 153. 1943.
21. LEVY, M. J. Brit. Inst. Radio Engrs. 6: 64. 1946.
22. LEVY, M. J. Brit. Inst. Radio Engrs. 6: 228. 1946.
23. WHITTAKER, E. et ROBINSON, G. Calculus of observations. Blackie and Son Ltd., London. 1924.

CANADIAN JOURNAL OF PHYSICS

Notice to Contributors

GENERAL: Manuscripts should be typewritten, double spaced, and the **original and one extra copy** submitted. Style, arrangement, spelling, and abbreviations should conform to the usage of this Journal. Names of all simple compounds, rather than their formulas, should be used in the text. Greek letters or unusual signs should be written plainly or explained by marginal notes. Superscripts and subscripts must be legible and carefully placed. Manuscripts should be carefully checked before being submitted, to reduce the need for changes after the type has been set. If authors require changes to be made after the type is set, they will be charged for changes that are considered to be excessive. **All pages, whether text, figures, or tables, should be numbered.**

ABSTRACT: **An abstract of not more than about 200 words, indicating the scope of the work and the principal findings, is required.**

ILLUSTRATIONS:

(i) *Line Drawings:* All lines should be of sufficient thickness to reproduce well. Drawings should be carefully made with India ink on white drawing paper, blue tracing linen, or co-ordinate paper **ruled in blue only;** any co-ordinate lines that are to appear in the reproduction should be ruled in black ink. Paper ruled in **green, yellow, or red should not be used** unless it is desired to have all the co-ordinate lines show. Lettering and numerals should be neatly done in India ink preferably with a stencil (**do not use typewriting**) and be of such size that they will be legible and not less than one millimeter in height when reproduced in a cut three inches wide. All experimental points should be carefully drawn with instruments. Illustrations need not be more than two or three times the size of the desired reproduction, but the ratio of height to width should conform with that of the type page. **The original drawings and one set of small but clear photographic copies are to be submitted.**

(ii) *Photographs:* Prints should be made on glossy paper, with strong contrasts; they should be trimmed to remove all extraneous material so that essential features only are shown. Photographs should be submitted **in duplicate;** if they are to be reproduced in groups, one set should be so arranged and mounted on cardboard with rubber cement; the duplicate set should be unmounted.

(iii) *General:* **The author's name, title of paper, and figure number should be written in the lower left hand corner (outside the illustration proper) of the sheets on which the illustrations appear.** Captions should not be written on the illustrations, but typed together at the end of the manuscript. All figures (including each figure of the plates) should be numbered consecutively from 1 up (arabic numerals). **Each figure should be referred to in the text.** If authors desire to alter a cut, they will be charged for the new cut.

TABLES: Each table should be typed on a separate sheet. Titles should be given for all tables, which should be numbered in Roman numerals. Column heads should be brief and textual matter in tables confined to a minimum. **Each table should be referred to in the text.**

REFERENCES: **These should be listed alphabetically by authors' names, numbered in that order, and placed at the end of the paper.** The form of literature citation should be that used in this Journal. **Titles of papers should not be given.** The first page only of the references cited should be given. **All citations should be checked with the original articles.** Each citation should be referred to in the text by means of the key number.

REPRINTS: A total of 50 reprints of each paper, without covers, are supplied free to the authors. Additional reprints will be supplied according to a prescribed schedule of charges. On request, covers can be supplied at cost.

Approximate charges for reprints may be calculated from the number of printed pages, obtained by multiplying by 0.6 the number of manuscript pages (double-spaced typewritten sheets, 8½ in. by 11 in.) and making allowance for space occupied by line drawings and half-tones (not inserts). The cost per page is tabulated at the back of the reprint request form sent with the galley.

Contents

Printed in Canada *by* University of Toronto Press